N69-34913

NASA TECHNICAL MEMORANDUM

NASA TM X-52621

NASA TM X-52621

CASE FILE COPY

INTERNAL THRUST AND PUMPING PERFORMANCE OF AN AUXILIARY INLET EJECTOR NOZZLE WITH CLAMSHELL THRUST REVERSER

by Ali H. Mansour and Richard R. Burley
Lewis Research Center
Cleveland, Ohio
June 1969

This information is being published in preliminary form in order to expedite its early release.

NASA TM X-52621

INTERNAL THRUST AND PUMPING PERFORMANCE OF AN AUXILIARY INLET EJECTOR NOZZLE WITH CLAMSHELL THRUST REVERSER

by Ali H. Mansour and Richard R. Burley

Lewis Research Center
Cleveland, Ohio

NATIONAL AERONAUTICS AND SPACE ADMINISTRATION

Page Intentionally Left Blank

ABSTRACT

Data were obtained over a range of pressure ratio from 2 to 31 and corrected secondary weight-flow ratio from 2 to 8% for three configurations which simulated take-off, transonic acceleration, and supersonic cruise flight conditions. A clamshell thrust reverser was fixed in positions approximately corresponding to those in flight operation. Adding tertiary air to the ejector improved performance at low pressure ratios. A maximum thrust coefficient of about 99% was obtained at take-off, and about 99.5% at supersonic cruise.

E-5124

Page Intentionally Left Blank

INTERNAL THRUST AND PUMPING PERFORMANCE OF AN AUXILIARY INLET EJECTOR NOZZLE WITH CLAMSHELL THRUST REVERSER

By Ali H. Mansour and Richard R. Burley

E-5124

CONTENTS

TM X-52621

Page Intentionally Left Blank

SUMMARY

An investigation was conducted to determine pumping and internal-thrust performance of an auxiliary inlet ejector nozzle (AIE), with clamshell thrust reverser, over a range of corrected secondary flow ratio from about 0.02 to about 0.08. A turbojet (J85-GE-13) was used as a gas generator to provide nozzle inlet flow. The engine primary nozzle area was varied to give a range of ejector area ratios between 2.25 and 4.507. The nozzle inlet gas temperature was varied from about 1640°R (900°K) to about 3200°R (1777°K). Three configurations were tested which simulated take-off (flaps closed; open fixed doors), transonic acceleration (flaps closed; doors closed), and supersonic cruise (flaps open; doors closed) flight conditions.

Pumping performance for the take-off ejector (doors open) was adequate and no apparent limit was reached. A thrust coefficient of about 99 percent was obtained with this configuration at low nozzle pressure ratios (between two and three) with about 0.05 corrected secondary flow ratio. The 20° door seems to have a slightly (less than one percent) better thrust coefficient than the 8°-16°, 16°, 10°-20° doors.

Pumping was limited due to a choking condition in the transonic ejector (doors closed). An improvement in thrust coefficient was obtained with this configuration as secondary flow was increased. A thrust coefficient approaching 97 percent was obtained at a nozzle pressure ratio of about 6.5.

Adding tertiary air through the open doors to the ejector improved thrust coefficient at low pressure ratios.

Pumping was limited due to a choking condition in the supersonic cruise ejector (flaps open; doors closed). A thrust coefficient of about 99.5 percent was obtained at a nozzle pressure ratio of about 24 for the highest area ratio (4.507) tested with a corrected secondary flow ratio of about 0.06.

A corrected secondary flow ratio of as low as 0.02 was sufficient for cooling the shroud and the clamshell for a maximum primary gas temperature of about 3200°R (1777°K).

INTRODUCTION

A flight test program has been initiated at Lewis Research Center to evaluate airframe installation effects on a variety of exhaust nozzle concepts. Prior to flight testing, it is necessary to determine the internal performance of these nozzles. This report presents the pumping and internal thrust performance of an auxiliary inlet ejector nozzle with a clamshell thrust reverser which was investigated in a Propulsion Systems Laboratory altitude chamber at the Lewis Research Center.

The nozzle system included an ejector shroud with a fixed contour simulating flaps at the shroud exit (trailing-edge flaps) and a series of auxiliary inlet doors located around the periphery of the external skin just ahead of the primary

nozzle exit. The basic operation of this type of nozzle system is described in reference 1. For this investigation, the auxiliary inlet doors and simulated trailing-edge flaps were fixed in positions corresponding to operations at take-off (flaps closed; fixed open doors), transonic operation (flaps closed; doors closed), and supersonic cruise operation (flaps open; doors closed). The clamshell was fixed in positions approximately corresponding to those in flight operations. A 17 degree position was set for take-off and a zero degree position was set for the transonic acceleration and supersonic cruise operations. (A simulated clamshell surface was provided for the supersonic cruise operation). The clamshell was not used as a thrust reversing device in this test.

The primary nozzle gas was provided by a variable exhaust area turbojet engine (J85-GE-13) and the secondary air was furnished by a facility air system.

Thrust and pumping characteristics are presented for a range of primary nozzle pressure ratios from about two to 31.0 and a range of corrected secondary flow ratio from about 0.02 to 0.08. The turbojet engine nozzle area was varied to provide a range of area ratios, A_9/A_8, (see Appendix A for symbol identifications) from 2.25 to 4.507. The engine exhaust gas temperature was varied from about $1640^{\circ}R$ ($900^{\circ}K$) to $3200^{\circ}R$ ($1777^{\circ}K$). Temperature and pressure profiles for the ejector, and pressure profiles for the clamshell are presented. Nozzle thrust coefficients are presented in two forms; F_G/F_{IP} and $F_G/(F_{IP} + F_{IS})$. The discussion of thrust coefficients in this report considers only the second form.

APPARATUS AND PROCEDURE

Installation

A schematic view and a photograph of the research hardware installation in the Propulsion System Laboratory altitude chamber are shown in figures 1 and 2. A General Electric J85-13 turbojet engine with afterburner was used as a gas generator for the auxiliary inlet ejector. The nacelle which supported the ejector assembly was mounted from a bed plate freely suspended by four flexure rods. Pressure forces acting on engine, nacelle, and nozzle were transmitted to a load cell which measured thrust. The load cell was water cooled to provide a constant temperature environment and eliminate errors due to heating of the test section during engine operation. A minimal amount of air was admitted to the test section of the altitude chamber through a bypass valve to reduce heating and keep the test section at an acceptable temperature level. A front bulkhead with a labyrinth seal around the inlet section of the primary air venturi separated the engine inlet air from the exhaust and provided a means of adjusting exhaust pressure independent of inlet air pressure. A flow deflector was used to divert air leakage through the seal from impinging on the nacelle. Pressure measurements on either side of the labyrinth seal were used to obtain the seal force applied to the thrust load cell.

Secondary airflow was supplied through a torroidal manifold and entered the front of the nacelle to cool the engine and primary nozzle. A rotary valve at the front of the nacelle was used to regulate upstream secondary air pressure to the same value as engine inlet air pressure. This was done to simulate realistic valve positions (as compared to in-flight operation) and minimize air leakage in a slip seal between the two sources of air.

Primary Nozzle

The J-85 has a variable area primary nozzle that closely approximates a circular geometry. As the exit area is modulated for changes in power, the primary nozzle translates longitudinally and a corresponding change in exit-flow convergence angle occurs (see fig. 3). The overlapping primary leaves translate on roller-track-cage arrangement into a nozzle-housing ring. The nozzle-housing ring has a series of 24 rectangular cut-outs located circumferentially about the ring. A flow diverter was used (see fig. 4) with all ejectors to force secondary cooling air underneath the nozzle-housing ring and over the primary leaves.

Auxiliary Inlet Ejector Nozzle

Schematic views and photographs of the ejector nozzles tested are shown in figures 4 through 7. The ejector assembly was attached to the 25-inch (63.50 cm) diameter nacelle. Door sections were removable. Four sets of doors were used; two single hinge doors with 16° and 20° angles and two double hinged doors with 8°-16° and 10°-20° angles. Ejector geometrical ratios (diameter and length to diameter ratios) are plotted as a function of the primary area in figure 8.

Two photographs for the clamshell at zero and 17 degree positions are shown in figures 9a and 9b. Two identical sections, a top and a bottom, hinged at both ends, made up the clamshell.

Instrumentation

Static pressures in the primary air venturi (station 1, see figure 1), and total pressures and temperatures ahead of the bellmouth were used to obtain inlet momentum and engine airflow. Metered engine fuel flow and afterburning fuel flow were added to engine flow to obtain the primary nozzle gas flow. With no afterburning, primary nozzle gas temperature (station 8) was assumed equal to the measured turbine discharge temperature (station 5). Afterburning nozzle temperature (station 8) was the sum of the turbine discharge temperature (station 5) and the afterburner temperature rise which is a function of afterburner fuel-air ratio and turbine discharge pressure (station 5). Primary gas total pressure (station 8) was a function of the total pressure at station 5 and the afterburner pressure drop ratio which is a function of gas flow, pressure, and temperature at station 5 and effective nozzle area at station 8. For more detailed engine instrumentation and functional relationships, see reference 2.

Two standard ASME sharp-edged orifices were used to determine the secondary nozzle airflow. Secondary nozzle total pressure and temperature were measured at station 200.35 as shown in figure 10.

Static pressure taps were installed at the inner and outer surface of auxiliary doors (a maximum of four doors were instrumented). Thermocouples were installed inside the doors only, as shown in figure 11. Figures 12a and 12b show ejector instrumentations. Figure 13 shows clamshell instrumentation; only the top half of the clamshell was instrumented.

Procedure

Engine inlet pressure was maintained at about 0.638 atm. for take-off and transonic acceleration test conditions and at one atm. for supersonic cruise test conditions. Engine inlet temperature and secondary air temperature were supplied at nominal values of 535°R (297°K). With no afterburning, the engine was operated at rated conditions (16500 RPM). With afterburning, using a nozzle area position indicator, the engine power was obtained by setting a nozzle area at station 8. At rated speed and no afterburning, the primary nozzle corrected gas flow obtained was about 44 lbs/sec. at a temperature of about 1640°R (900°K). The maximum corrected afterburning gas flow obtained was about 45.5 lbs/sec. at a nozzle inlet temperature of about 3200°R (1777°K).

Performance characteristics of each nozzle configuration were investigated over a range of pressure ratios. The take-off and transonic acceleration configurations were tested over a range of pressure ratios from two to 6.5. The supersonic cruise configuration was tested between five and 31.0 pressure ratio. Nozzle pressure ratio was varied by changing the exhaust pressure. At each setting of pressure ratio, the secondary airflow was adjusted to each of three values covering a nominal range of two to eight percent corrected secondary weight flow ratio. At each setting of secondary airflow, the secondary air pressure upstream of the rotary value at the nacelle inlet was adjusted to the same value as engine inlet air pressure. For methods used for data reduction, see reference 3.

RESULTS AND DISCUSSION

Nozzle thrust coefficients, secondary total pressure ratios, and nozzle pressure ratios for each nozzle configuration was initially plotted as a function of corrected secondary weight flow ratio ($\frac{W\sqrt{T}}{P}$); values of each of these parameters were then interpolated or extrapolated to obtain values at corrected secondary weight flow ratios of 0.02, 0.04, 0.06, and 0.08. These values were then plotted against nozzle pressure ratio for each weight flow ratio to make up thrust and pumping characteristics curves. The symbols on these curves are, therefore, not necessarily actual data points. Actual data points are used for pressure and temperature profiles for the ejector and the clamshell.

Pumping and Thrust Characteristics

Pumping and thrust characteristics of the auxiliary inlet ejector are presented as a function of nozzle pressure ratio for corrected secondary flow ratios of 0.02, 0.04, 0.06, and 0.08 for each configuration. For the take-off configuration and four door geometries, the pumping characteristics are presented in figures 14 through 17 and the corresponding thrust characteristics are presented in figures 18 through 25. For the transonic configuration, pumping characteristics are presented in figure 26 and the corresponding thrust characteristics are presented in figures 27 and 28. For the supersonic cruise configuration, the pumping characteristics are presented in figure 29 and the corresponding thrust characteristics are presented in figures 30 and 31.

Pumping characteristics are presented in the form P_{TS}/P_{T8}, where P_{TS} is the total pressure near the exit passage of the secondary and P_{T8} is the total pressure at the primary nozzle. Thrust coefficients are shown in two forms, $F_G/(F_{IP} + F_{IS})$ and F_G/F_{IP}; where F_G is actual jet thrust, F_{IP} is the isentropic thrust of the primary flow, and F_{IS} is the isentropic thrust of the secondary flow. F_{IS} was set to zero when the secondary total pressure was less than altitude pressure. The discussion of thrust coefficients in this report considers only the first definition, $F_G/(F_{IP} + F_{IS})$.

For the take-off configuration (flaps closed; open fixed doors) all four door geometries (16^o, 8^o-16^o, 20^o, 10^o-20^o) exhibited similar trends in pumping and thrust. The secondary pressure required to pump a given flow decreased as nozzle pressure ratio was increased, and was increased for a given nozzle pressure ratio as the amount of secondary flow was increased (figures 14 through 17). The effect of door angle on pumping performance was small. A slight improvement in pumping was obtained for all door geometries as area ratio was increased from 2.25 to 3.115.

The thrust coefficient of the 20^o door (figure 20) was slightly (less than one percent) higher than for the other door geometries (figures 18, 19, and 21). Thrust coefficients for the 20^o door at low pressure ratios (about three) and area ratio of 3.115 were as high as 99 percent and at high pressure ratios (about 5.7) were as low as 94 percent with moderate amount of secondary air (figure 20a). Increasing area ratio from 2.25 to 3.115 for all door geometries increased thrust coefficient less than one percent at low pressure ratios and about three percent at high pressure ratios with moderate amount of secondary air. In this configuration, it should be noted that the 17-degree clamshell position was set to yield near optimum performance. This near-optimum clamshell position was estimated from unpublished cold-flow data at Lewis Research Center. A comparison of the thrust characteristics of the take-off configurations (figures 18 through 21) with similar data for the transonic configurations (figure 27) shows that tertiary air (air through doors) which was not included in the calculation of ideal thrust, improved the thrust coefficient at low pressure ratios.

For the transonic acceleration configuration (flaps closed; doors closed), three area ratios were tested (figures 26, 27 and 28) and all exhibited similar trends in pumping and thrust characteristics. When a maximum amount of jet overexpansion existed, the low pressure on the back side of the primary nozzle leaves made the secondary pressure insensitive to further decreases in ambient pressure. This condition existed beyond the "knee" of the pumping curves in figure 26. At the nozzle pressure ratios corresponding to the knee of each pumping curve in figure 26, the thrust coefficients (figures 27 and 28) reached minimum values. For this ejector several observations can be made:

1. Pumping pressure (secondary pressure) was decreased as area ratio was increased, and was increased as secondary flow was increased for a constant nozzle pressure ratio.

2. Secondary flow markedly improved thrust coefficient at all area ratios tested.

3. Thrust coefficients approaching 95 percent were measured when operating near 2.5 nozzle pressure ratio (figure 27a) and approaching 97 percent near 6.5 pressure ratios (figure 27c).

For the supersonic cruise configuration (flaps open; doors closed), the pumping curves were flat (straight lines) across the pressure ratio range covered, figure 29. It is evident that secondary pressure was not affected by lowering ambient pressure. Increasing area ratio increased pumping performance at a constant nozzle pressure ratio. A nozzle thrust coefficient of about 99.5 percent was obtained at a nozzle pressure ratio of 24 with the largest area ratio (4.507) tested using a moderate amount of secondary flow (about 0.06), figure 30a. The other three area ratios (3.445, 3.210, 2.958) yielded a thrust coefficient of about 97.0 to 98.0 percent at a nozzle pressure ratio of about 18 with moderate amounts of secondary flow, figure 30b, c, d. Thrust coefficient peaked at about 0.06 corrected secondary ratio.

A corrected secondary flow ratio of as low as 0.02 was sufficient for cooling ejector shroud and clamshell for a maximum primary gas temperature of about 3200°R (1777°K) for all configurations.

Ejector and Clamshell Profiles

Typical ejector and clamshell wall pressure and temperature profiles are presented in figures 32 through 38. The static pressure along the wall is ratioed to the total pressure at the primary nozzle throat. For ejector profiles this ratio is plotted versus X/D_{E8}, where X is the distance from the primary exit nozzle edge to the static pressure tap and temperature locations inside the ejector, and D_{E8} is the effective diameter of the primary throat. For the supersonic cruise ejector the profiles are presented as a function of area ratio (A/A^*) and X/D_{E8}.

For the clamshell, the wall pressure ratio (P_C/P_{T8}) is plotted versus X_C, where X_C is the distance of the static pressure tap from the leading edge of the clamshell.

Figures 32a and 33a present typical ejector pressure profiles for the take-off configuration (only 8^o-16^o and the 20^o doors are presented). Typical clamshell pressure profiles are presented in figures 34a, b. Pressure profiles for zero (doors closed) and 17^o (20^o doors) clamshell positions are plotted for two area ratios. When the clamshell was set at 17^o the profiles are shown for the inside and the outside of the clamshell surface. It appears that secondary flow had little or no effect on the pressure profiles at low pressure ratios and at high pressure ratios the pressure level on the outside surface of the clamshell was slightly higher as secondary flow was increased (figure 34b - $P_{T8}/P_0 = 5.25$). Figures 32a and 33a indicate that pressure levels were generally below ambient caused by overexpansion. As nozzle pressure ratio was increased, overexpansion of the gases inside the 17^o clamshell caused some thrust losses (see figure 34). The pressures inside the clamshell indicate the possible occurrance of a shock at the highest pressure ratio which caused a drop in performance. Other losses (as pressure ratio was increased) could be attributed to the fact that as pressure ratio was increased so did the auxiliary airflow through the ejector which caused a decrease of the effective primary nozzle area ratio (A_9/A_8) thus decreasing the thrust coefficient (as figures 18 through 21 indicate). Increasing secondary air decreased the wall temperature in the ejector (figures 32b and 33b). A maximum wall temperature of about 1800^oR (1000^oK) was recorded. The temperature inside the clamshell was hottest at about the center ($T_C/T_8 = .7$, or $T_C = 2200^oR = 1222^oK$) and decreased toward pin area where the two halves of the clamshell are hinged together.

Figures 35a and 36a present typical profiles for the transonic operation (thrust performance figure 27). The primary jet overexpansion is affecting ejector shroud static pressures and causing them to be lower than ambient. The peak loss due to this overexpansion occurs at a nozzle pressure ratio between three and four (figure 27). As pressure ratio is increased the wall pressures approach ambient so that the overexpansion losses are much smaller, thus causing a rise in thrust coefficient as figure 27 clearly shows. (Also see reference 4). Figures 35b and 36b present the temperature profiles for the transonic ejector. Temperatures are getting slightly colder toward the exit of the ejector and hotter as secondary airflow decreased. Pressure ratio didn't have a significant effect on temperature level.

Figures 37a and 38a present typical pressure profiles for two area ratios (4.507 and 3.445) for the supersonic cruise case. Pressure profiles were generally decreasing to approach ambient conditions. And at low pressure ratios (5.75 and 5.48 in figures 37a and 38a) a strong shock was generated thus bringing ejector pressures to about ambient conditions. Thrust curves (figure 30) indicate an increase in thrust coefficient as pressure ratio is increased beyond 12. The reason is that as pressure

ratio is increased these overexpansion losses were reduced and thus increased thrust coefficient.

Figures 37b and 38b present typical temperature profiles for this ejector. Pressure ratios had no effect on temperature profiles. A peak T_W/T_8 of about 0.8 was recorded.

SUMMARY OF RESULTS

The following results were obtained from static altitude tests of three ejector nozzle configurations representing three flight conditions; take-off, transonic acceleration, and supersonic cruise. Data were obtained over a range of area ratios from 2.20 to 4.50 and corrected secondary flow ratios from 0.02 to 0.08 and over a range of exhaust nozzle pressure ratios from 2 to 31.0.

1. For the take-off configuration, a slight improvement in pumping performance was obtained as area ratio was increased from about 2.25 to 3.10. Among the four different door geometries tested, the 20° door seems to have the best thrust performance (by less than one percent). Thrust coefficients for the 20° door at low pressure ratios (about three) and an area ratio of 3.115 were as high as 99 percent and at high pressure ratios (about 5.7) were as low as 94 percent with moderate amount of secondary air. Increasing area ratio from 2.25 to 3.10 increased thrust coefficient about one percent at low pressure ratios and about three percent at high pressure ratios with moderate amounts of secondary air ($w\sqrt{\theta}$ = 0.05).

2. For transonic configuration pumping was improved as area ratio was increased. Secondary flow markedly improved thrust coefficient at all area ratios tested. Thrust coefficients approaching 95 percent were measured when operating near 2.5 nozzle pressure ratio and approaching 97 percent near 6.5 nozzle pressure ratio.

3. Adding tertiary air through the open doors to the ejector improved thrust coefficient at low pressure ratios.

4. For the supersonic cruise configuration pumping performance was limited at the nozzle pressure ratios covered due to a choking condition in the ejector. Pumping performance was improved as area ratio was increased. A nozzle thrust coefficient of about 99.5 percent was obtained at a nozzle pressure ratio of 24 for the highest area ratio (4.507) tested with about 0.06 corrected secondary ratio. The area ratios 3.445, 3.210, and 2.958 yielded a thrust coefficient of about 97.0 to 98.0 percent at a nozzle pressure ratio of about 18 with 0.06 corrected secondary ratio.

5. A corrected secondary flow as low as 0.02 was sufficient for cooling shroud and clamshell for a maximum primary gas temperature of about 3200°R (1777°K).

APPENDIX A

The unit used for distance(D, L, X) was inches, for pressure (P) was pounds per square inches absolute, for temperature (T) degrees rankine, for flow (W) pounds per second, for thrust (F) pounds, and for area (A) inches squared.

Symbols

D_{MAX}	nacelle diameter (maximum)
D_8	primary throat diameter
T_P	primary temperature
W_P	primary flow
D_e	ejector throat diameter
T_S	secondary total temperature
W_S	secondary flow
P_{TS}	secondary total pressure
D_9	ejector exit diameter
L	distance from primary throat to ejector throat
L_e	distance from primary throat to ejector exit
F_G	actual jet thrust
F_{IP}	isentropic primary thrust
F_{IS}	isentropic secondary thrust
X	distance downstream from primary nozzle throat
X_C	distance downstream from leading edge of clamshell
$W\sqrt{T}$	corrected secondary to primary air ratio $\left(\frac{W_S}{W_P}\sqrt{\frac{T_S}{T_P}}\right)$
P_0	altitude static pressure

P_{T8}	primary nozzle total pressure
P_W	ejector wall static pressure
D_{E8}	effective primary throat diameter
T_8	gas temperature at primary throat (station 8)
T_W	ejector wall temperature
T_C	clamshell temperature
P_C	clamshell static pressure
A	area
A*	effective area at primary throat (A_{E8})

REFERENCES

1. Migdal, David; and Horgan, John J.: Thrust Nozzles for Supersonic Transport Aircraft. J. Eng. Power, vol. 86, no. 2, Apr. 1964, pp. 97-104.

2. Antl, Robert J.; and Burley, Richard R.: Steady-State Airflow and Afterburning Performance Characteristics of Four J85-GE-13 Turbojet Engines. NASA TM X-1742, 1969.

3. Samanich, Nick E.; and Huntley, Sidney C.: Thrust and Pumping Characteristics of Cylindrical Ejectors Using Afterburning Turbojet Gas Generator. NASA TM X-52565, 1969.

4. Trout, Arthur M.; Papell, S. Stephen; and Povolny, John H.: Internal Performance of Several Divergent-Shroud Ejector Nozzles with High Divergence Angles. NACA RM E57F13, 1957.

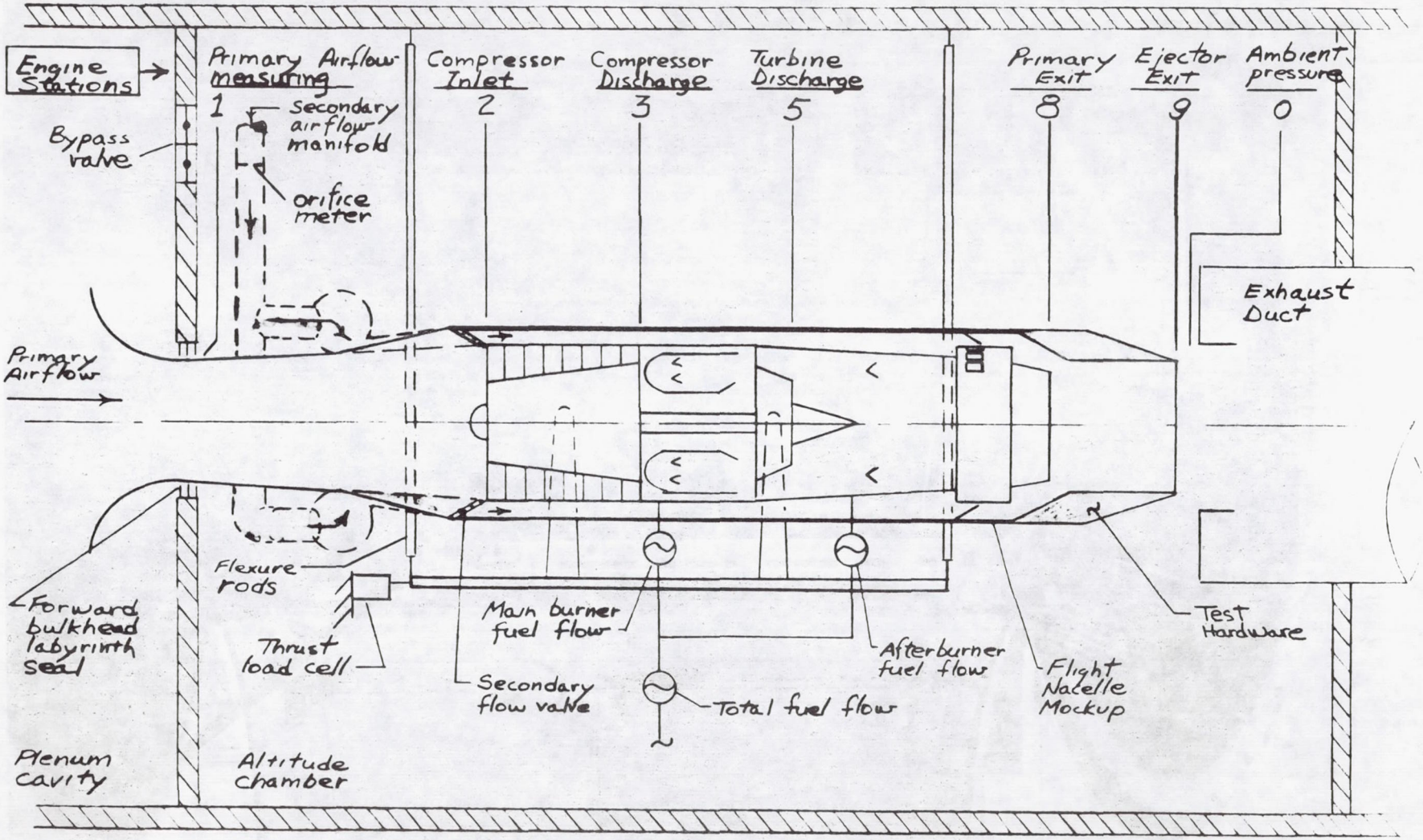

Figure 1 - Schematic of Test Installation

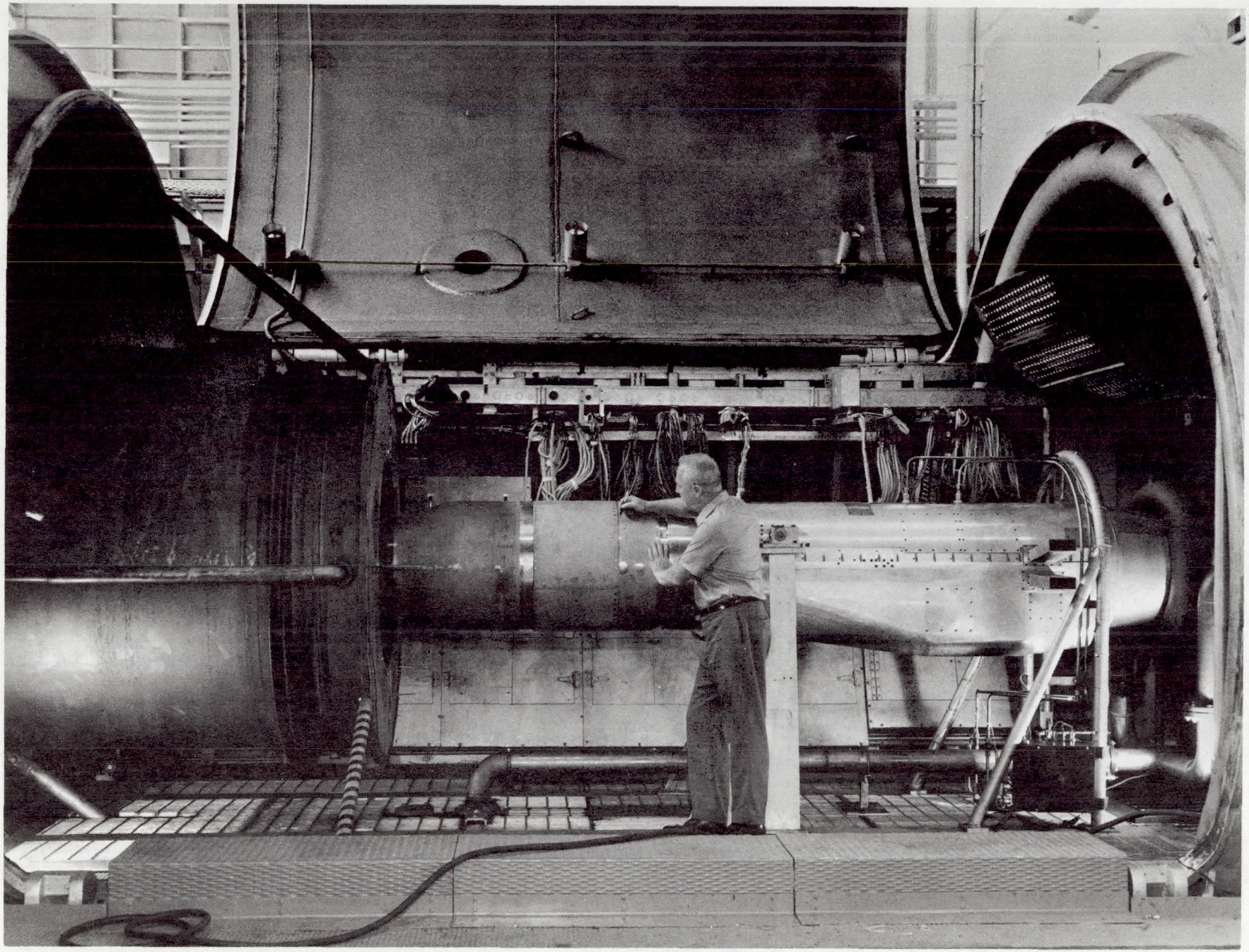

Figure 2 Photograph of Test Hardware
in Altitude Facility

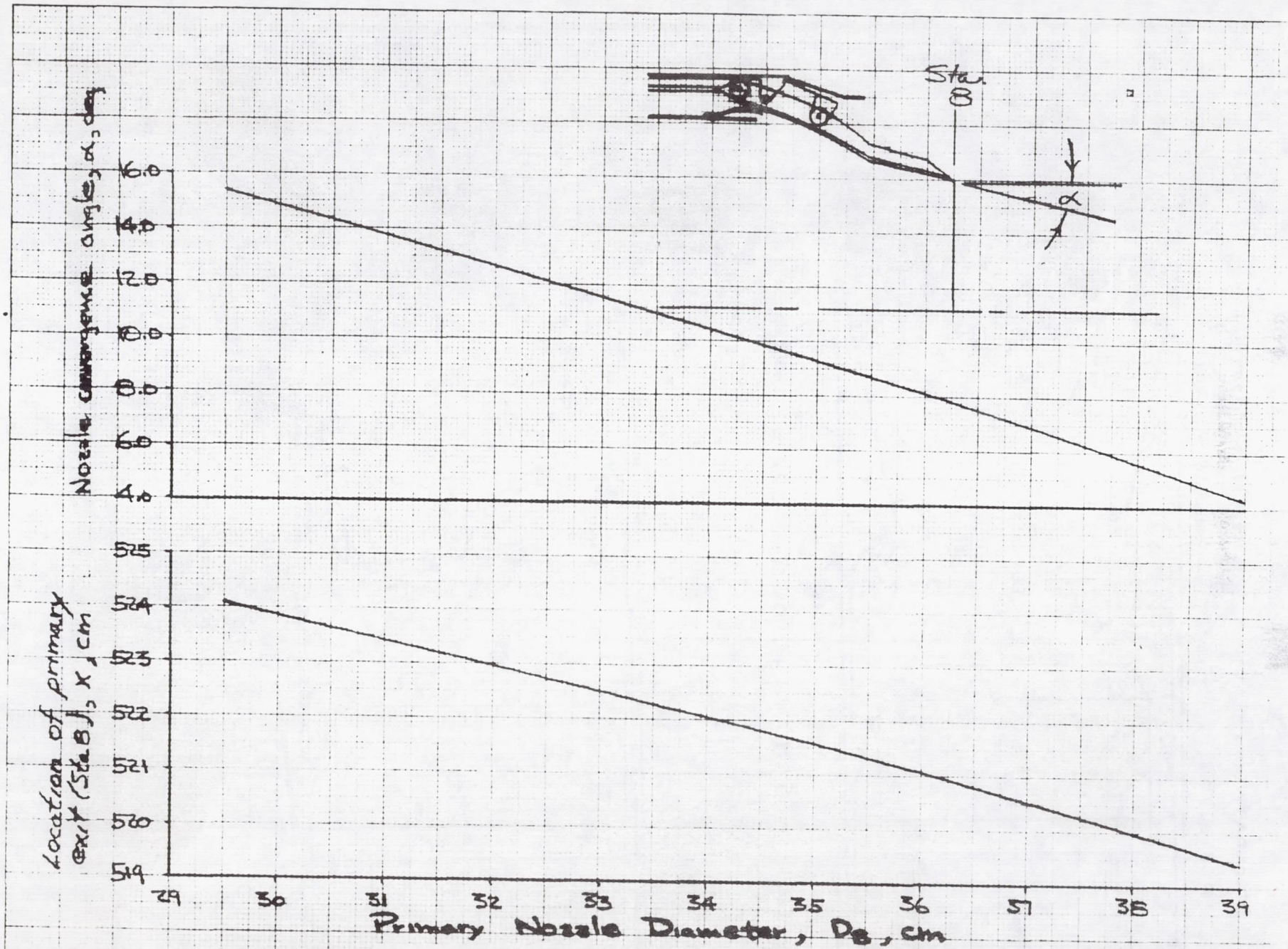

Figure 3 - Primary Nozzle Dimensional Characteristics

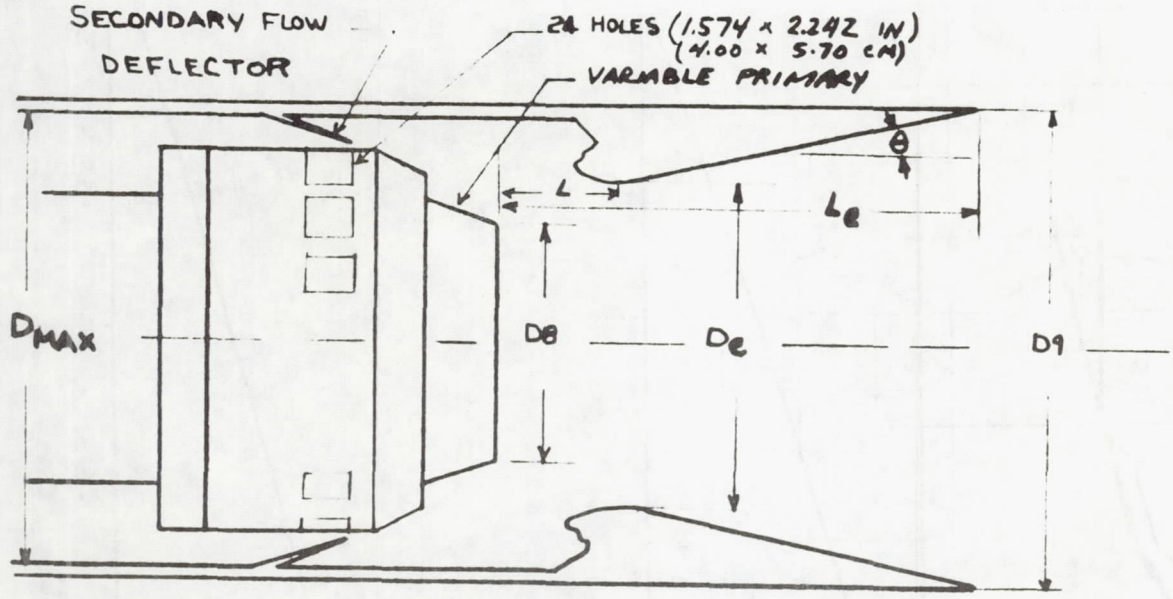

(a) TRAILING-EDGE FLAPS OPEN

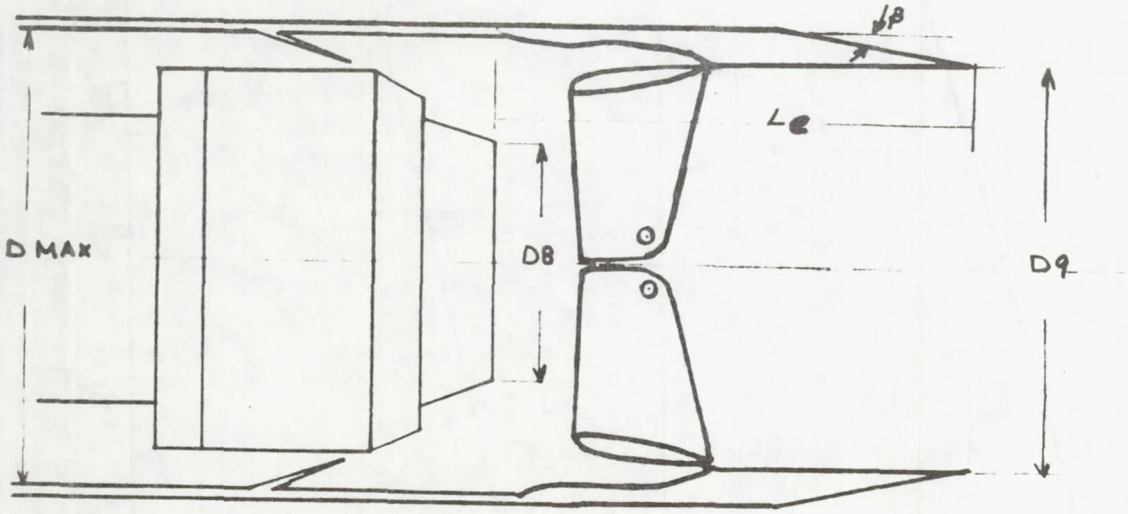

(b) TRAILING-EDGE FLAPS CLOSED
CLAMSHELL @ ZERO DEG. POSITION

FIGURE 4 SCHEMATIC VIEWS OF EJECTORS TESTED

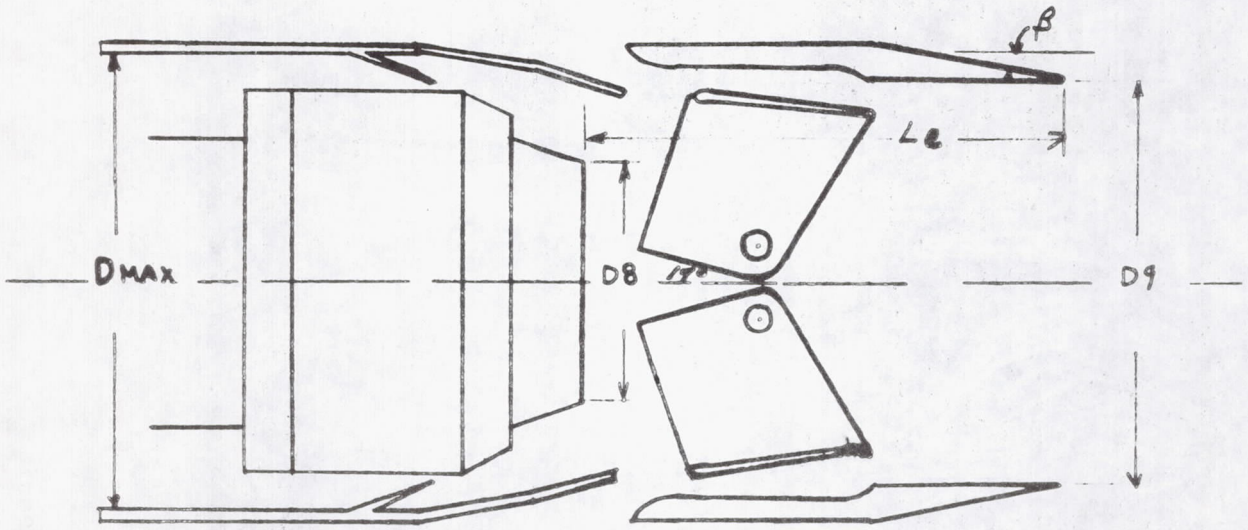

(c) TRAILING-EDGE FLAPS CLOSED, OPEN FIXED DOORS CLAMSHELL @ 17 DEG. POSITION

	TRAILING-EDGE FLAPS	
	CLOSED	OPEN
	—	
DMAX	25", (63.5 CM)	
De	20.70" (52.6 CM)	17.14" (43.5 CM)
D9	20.78" (52.8 CM)	24.72" (62.8 CM)
θ	—	9°
β	15°	—

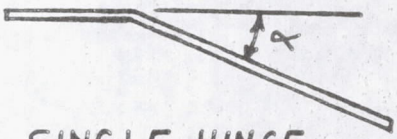

SINGLE HINGE

α°
0
16
20

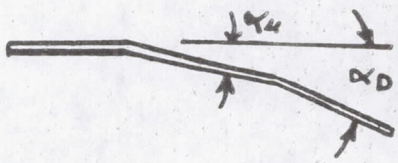

DOUBLE HINGE

αU°	αD°
8	16
10	20

FIGURE 4 CONCLUDED

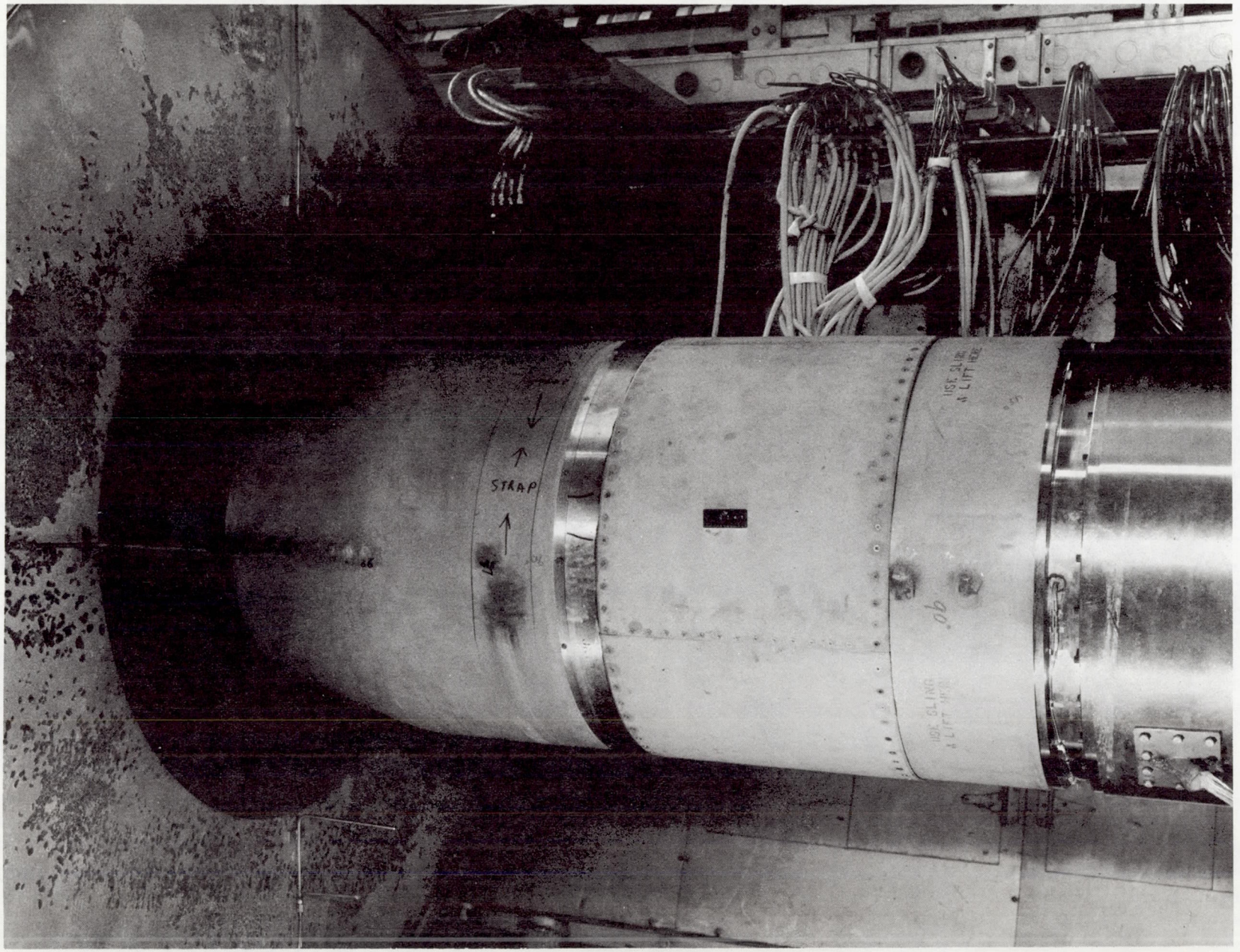

Figure 5 Photograph of Transonic Ejector (Flaps closed, Doors closed)

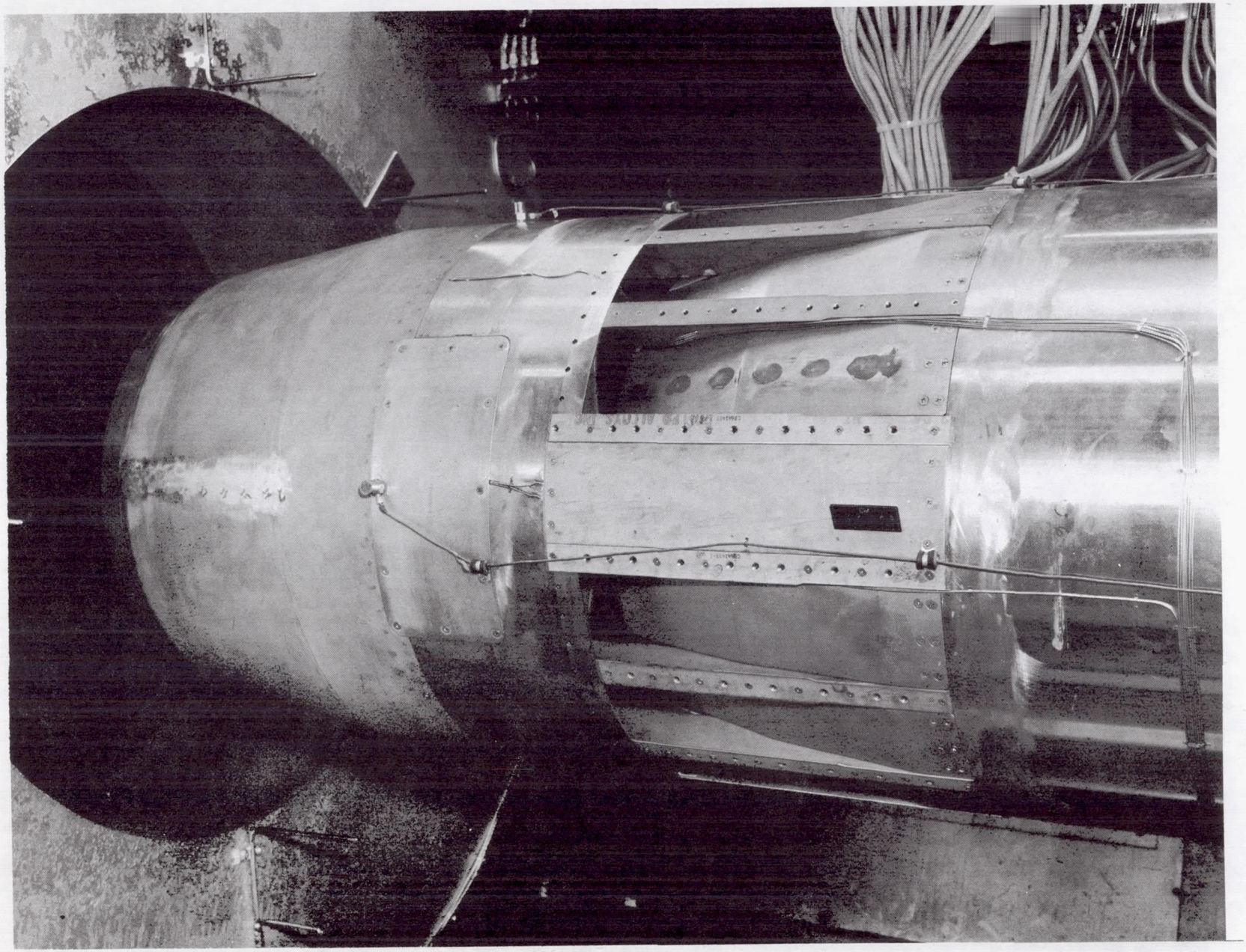

Figure 6 Photograph of Take-off Ejector (Flaps closed, Open fixed doors)

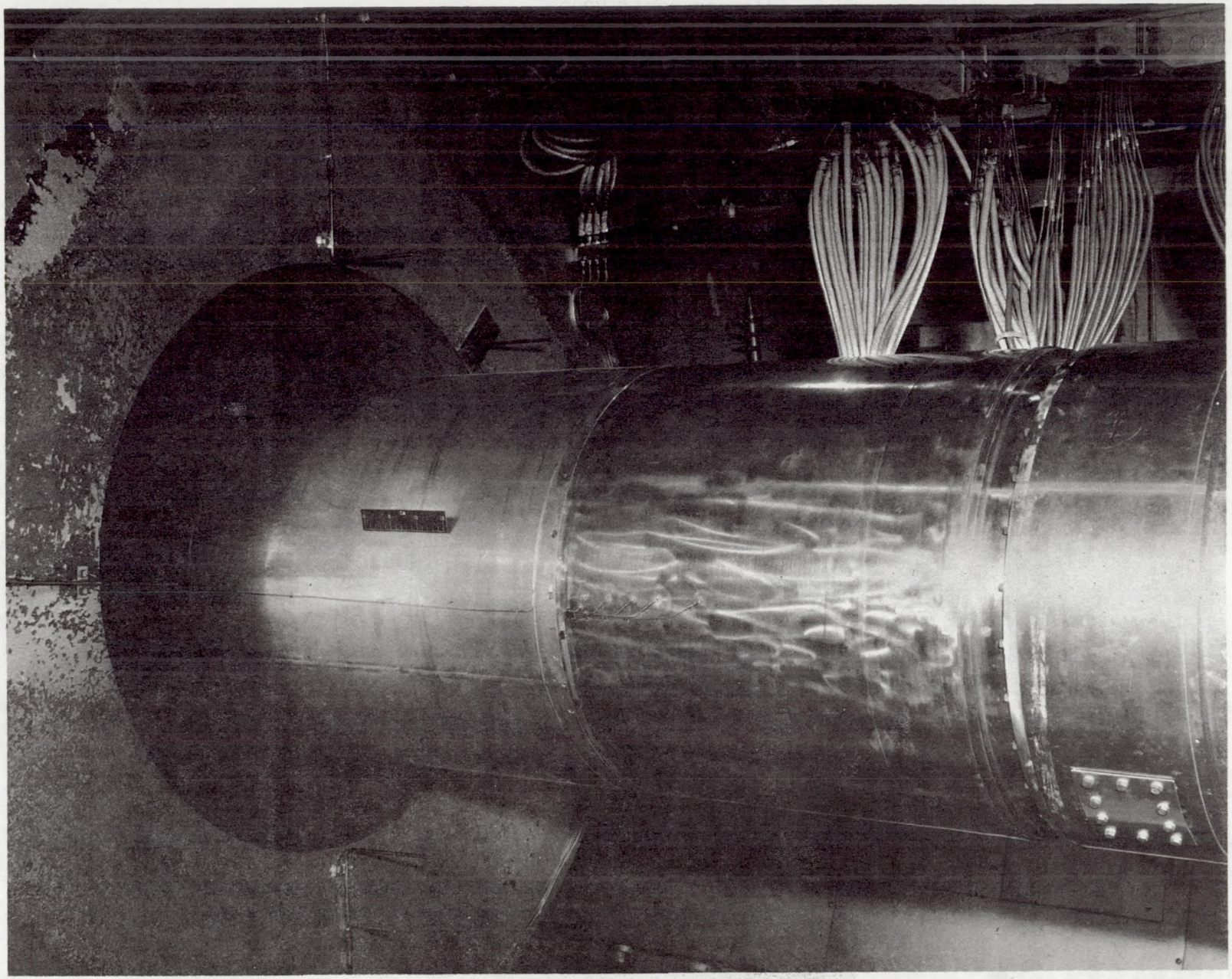

Figure 7 Photograph of Supersonic Cruise Ejector (Flaps open, Doors closed)

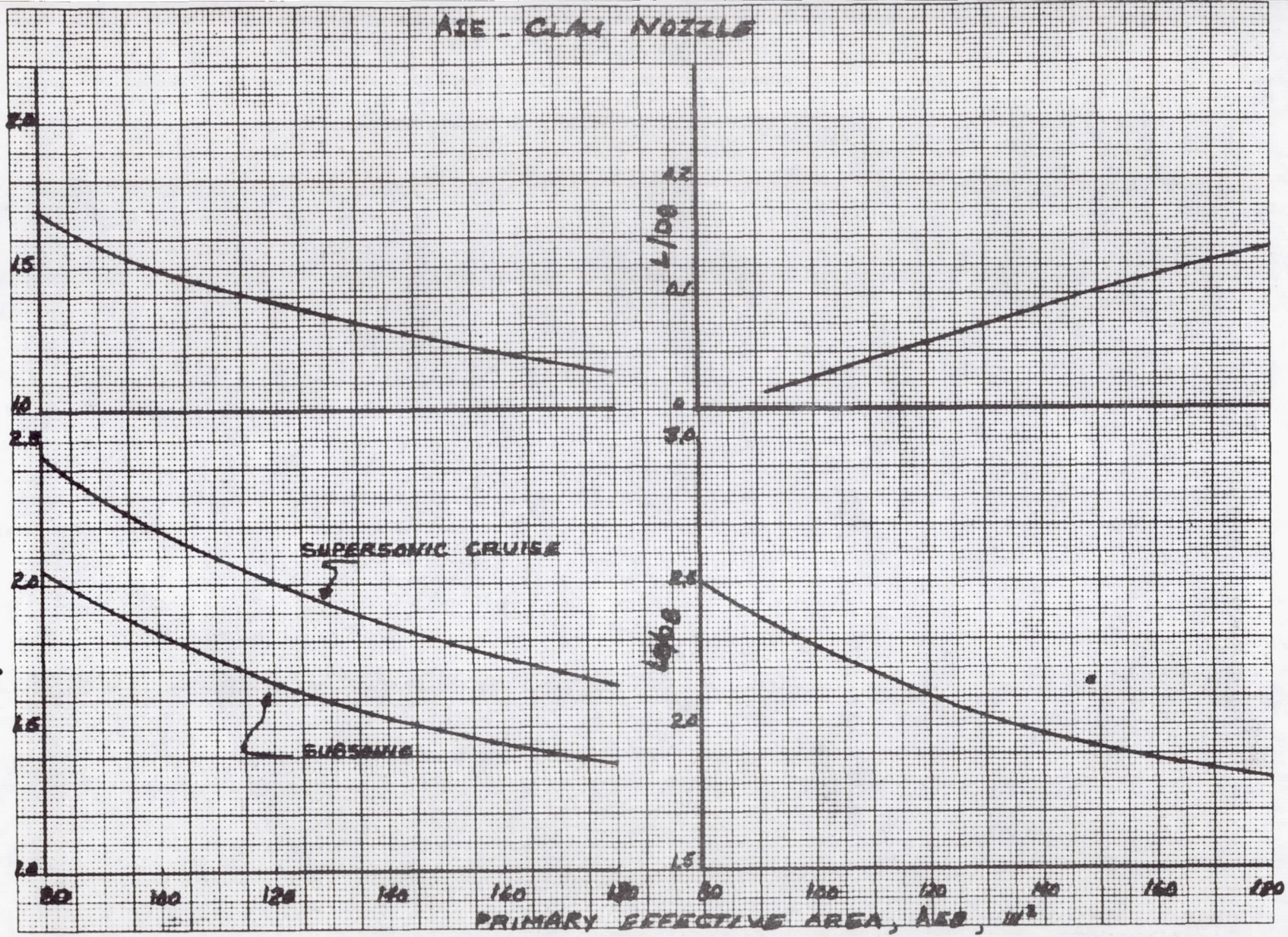

FIGURE 8 EJECTOR GEOMETRICAL CHARACTERISTICS

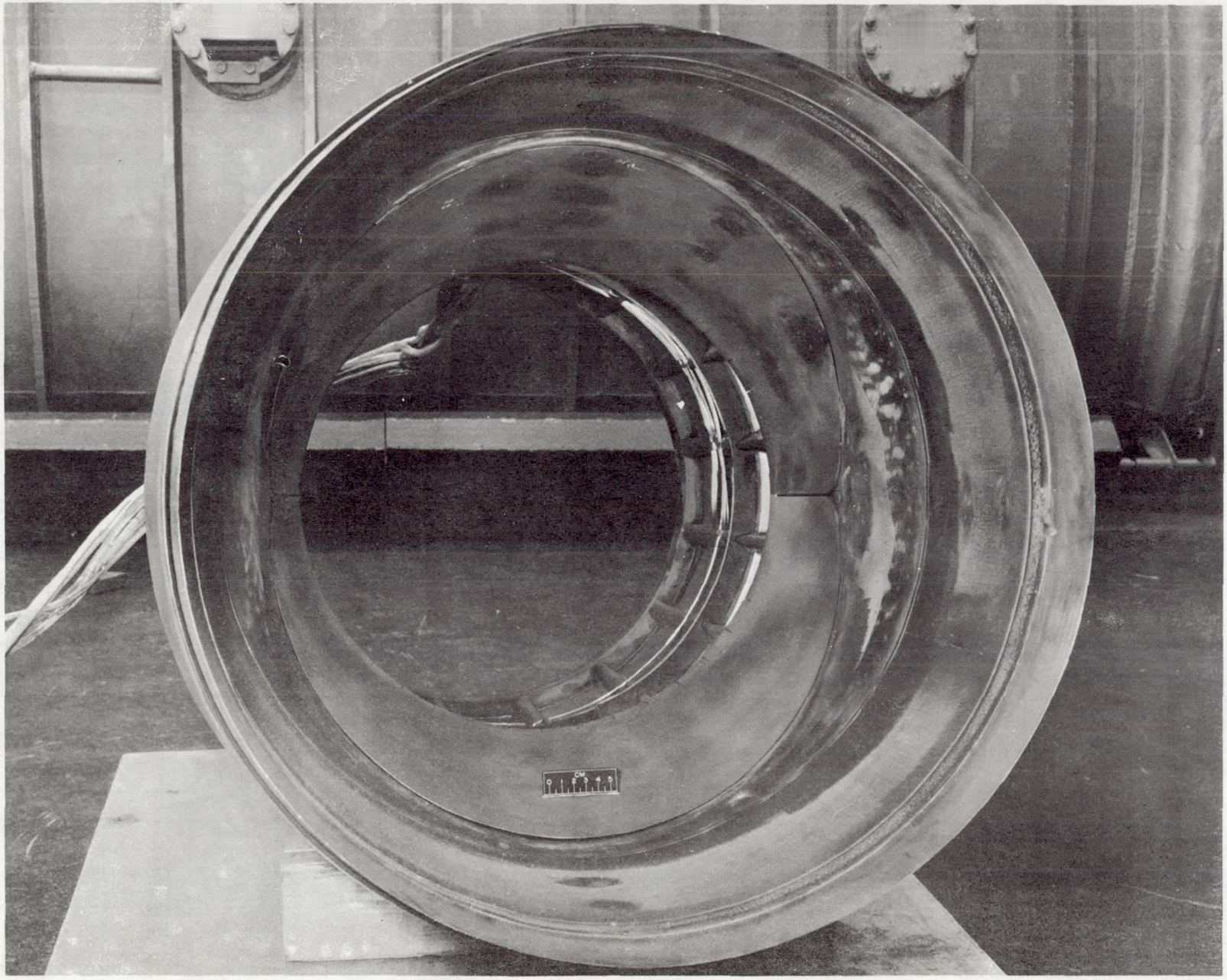

Figure 9a Photograph of Clamshell @
Zero degrees

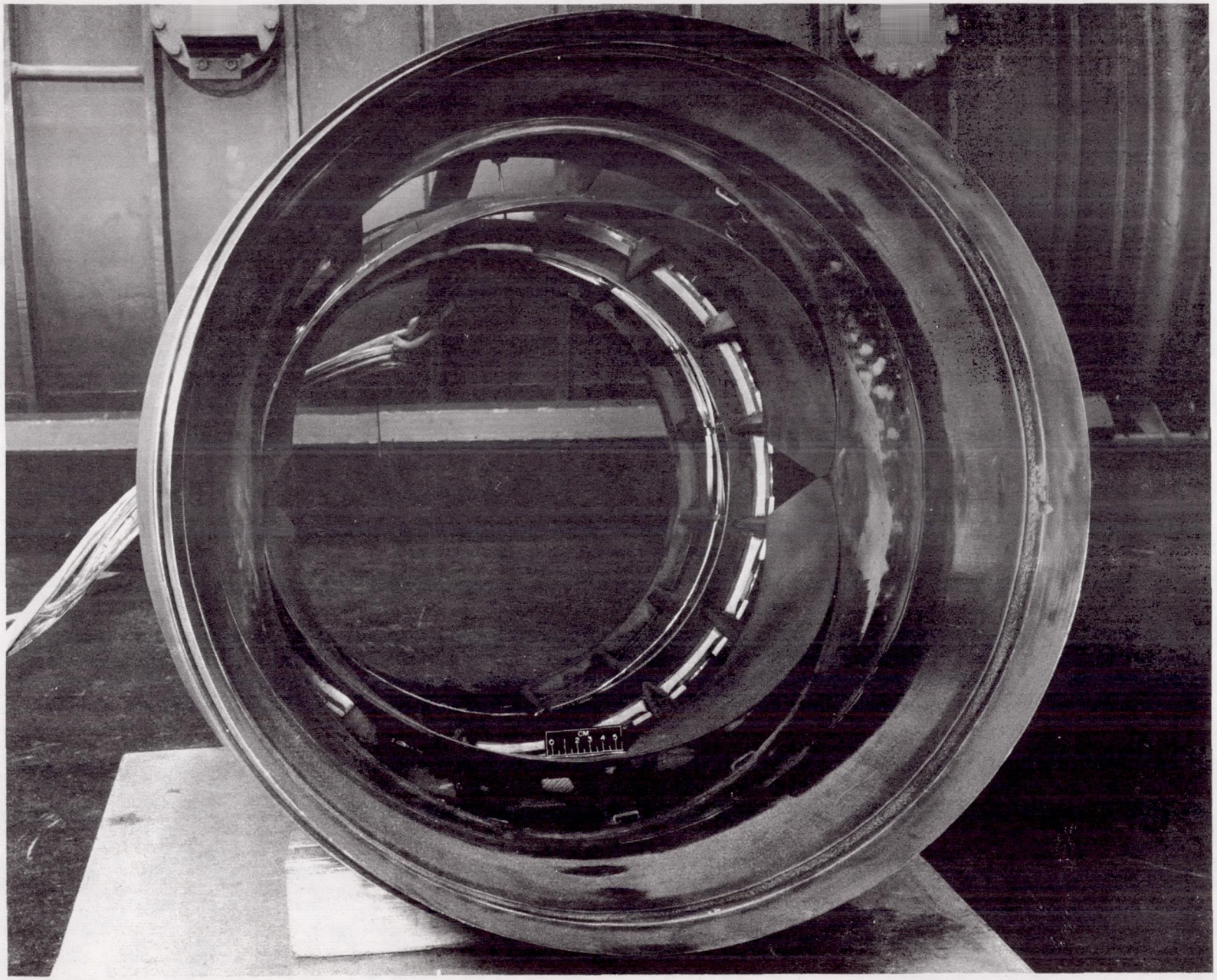

Figure 9b Photograph of Clamshell @
17 degrees

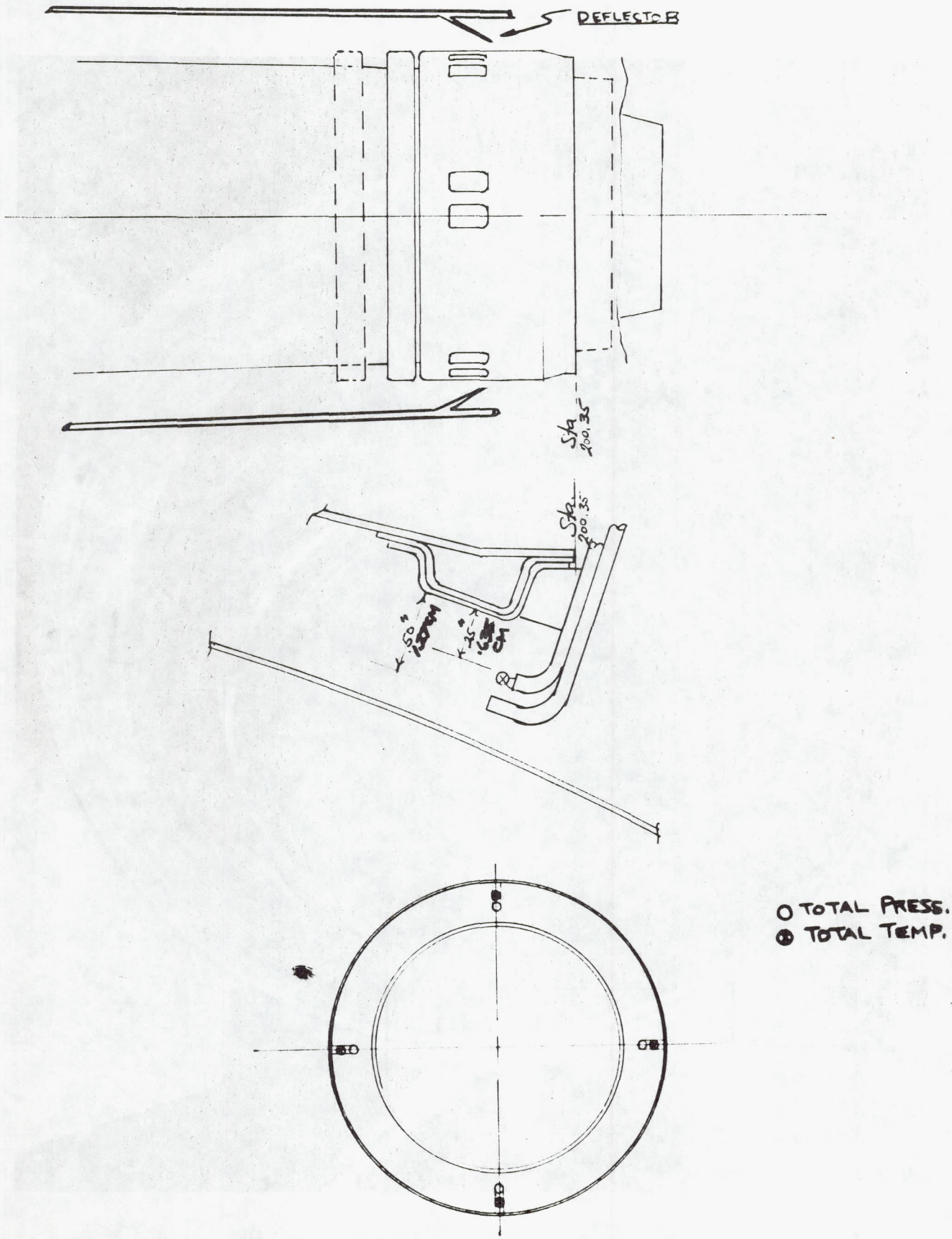

FIGURE. 10 SECONDARY PASSAGE INSTRUMENTATIONS

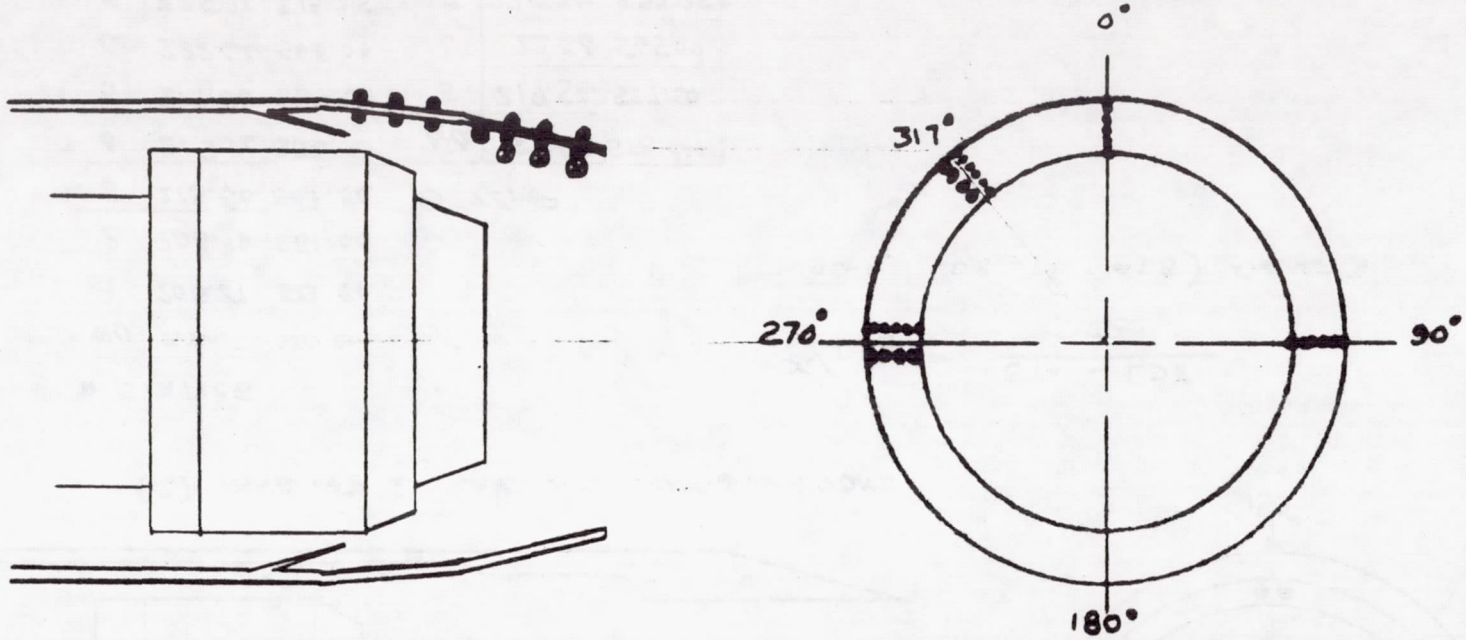

16 DOORS — ONLY FOUR WERE INSTRUMENTED (AS SHOWN ABOVE)

• STATICS
⊗ TEMPERATURS

FIGURE 11 AUXILIARY DOORS INSTRUMENTATION

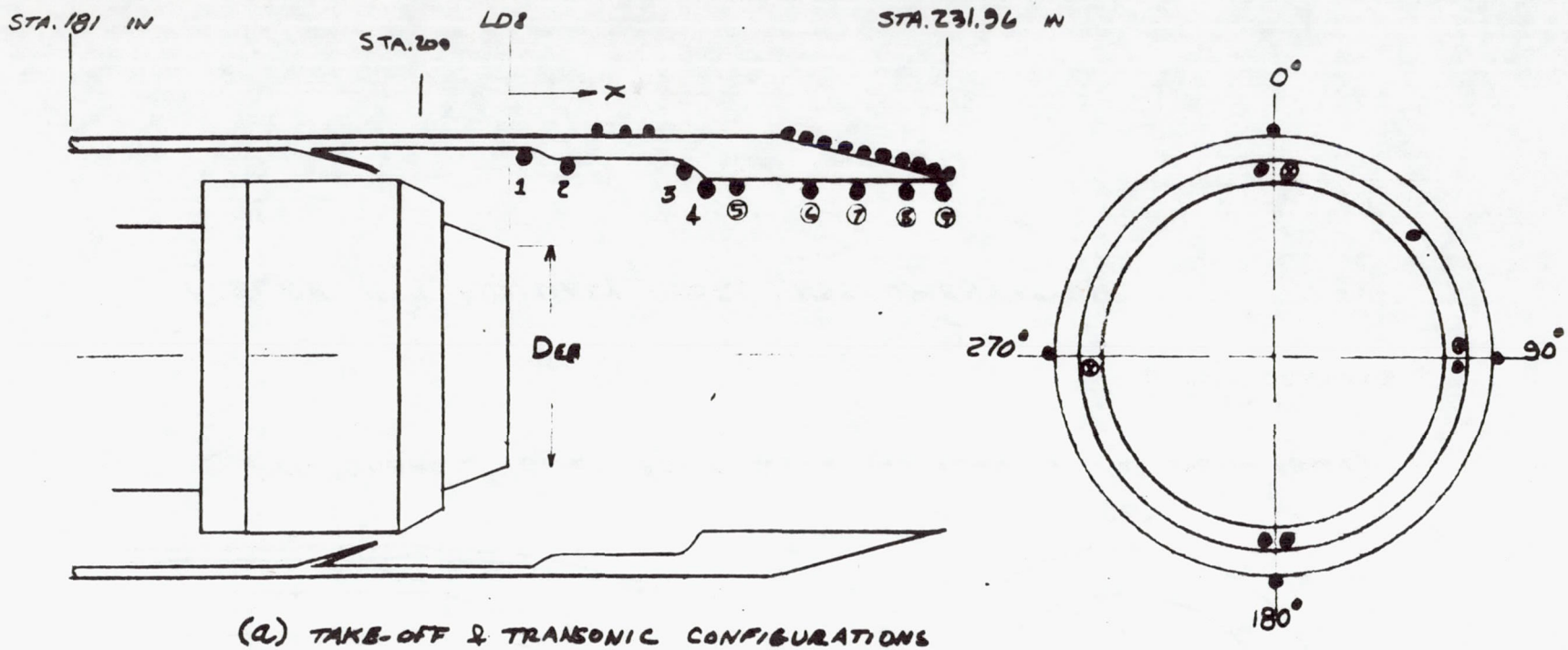

(a) TAKE-OFF & TRANSONIC CONFIGURATIONS

• STATICS

NO.	STA.*	STA. CM
1	205.27	521.80
2	208.96	531.00
3	213.56	542.50
4	217.56	552.50
5	219.56	557.50
6	222.66	565.00
7	225.76	573.25
8	228.86	581.25
9	231.96	589.30

⊗ TEMP.

NO.	STA.*	STA. CM
5	219.56	557.50
6	222.66	565.00
7	225.76	573.25
8	228.86	581.25
9	231.96	589.30

$$X/DEB = \frac{STA. - LDB}{DEB}$$

where, $LDB = f(AEB)$ FIGURE 3

FIGURE 12 AIE - CLAM EJECTORS INSTRUMENTATION

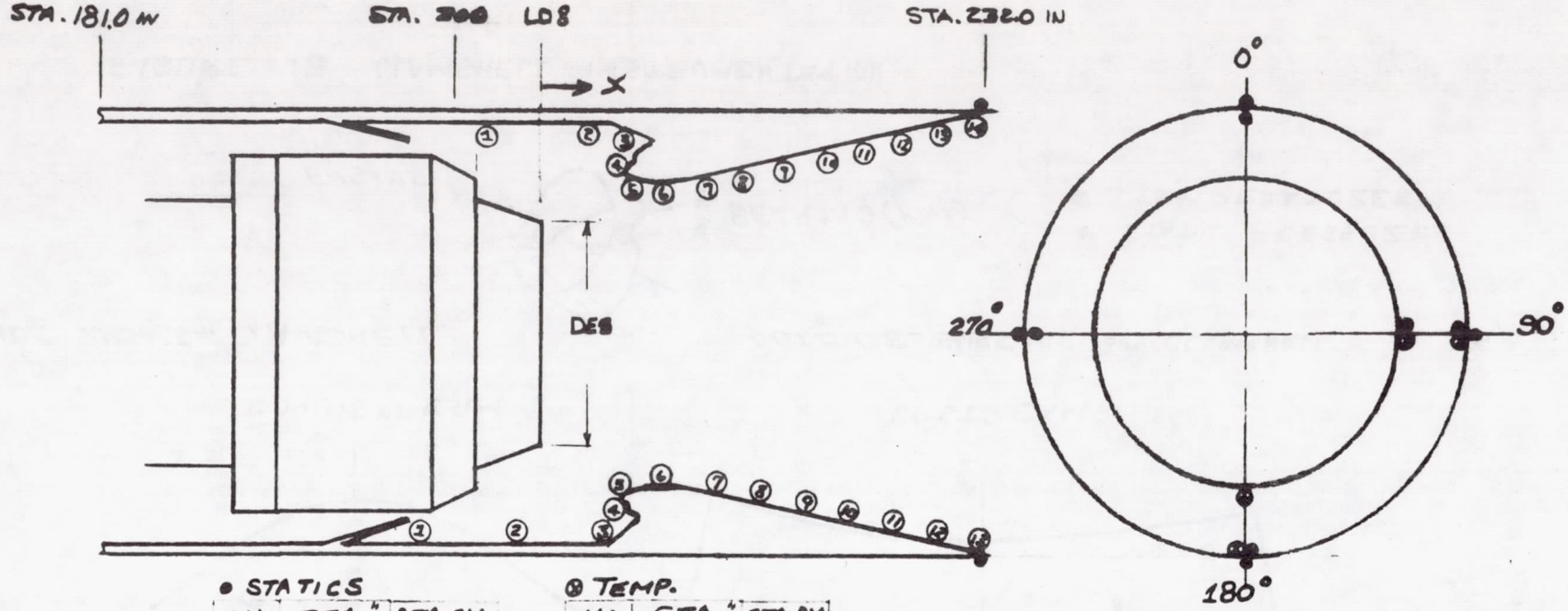

(b) SUPERSONIC CRUISE CONFIGURATION

• STATICS

NO.	STA."	STA.CM
1	199.00	505.50
2	202.00	513.00
3	204.45	519.20
4	206.60	522.00
5	206.32	521.70
6	206.92	524.70
7	208.90	530.50
8	213.05	541.00
9	216.98	551.00
10	220.36	560.00
11	223.98	569.00
12	227.20	577.00
13	230.37	585.00
14	232.00	589.30

⊗ TEMP.

NO.	STA."	STA.CM
1	196.50	499.00
2	200.60	509.00
3	204.55	519.20
4	205.60	522.0
5	206.32	521.70
6	206.72	524.70
7	210.15	533.80
8	213.67	542.60
9	217.20	551.58
10	220.72	561.45
11	224.25	569.70
12	227.77	578.30
13	231.50	588.00

FIGURE 12 CONCLUDED

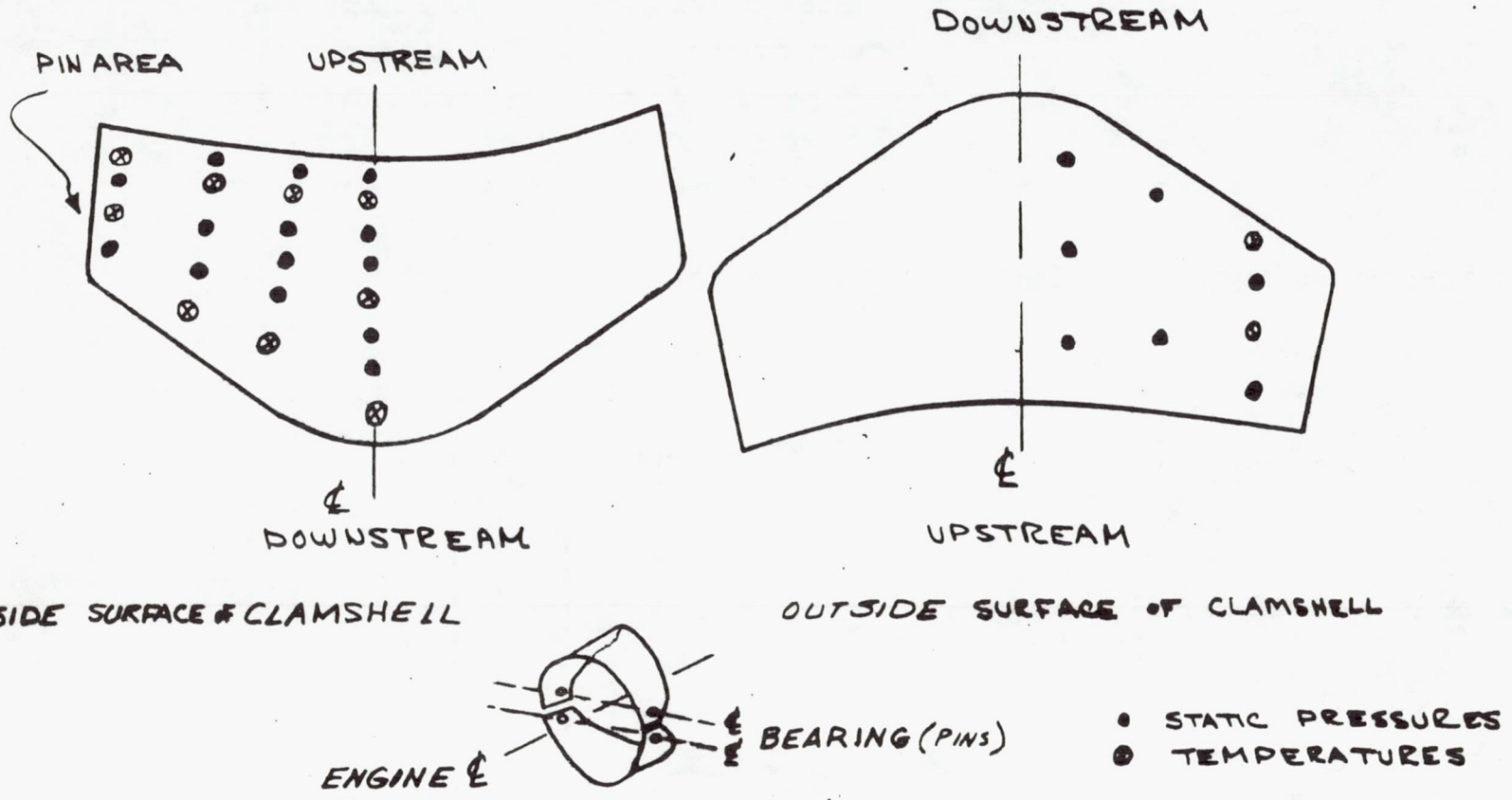

FIGURE: 18 CLAMSHELL INSTRUMENTATION

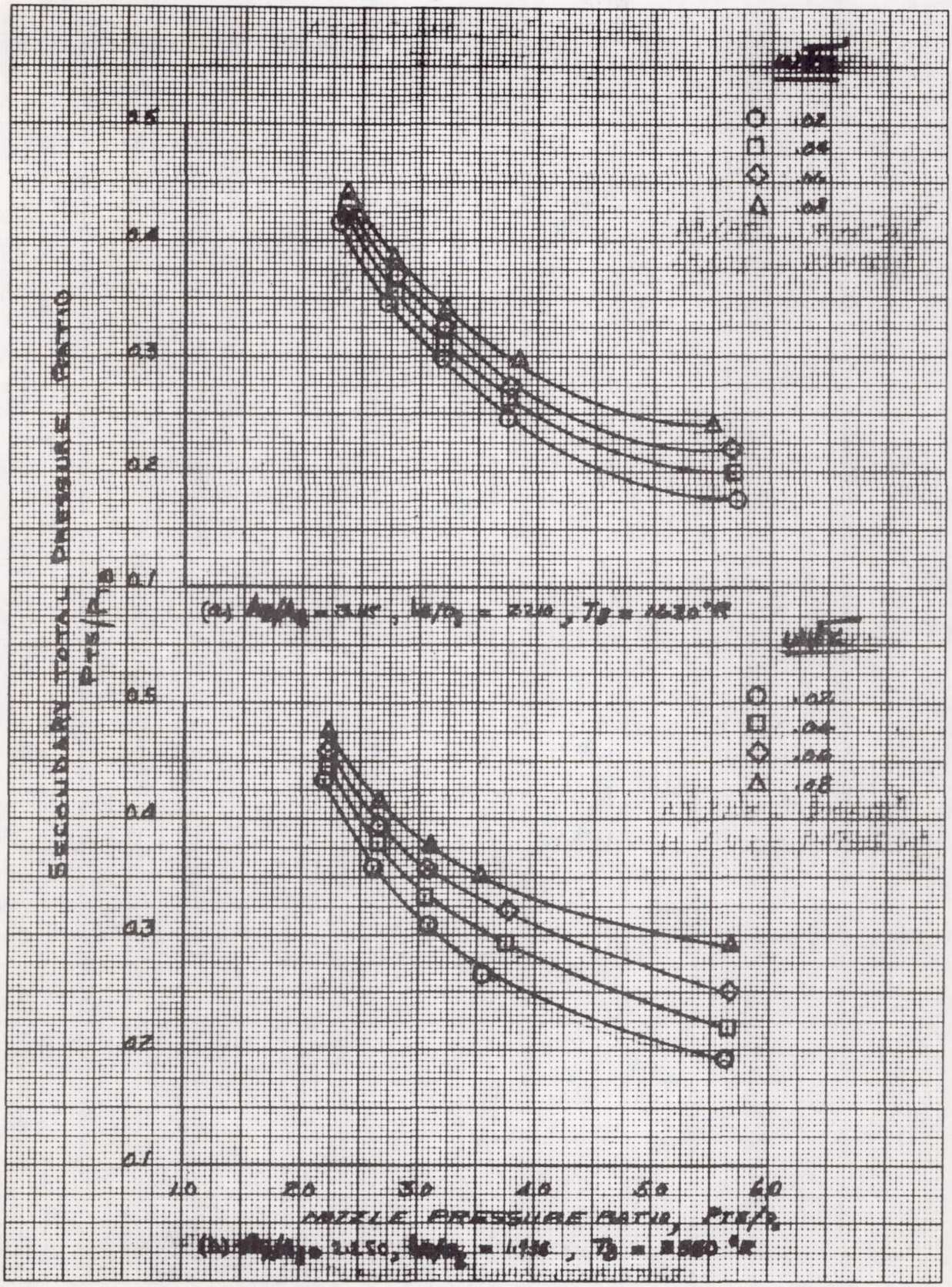

FIGURE 14 PUMPING CHARACTERISTICS
(TAKE-OFF, 16° DOORS)

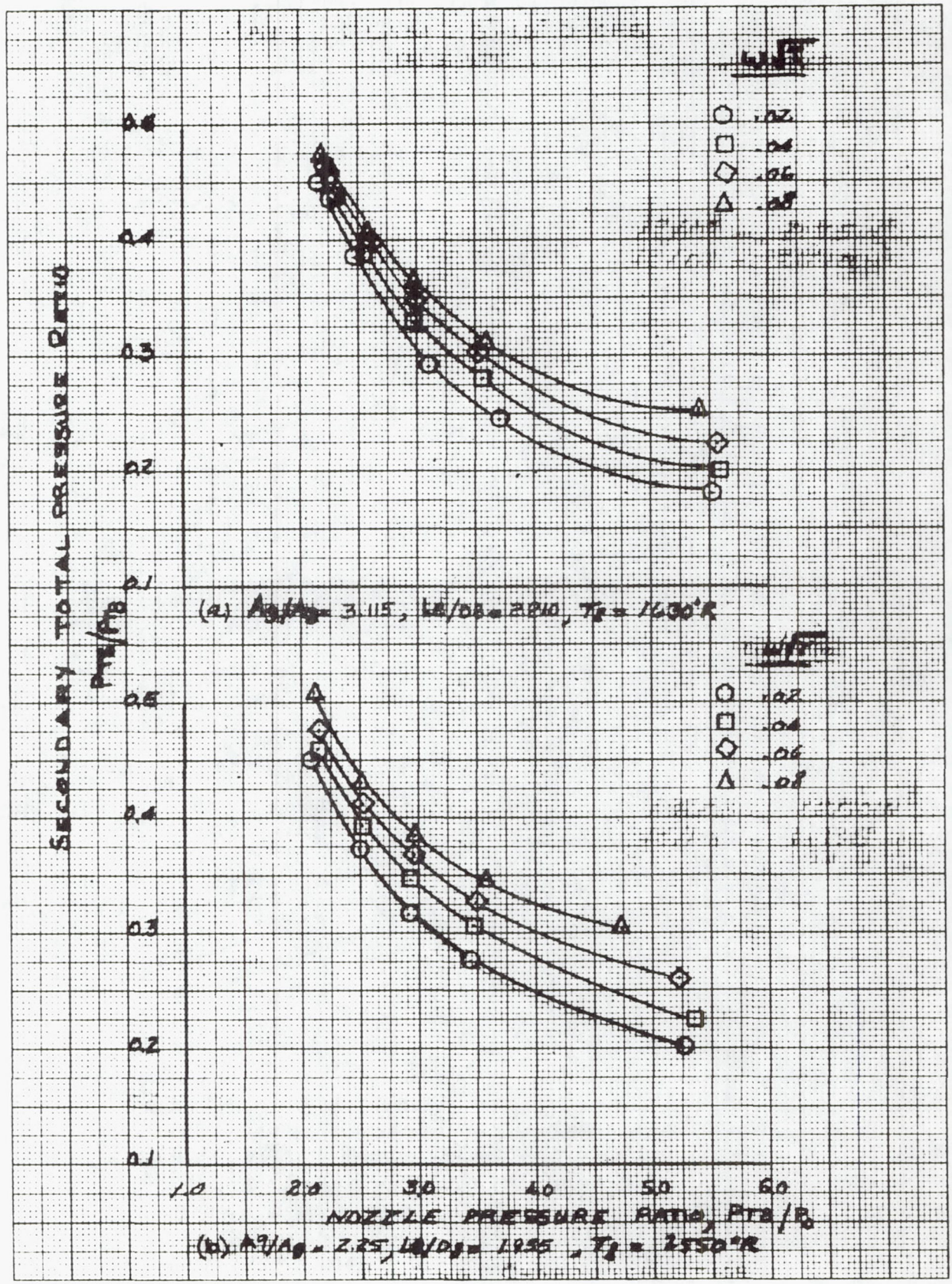

FIGURE 15 PUMPING CHARACTERISTICS
(TAKE-OFF 8°-16° DOORS)

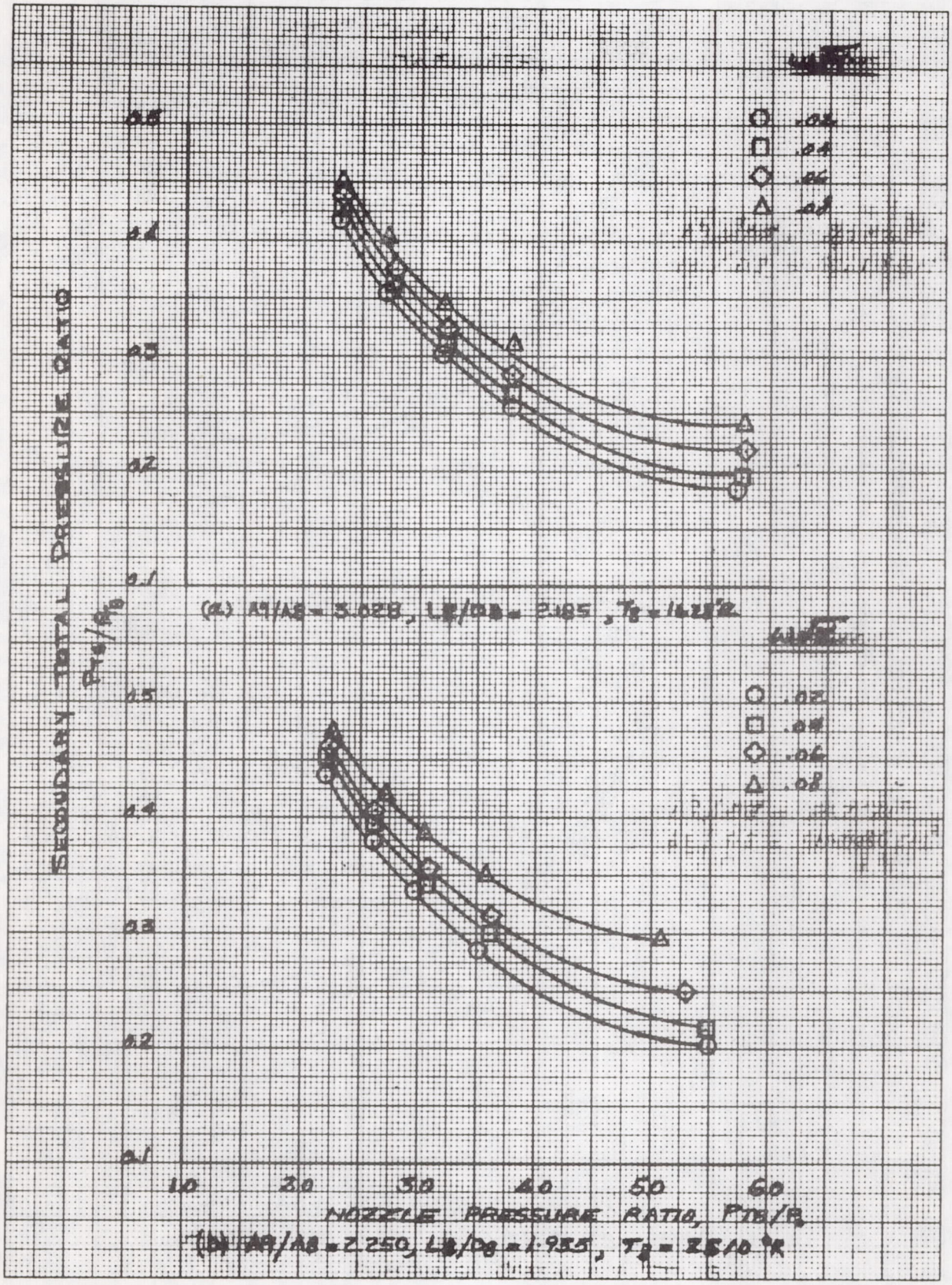

FIGURE 16 PUMPING CHARACTERISTICS
(TAKE-OFF, 20° DOORS)

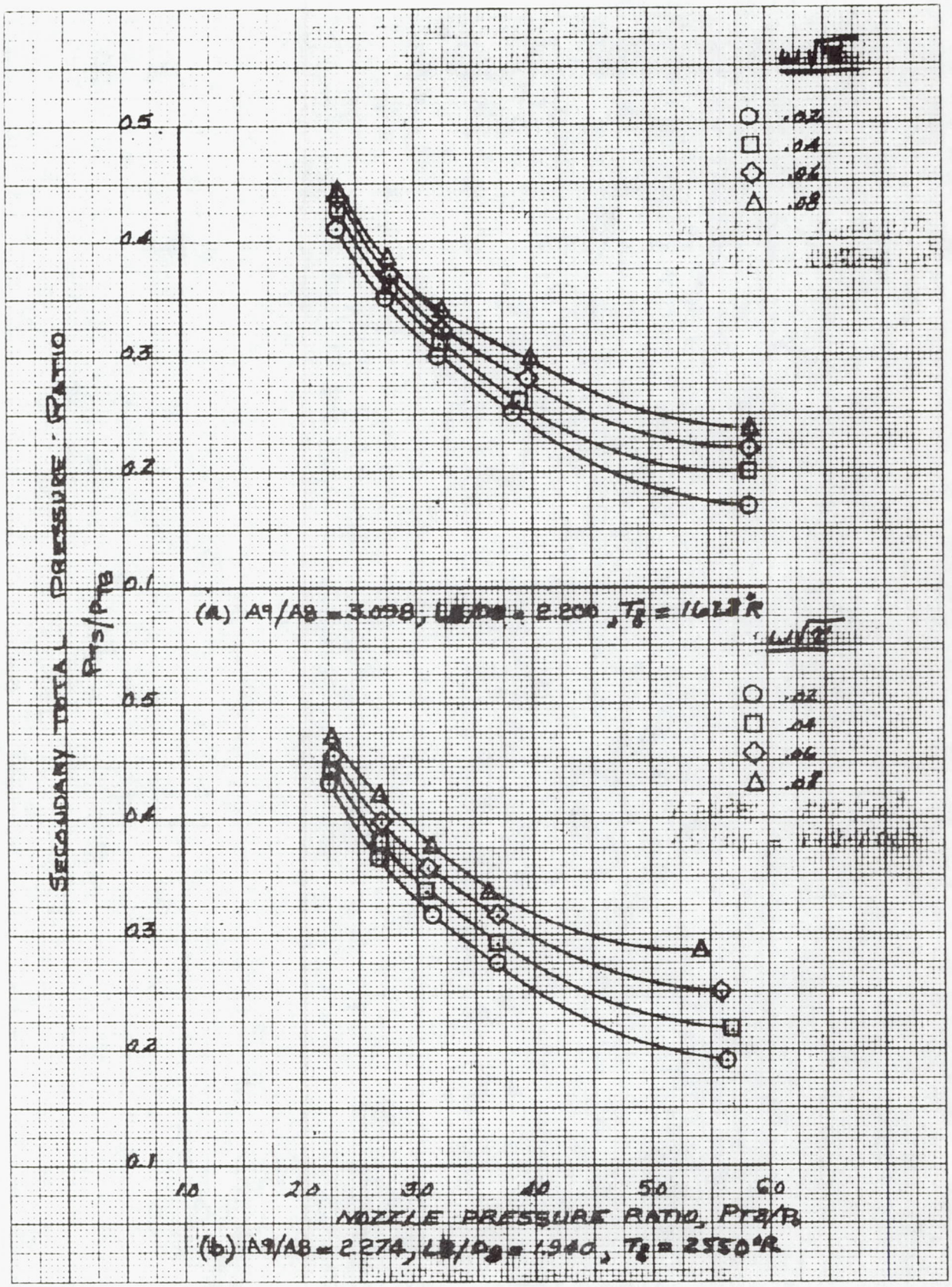

FIGURE 17 PUMPING CHARACTERISTICS
(TAKE-OFF, 10°-20° DOORS)

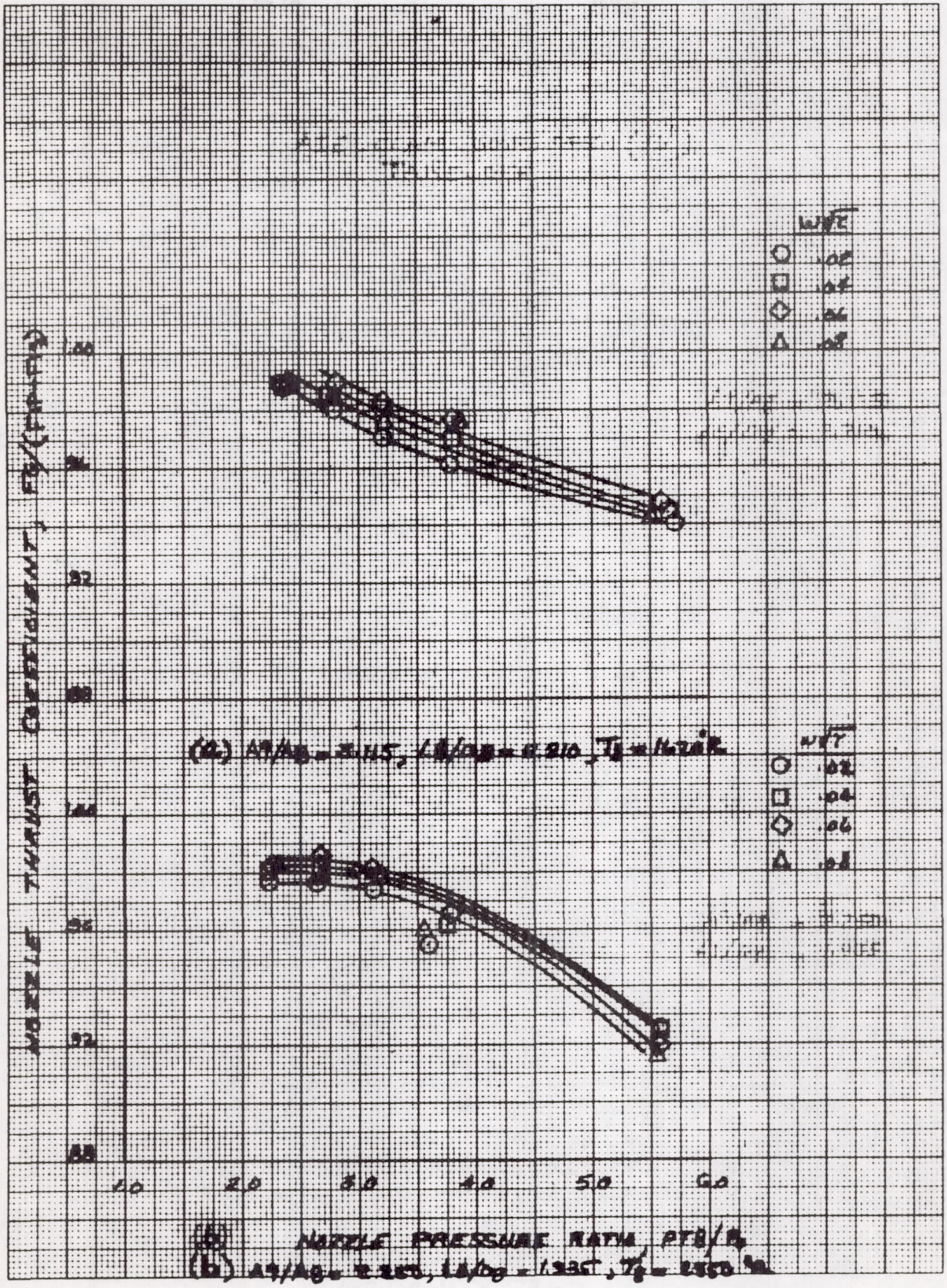

FIGURE 18 THRUST CHARACTERISTICS
(TAKE-OFF, 16° DOORS)

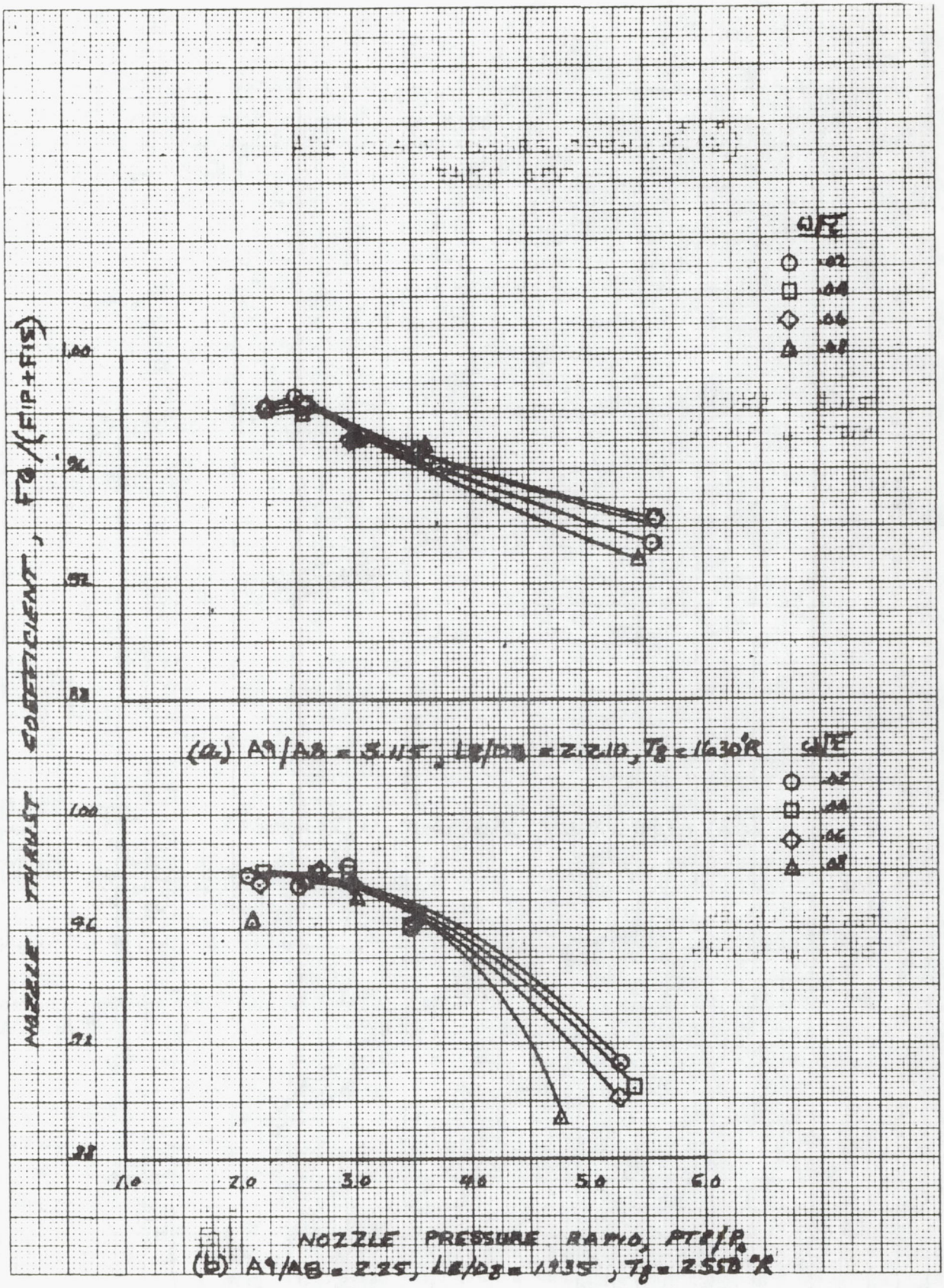

FIGURE 19 THRUST CHARACTERISTICS
(TAKE-OFF, 8°-16° DOORS)

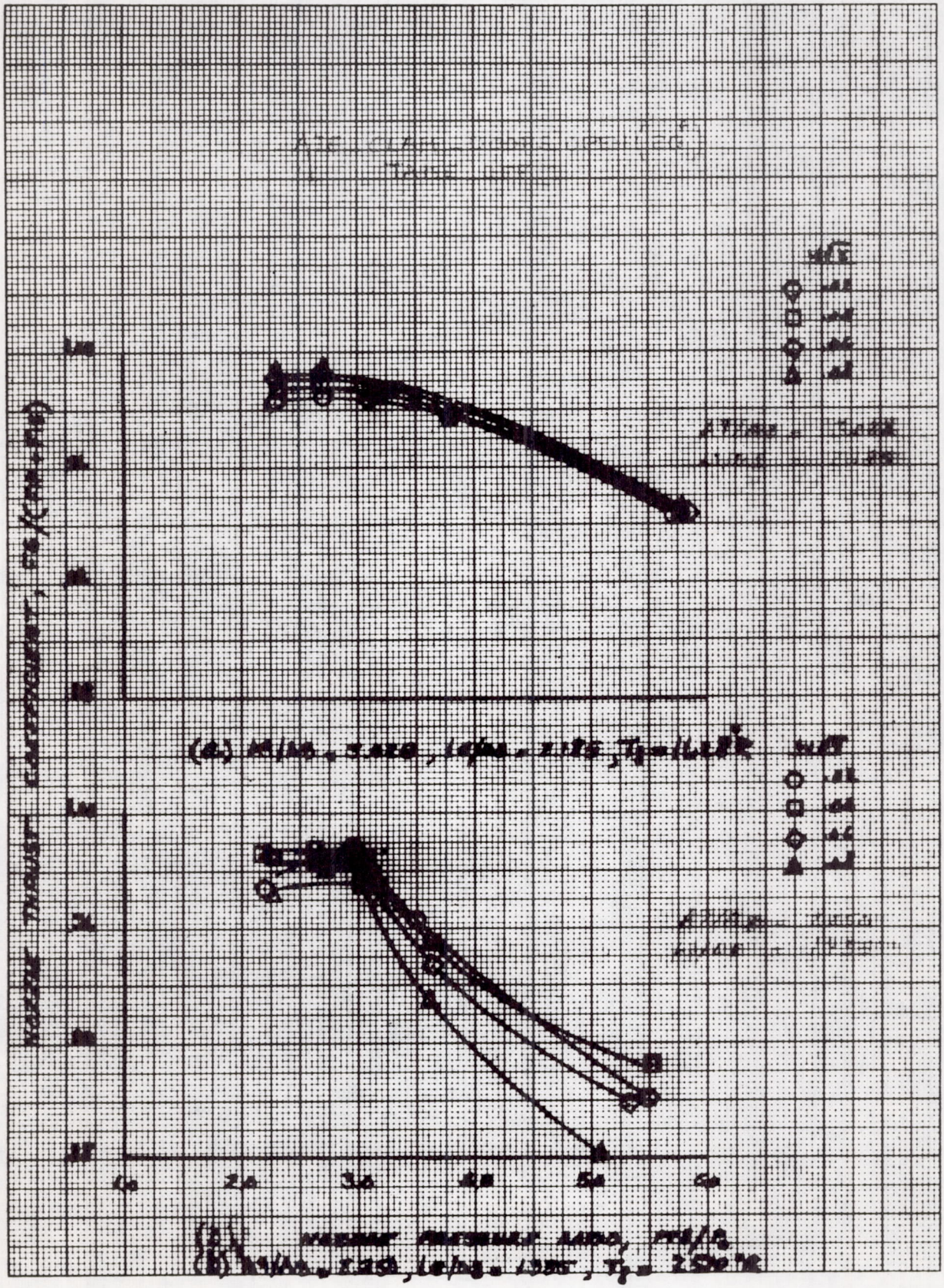

FIGURE 20 THRUST CHARACTERISTICS
(TAKE-OFF, 20° DOORS)

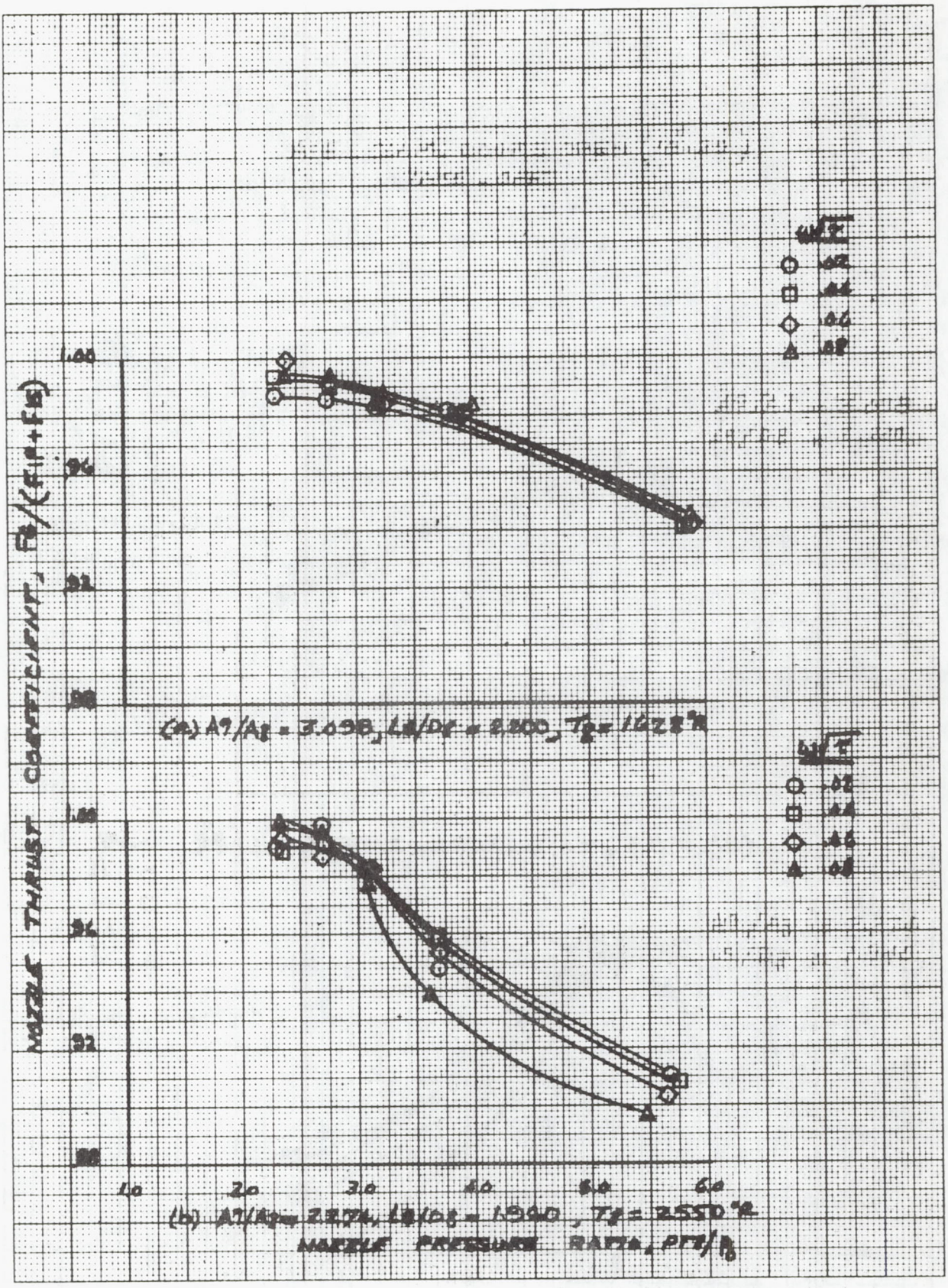

FIGURE 21 THRUST CHARACTERISTICS
(TAKE-OFF, 10°-20° DOORS)

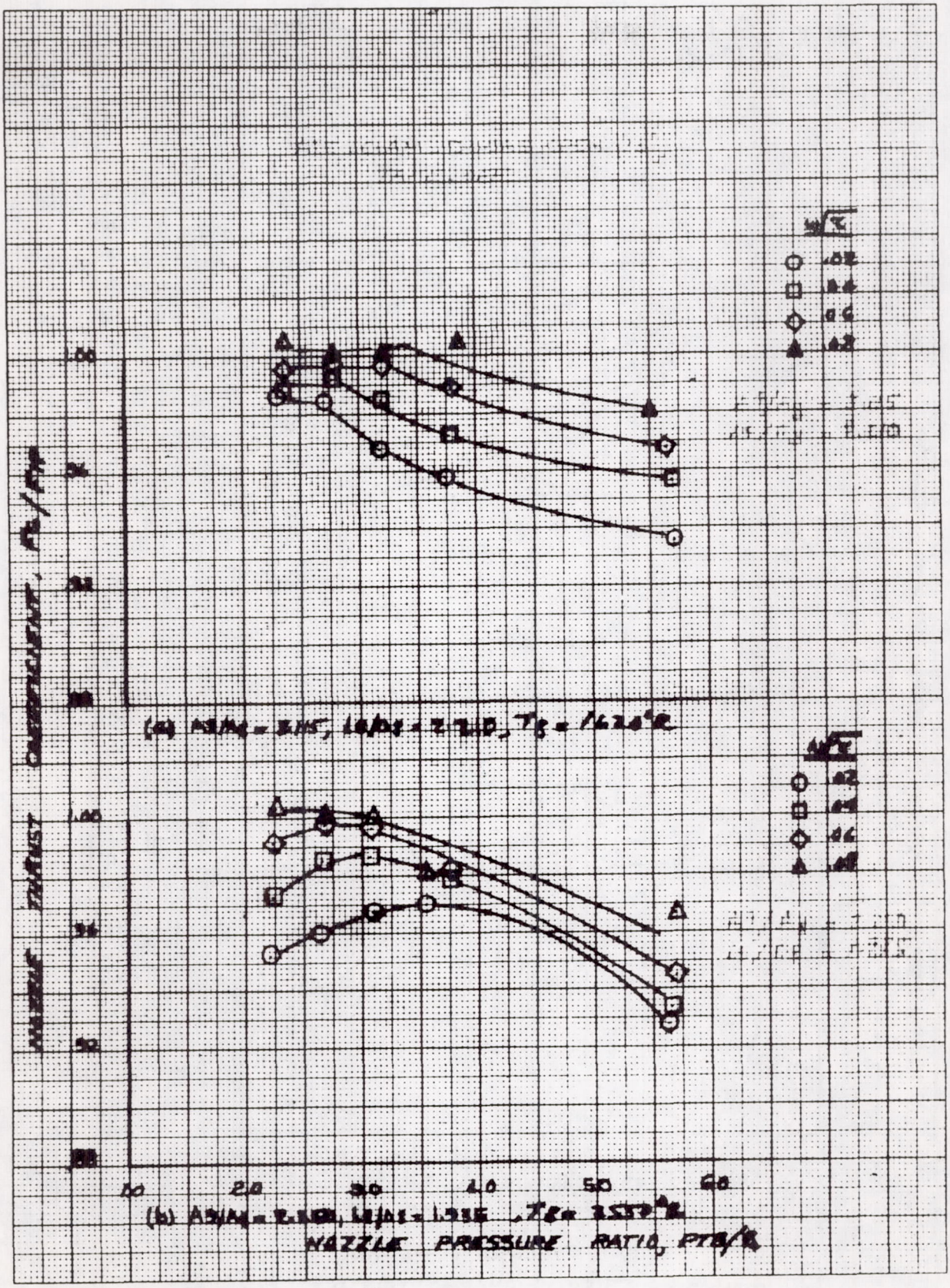

FIGURE 22 THRUST CHARACTERISTICS
(TAKE-OFF, 16° DOORS)

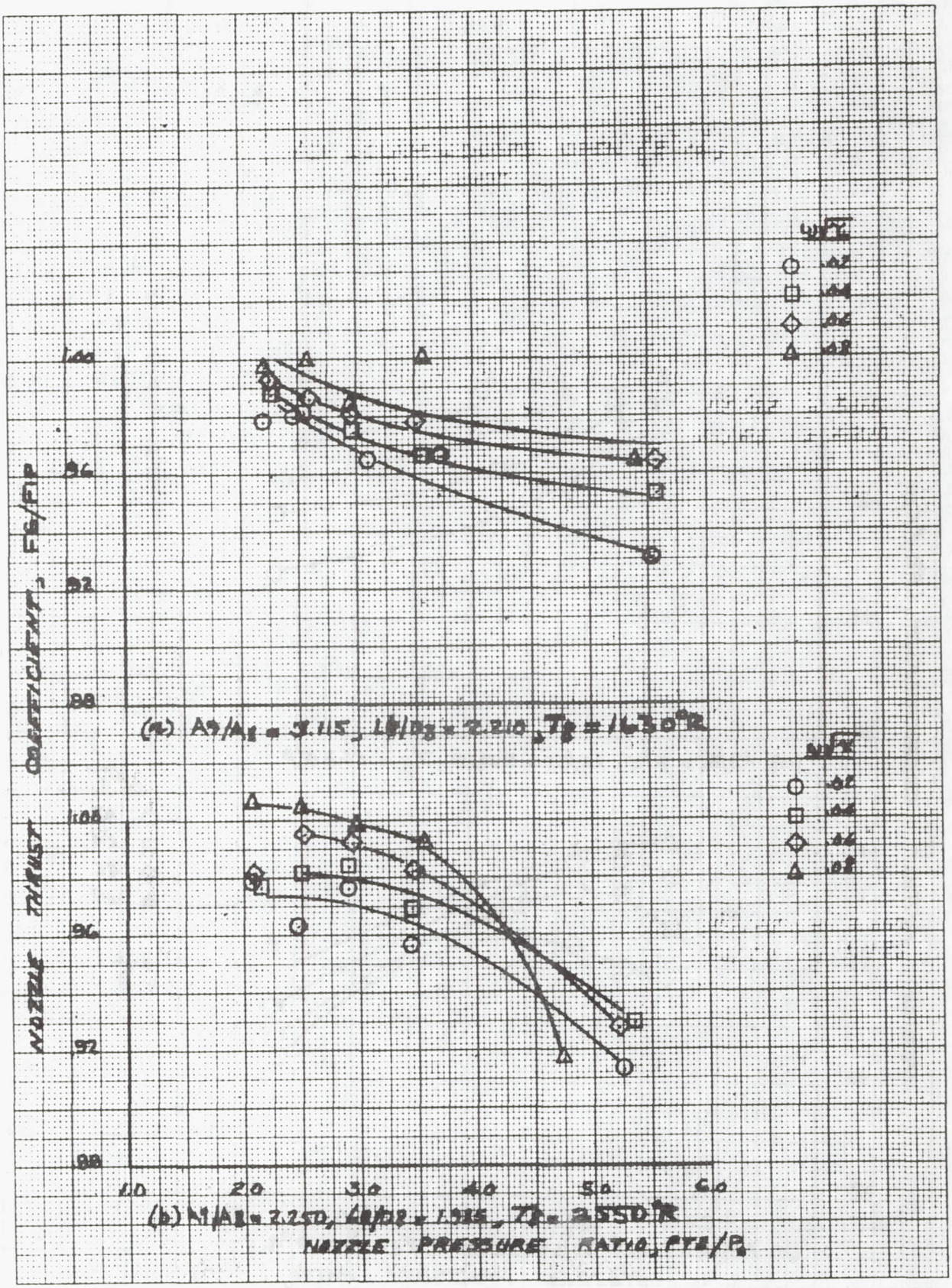

FIGURE 23 THRUST CHARACTERISTICS
(TAKE-OFF, 8°-16° DOORS)

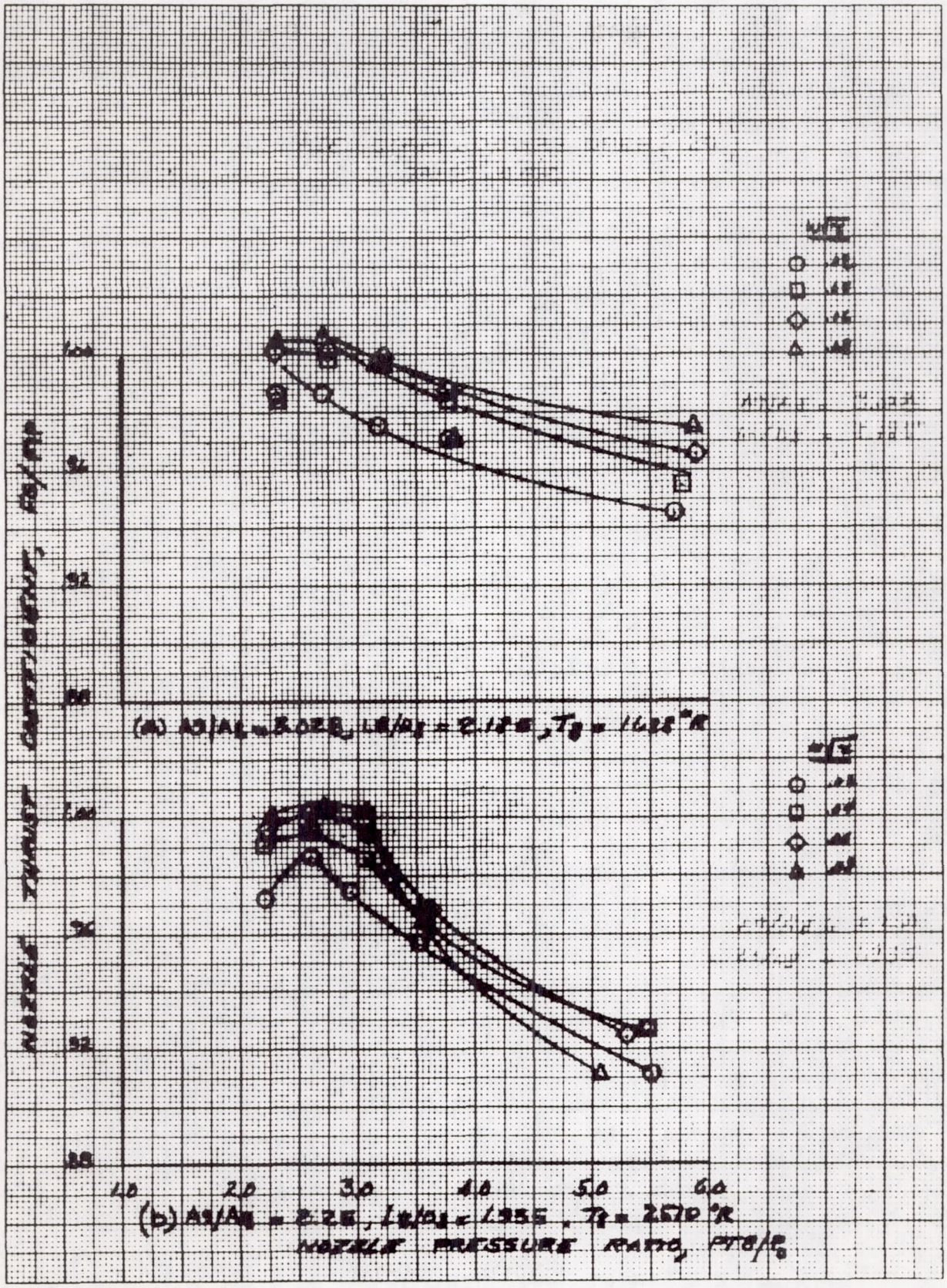

FIGURE 24 THRUST CHARACTERISTICS
(TAKE-OFF, 20° DOORS)

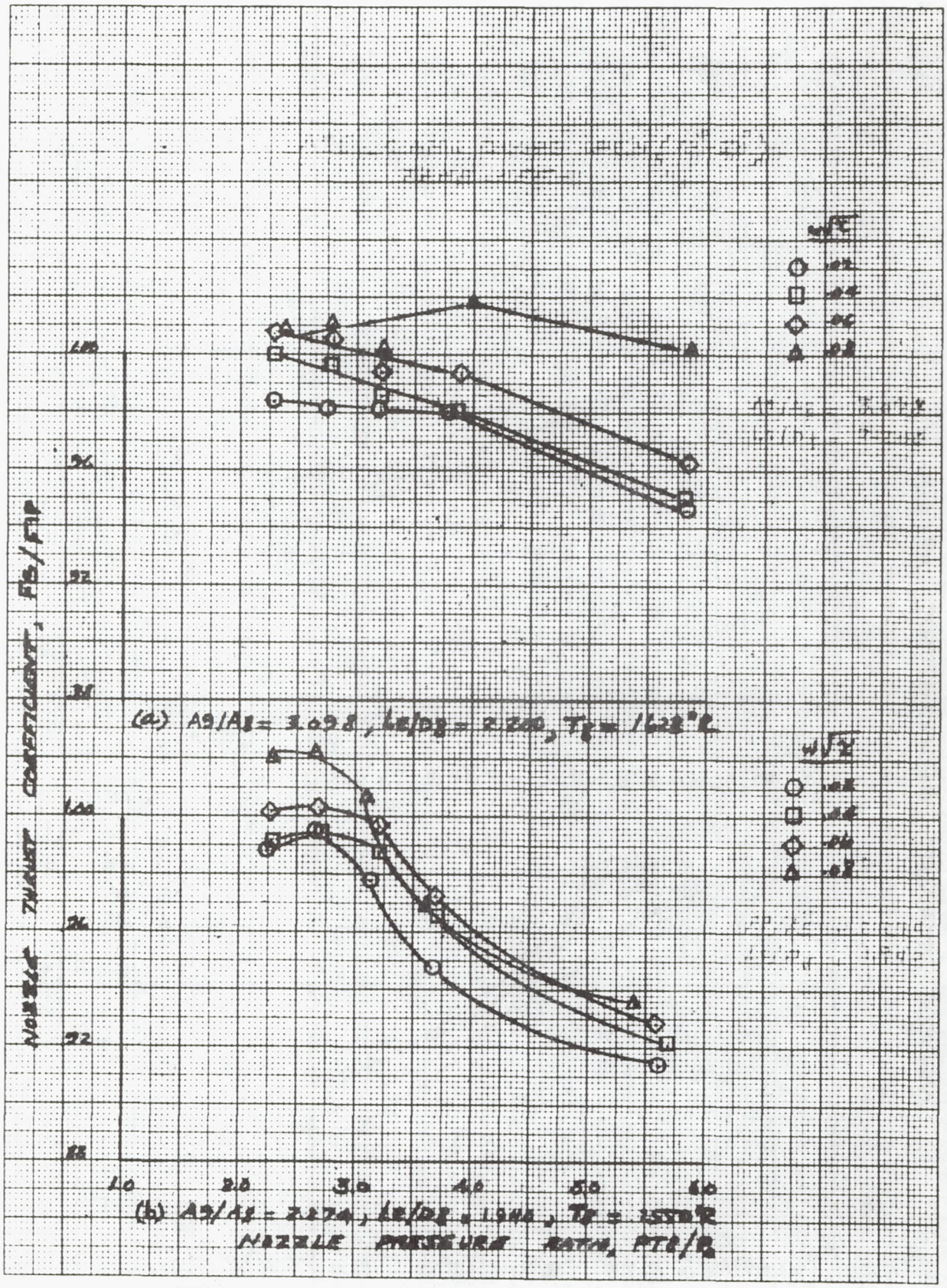

FIGURE 25 THRUST CHARACTERISTICS
(TAKE-OFF, 10°-20° DOORS)

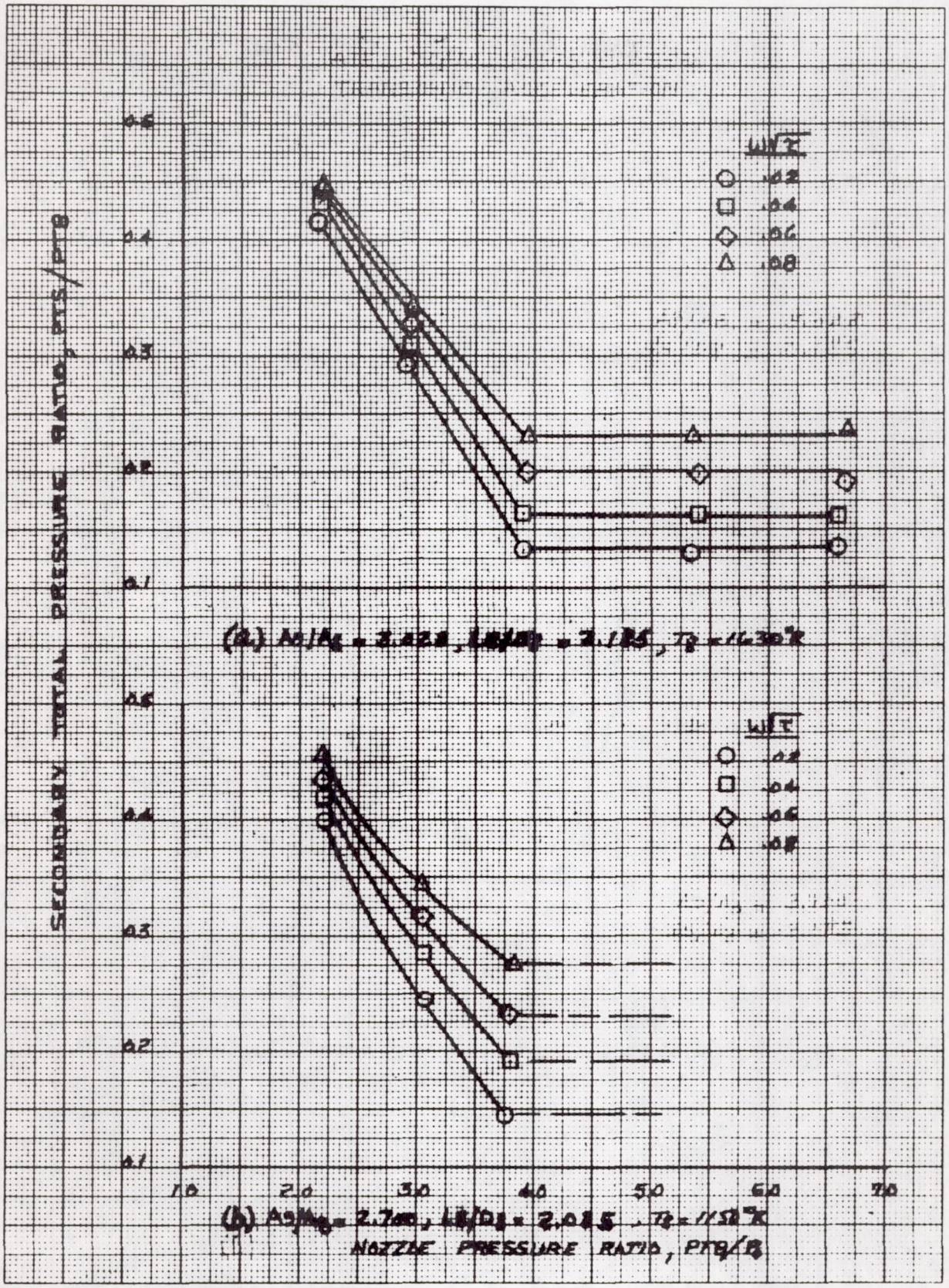

FIGURE 26 PUMPING CHARACTERISTICS (TRANSONIC, DOORS CLOSED)

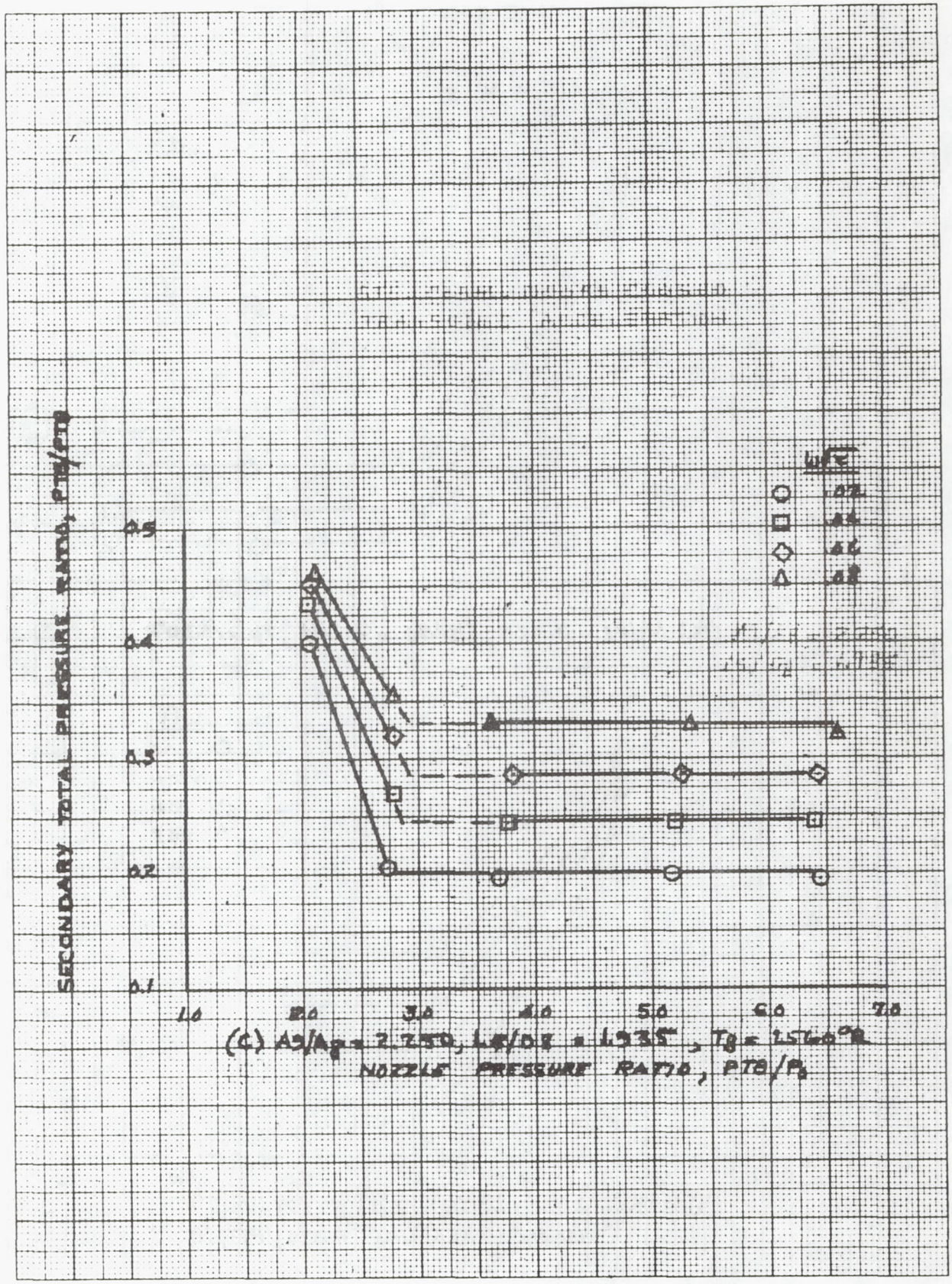

FIGURE 26 CONCLUDED

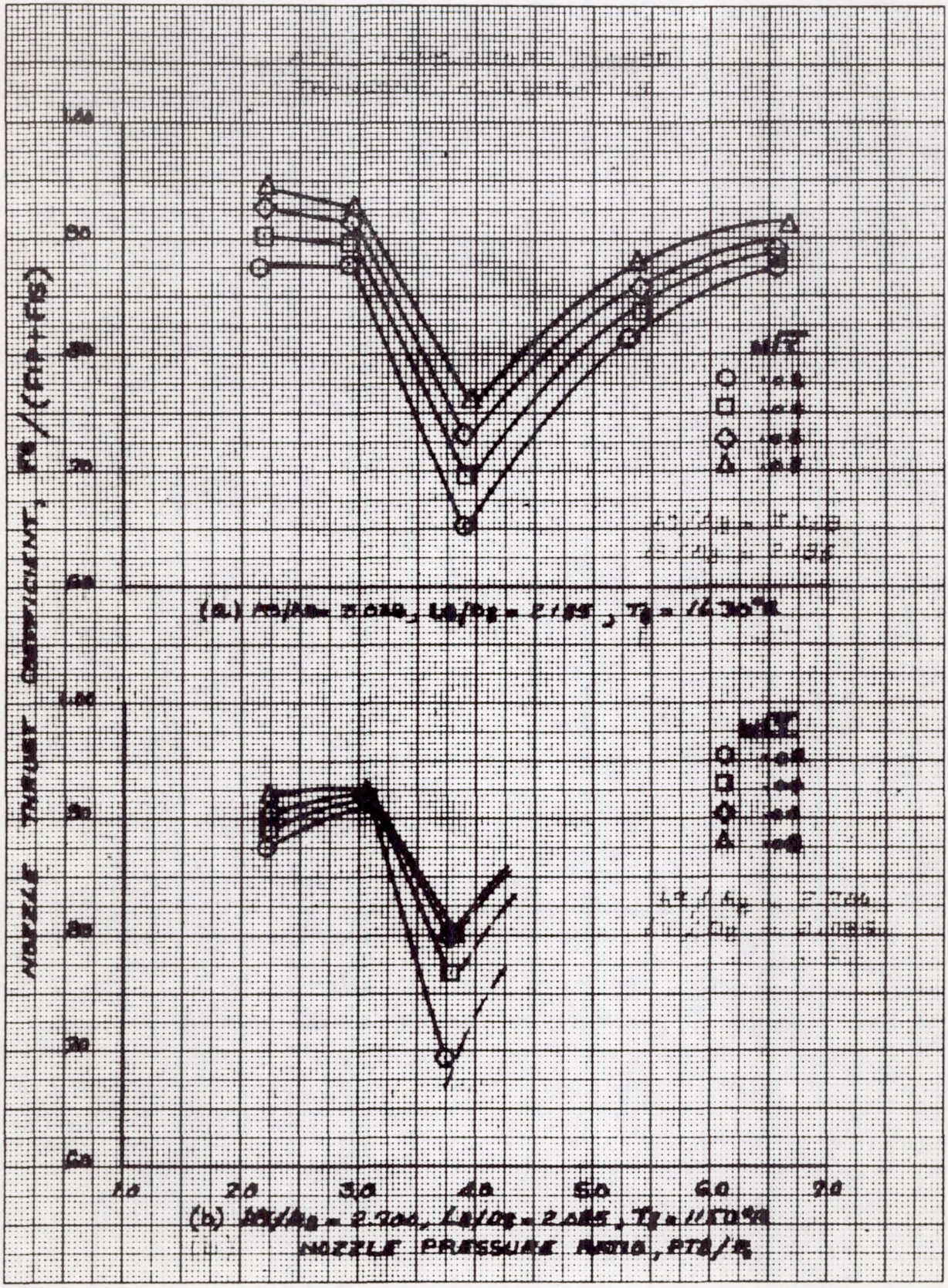

FIGURE 27 THRUST CHARACTERISTICS (TRANSONIC, DOORS CLOSED)

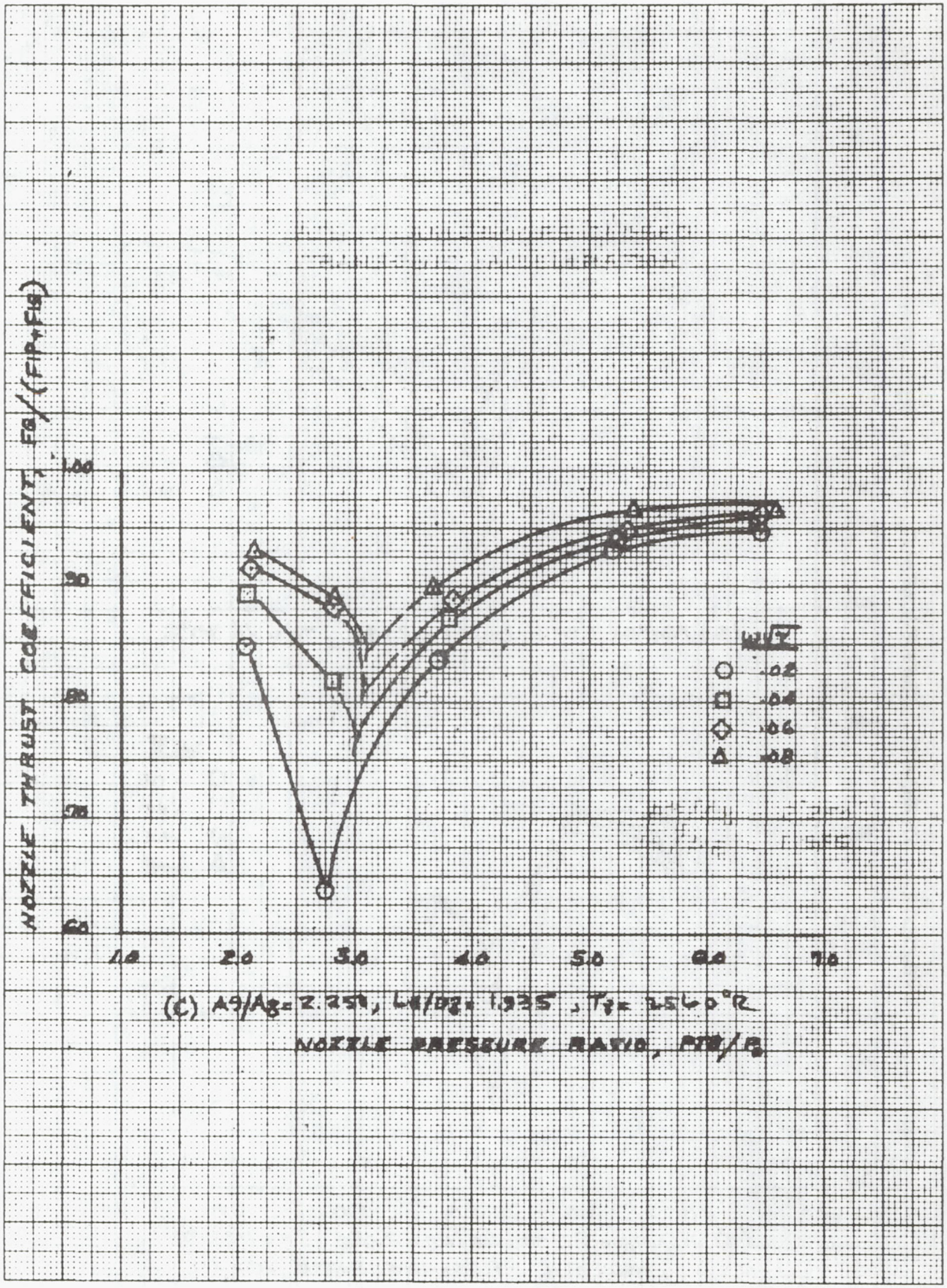

FIGURE 27 CONCLUDED

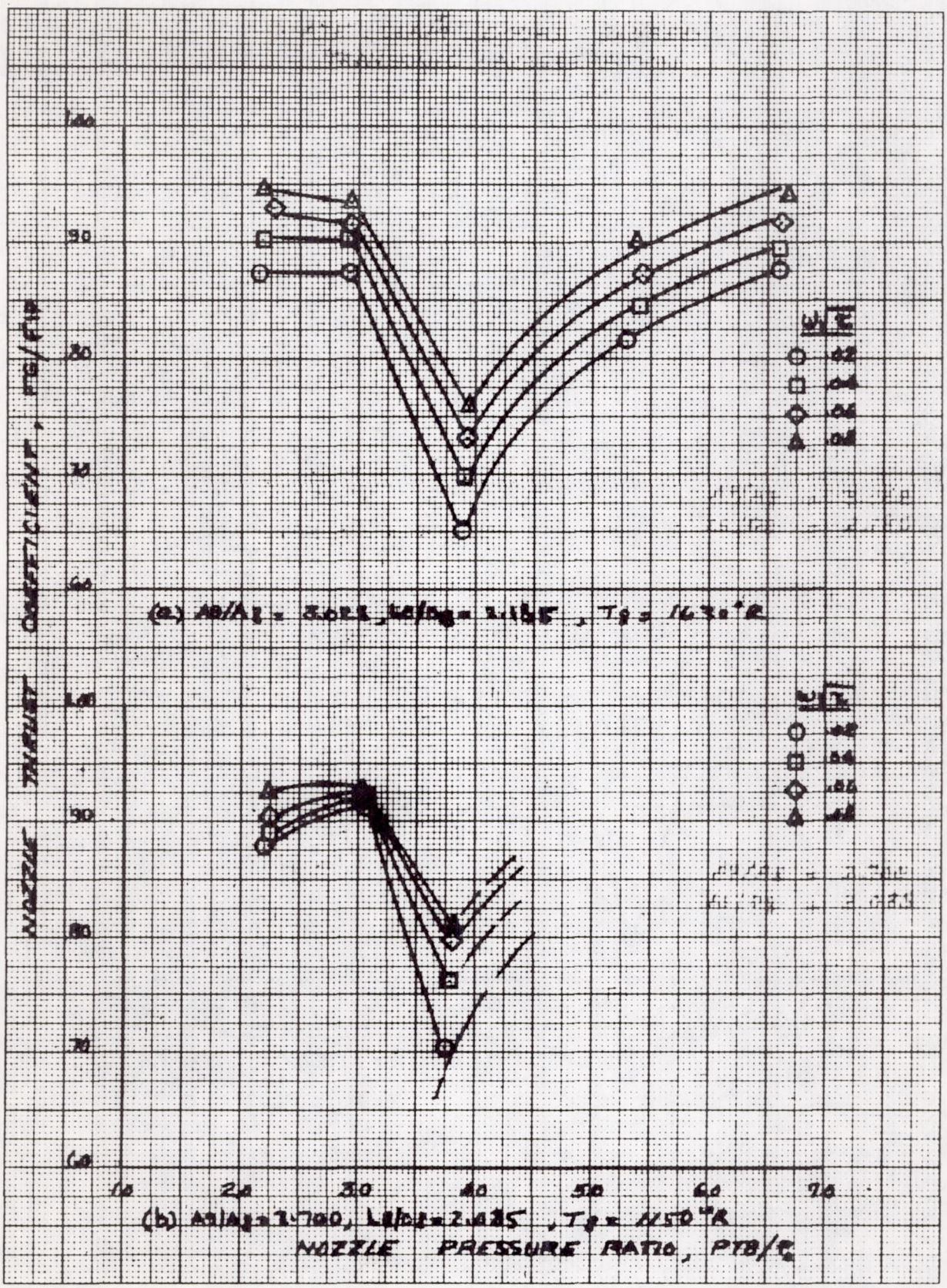

FIGURE 28 THRUST CHARACTERISTICS (TRANSONIC, DOORS LOCKED)

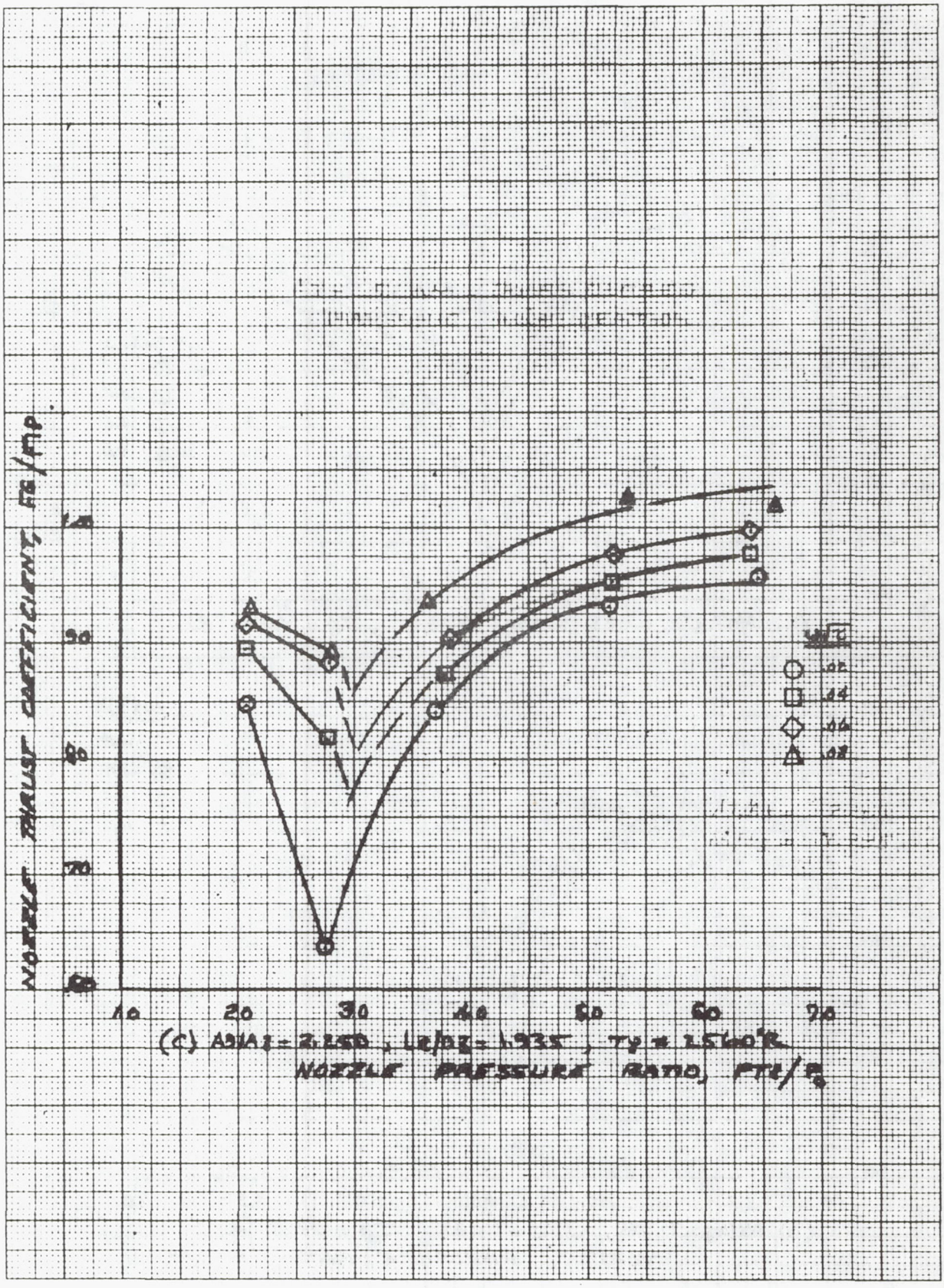

FIGURE 28 CONCLUDED

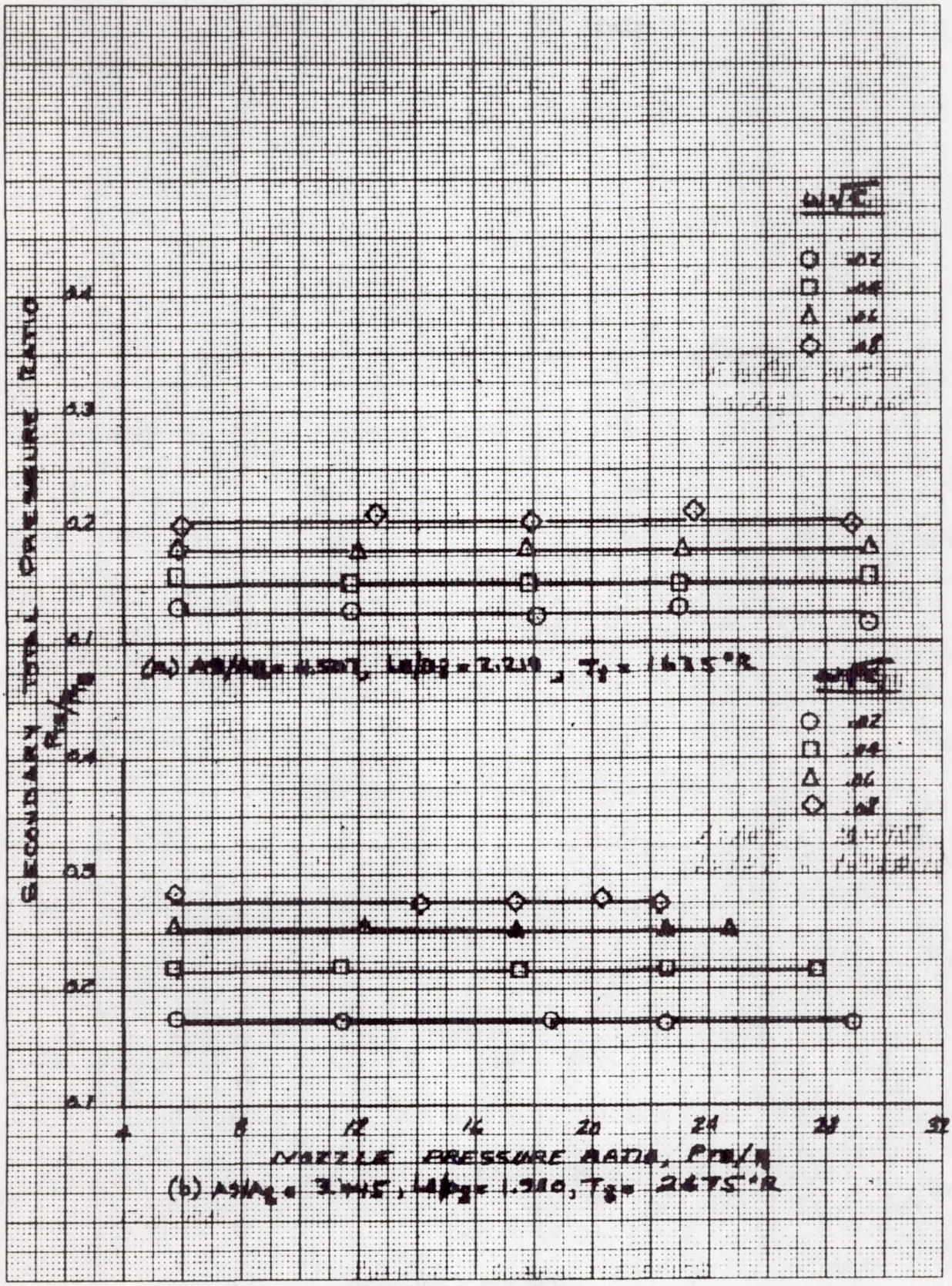

FIGURE 29 PUMPING CHARACTERISTICS
(SUPERSONIC CRUISE, DOORS CLOSED)

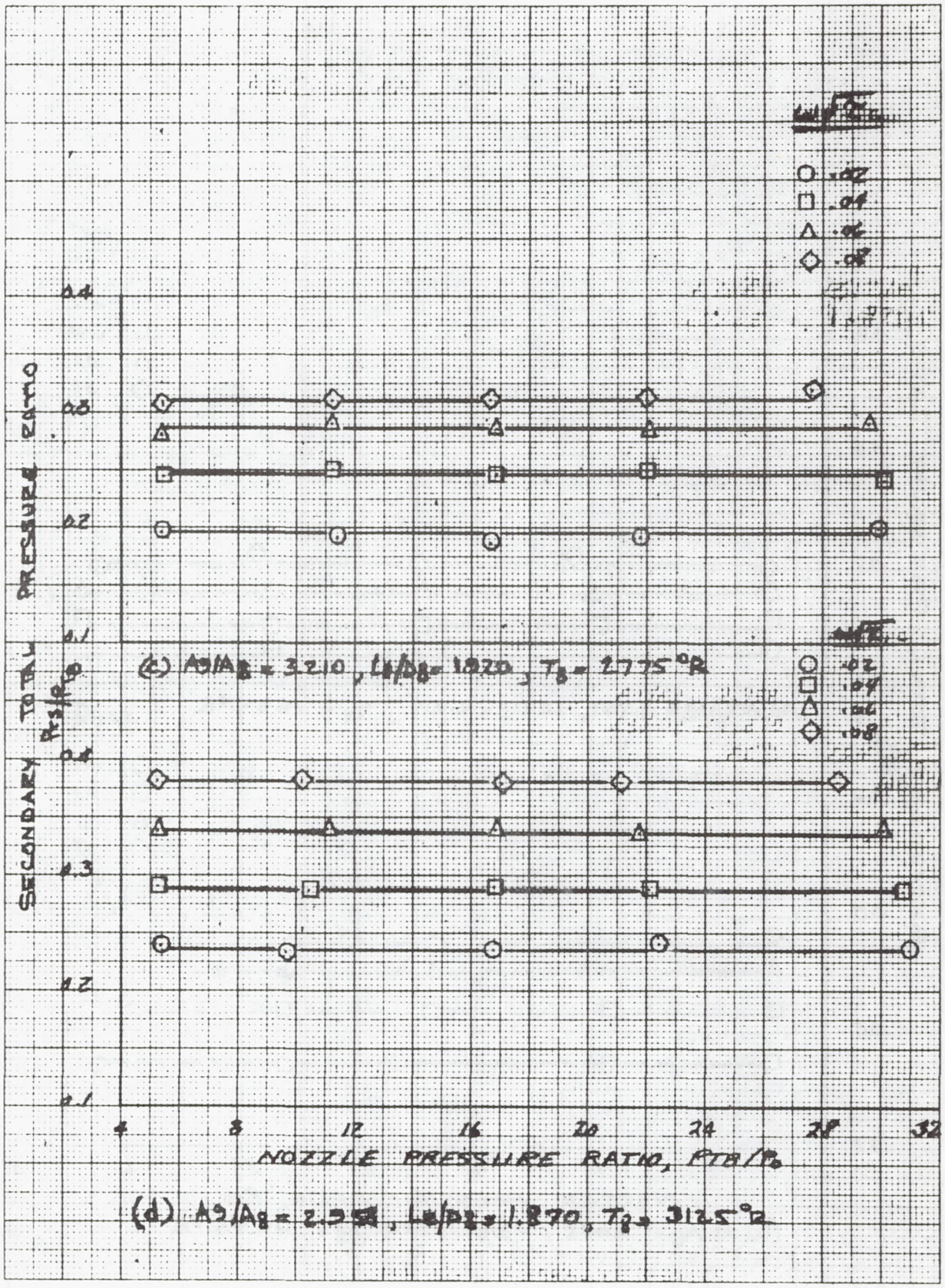

FIGURE 29 CONCLUDED

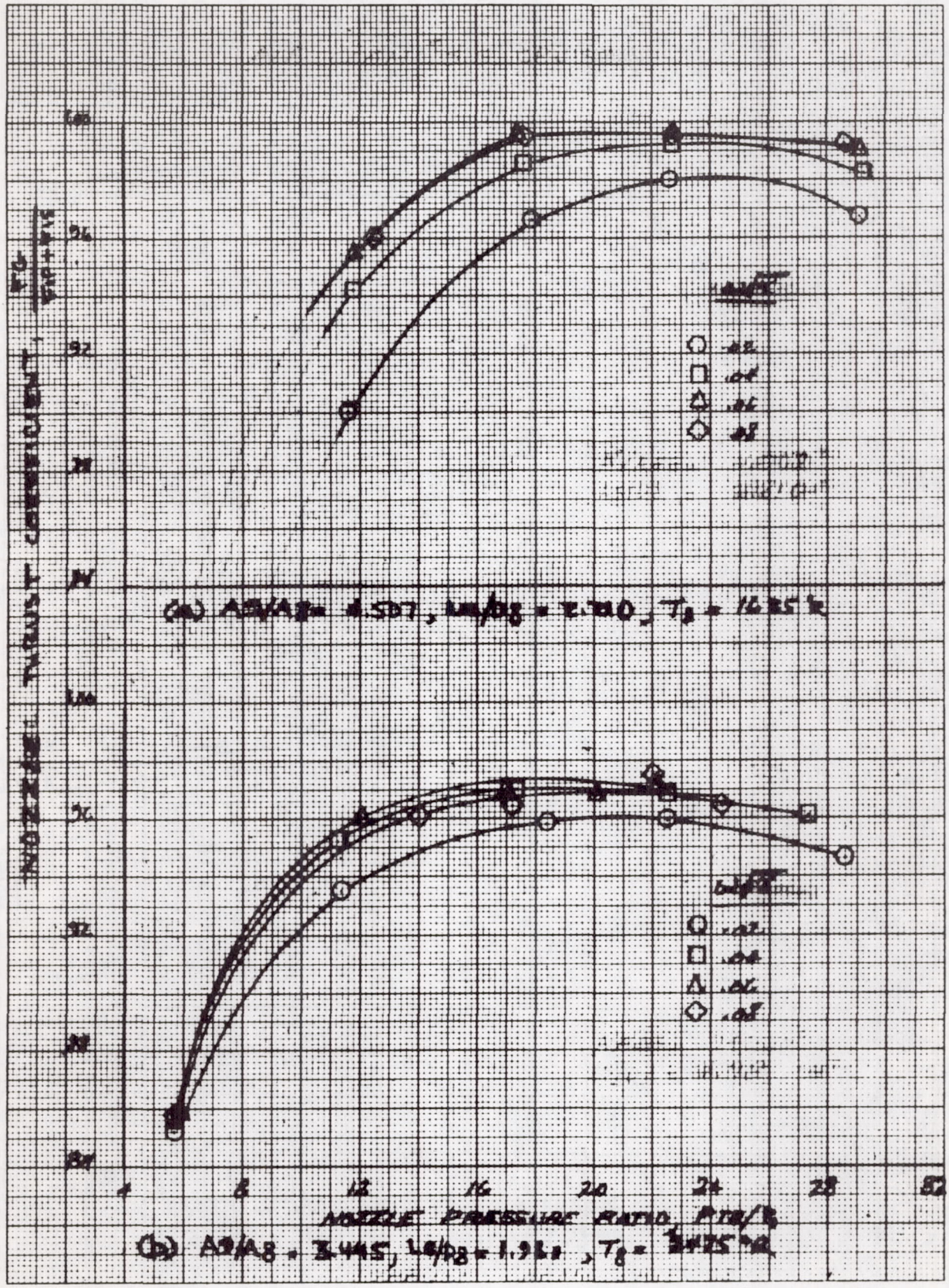

FIGURE 30 THRUST CHARACTERISTICS
(SUPERSONIC CRUISE, DOORS CLOSED)

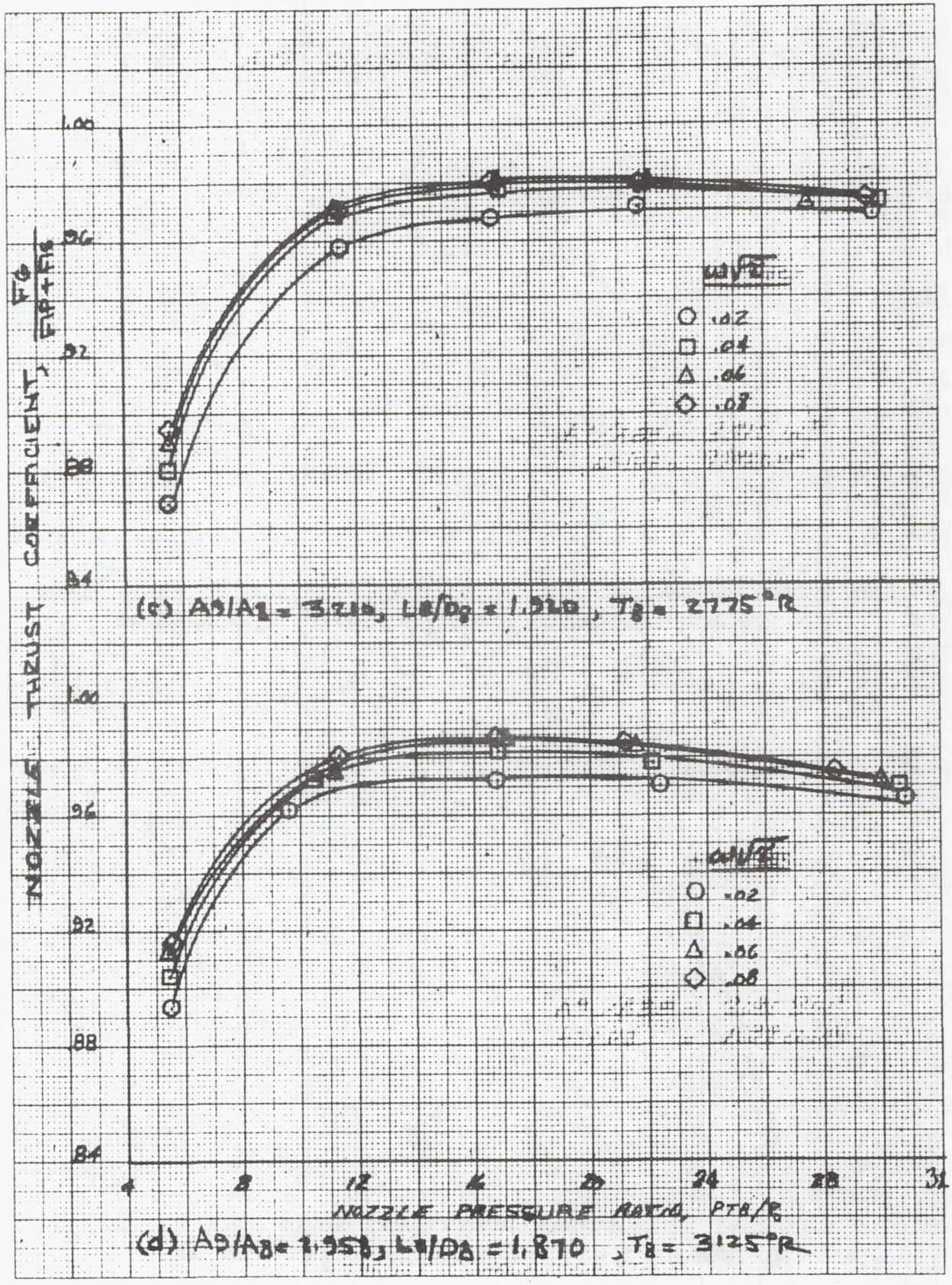

FIGURE 30 CONCLUDED

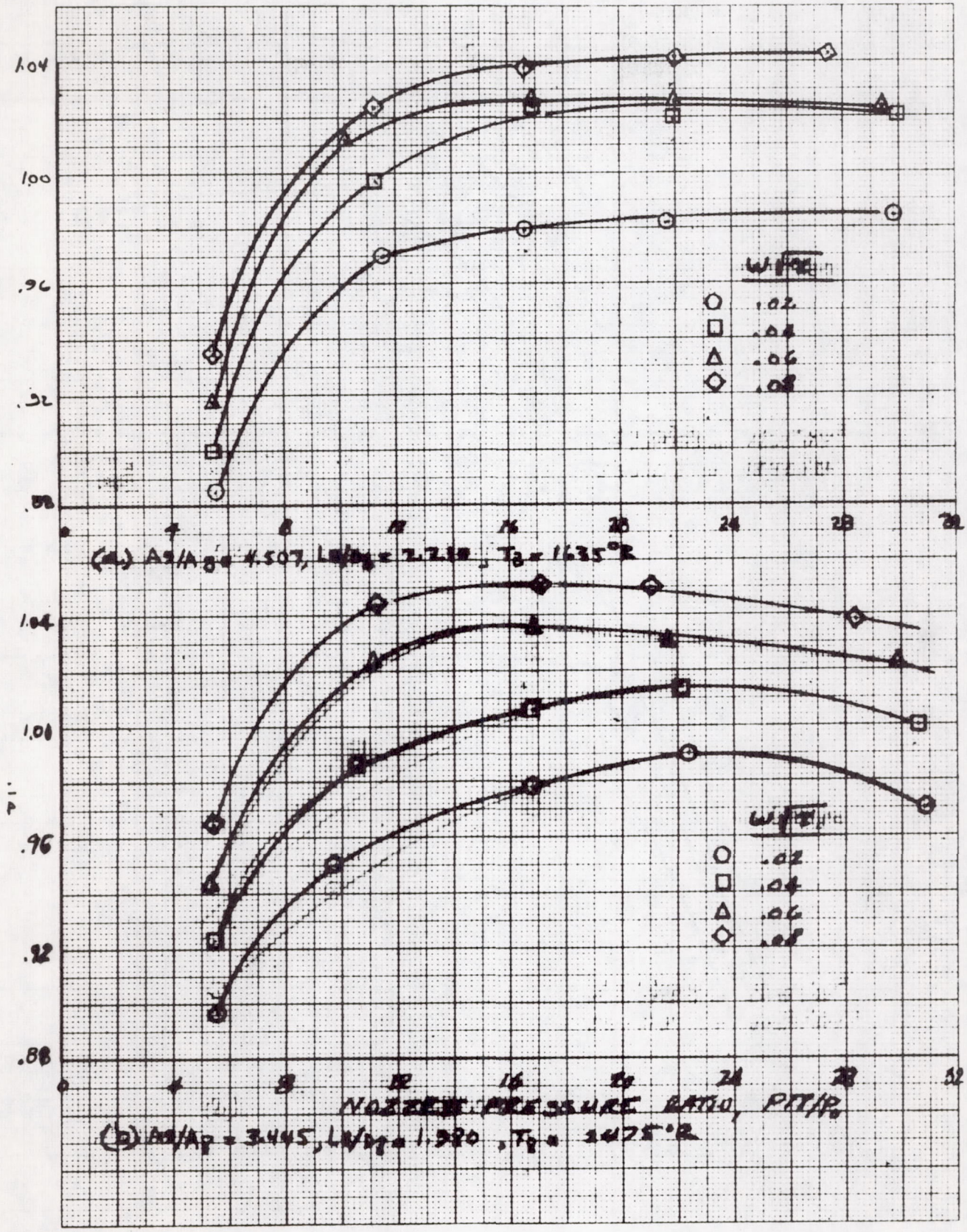

FIGURE 31 THRUST CHARACTERISTICS
(SUPERSONIC CRUISE, DOORS CLOSED)

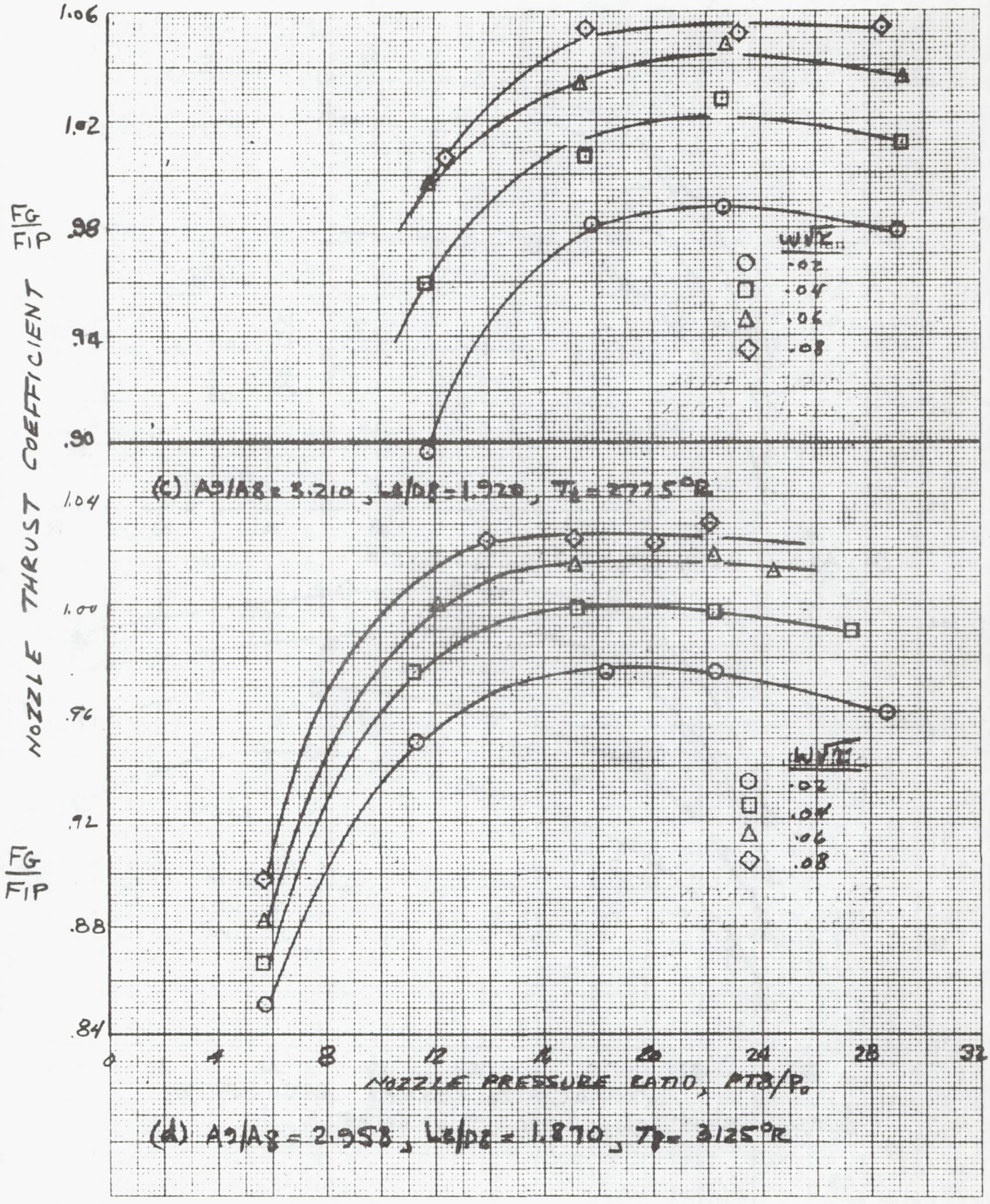

FIGURE 31 CONCLUDED

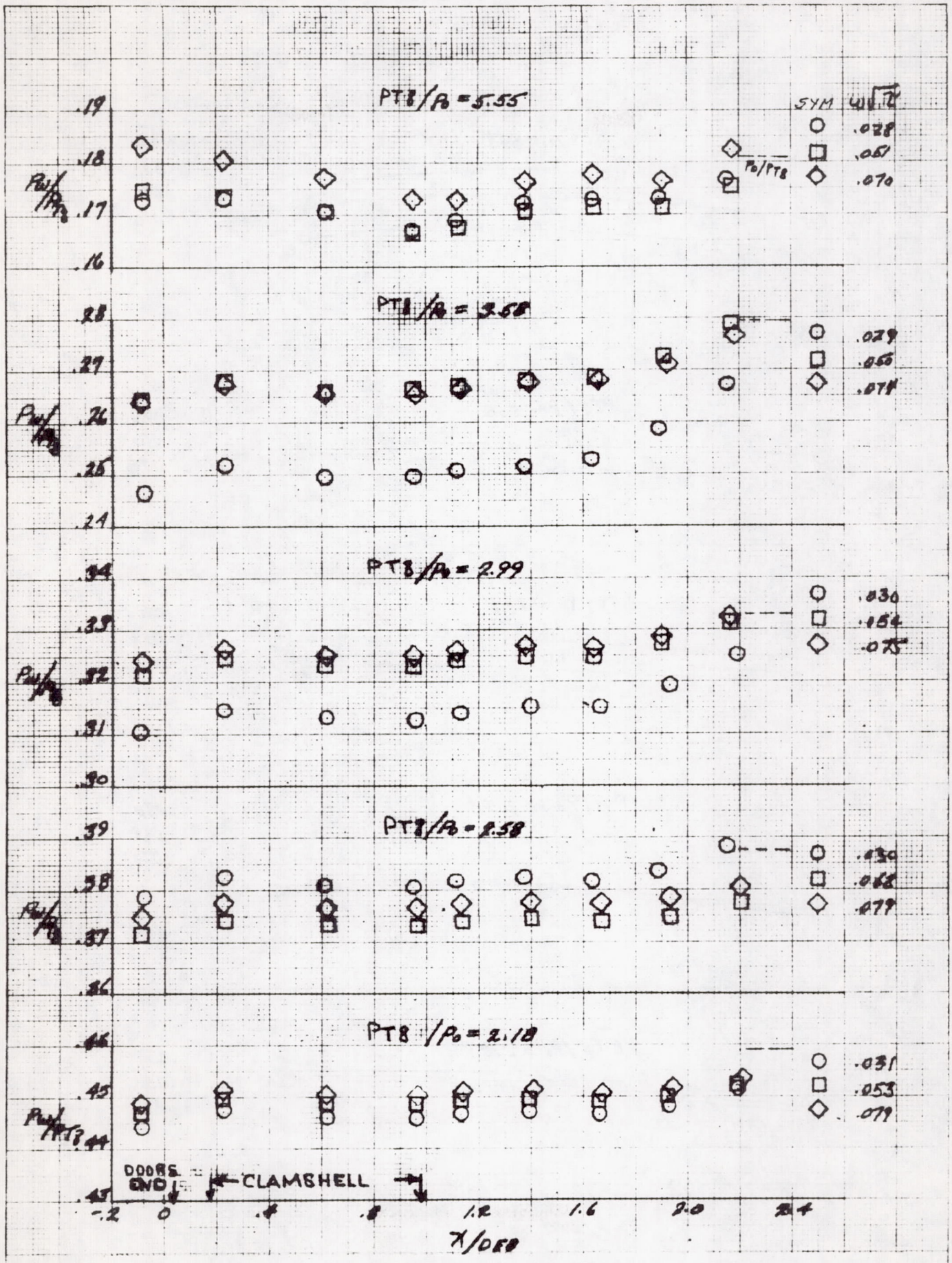

(a) PRESSURE PROFILES

FIGURE 32 EJECTOR WALL PROFILES (TAKE-OFF EJECTOR)
8°-16° DOOR, $A_9/A_8 = 3.115$, $L_e/D = 2.210$, $T_8 = 1630°R$

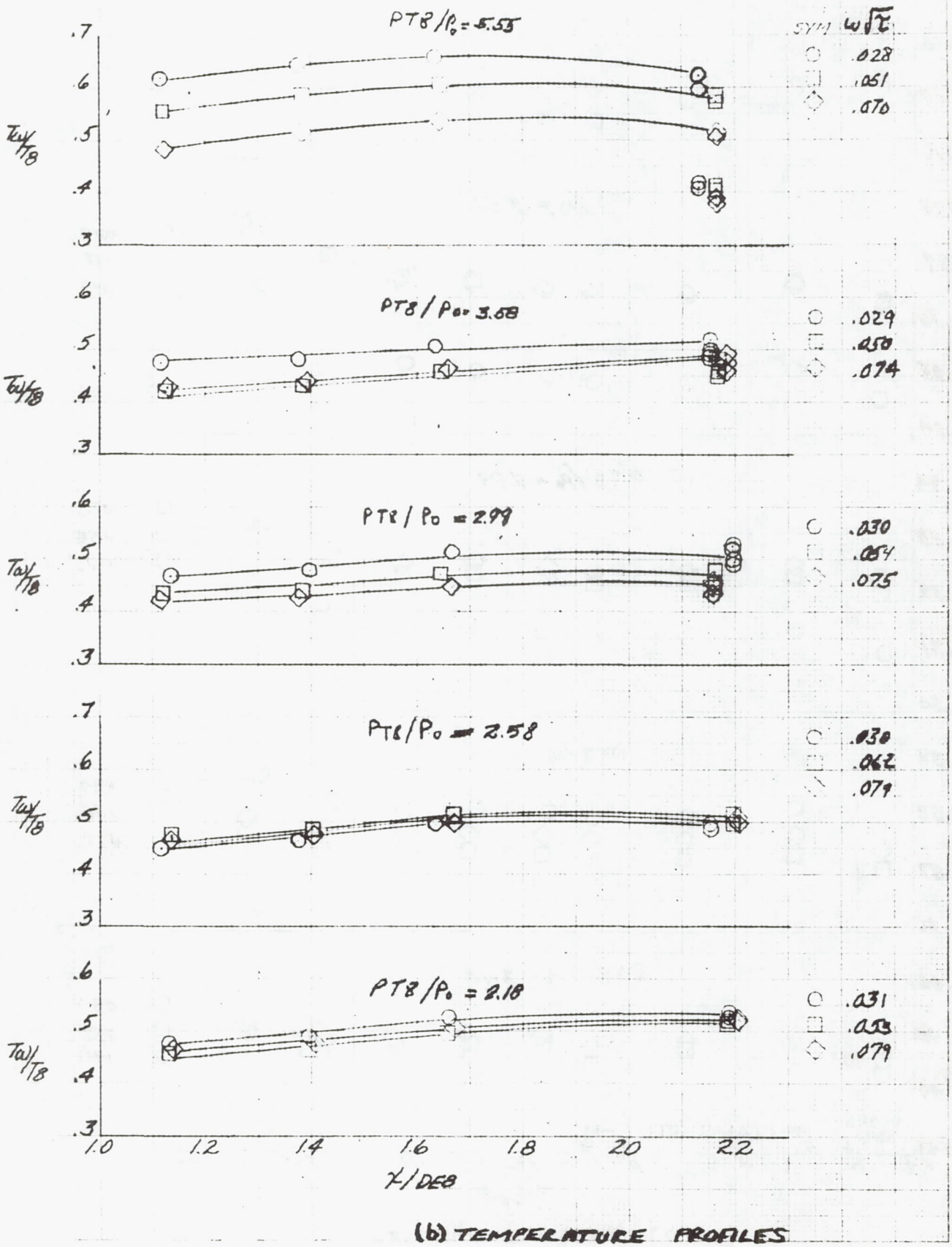

(b) TEMPERATURE PROFILES

FIGURE 32 CONCLUDED

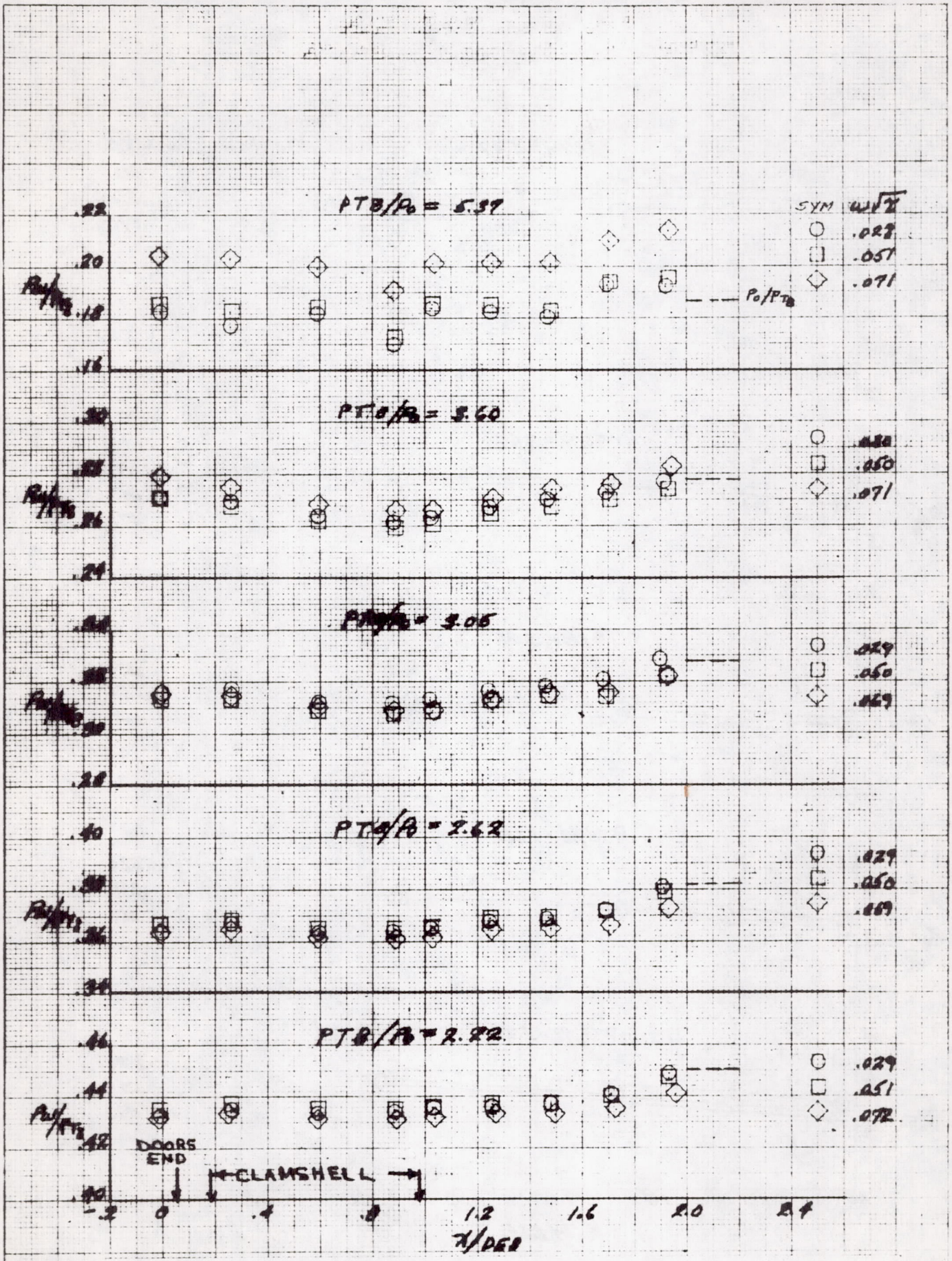

(a) PRESSURE PROFILES

FIGURE 33 EJECTOR WALL PROFILES (TAKE-OFF EJECTOR)
20° DOOR, $A_9/A_8 = 2.250$, $L_e/D_8 = 1.935$, $T_8 = 2510°R$

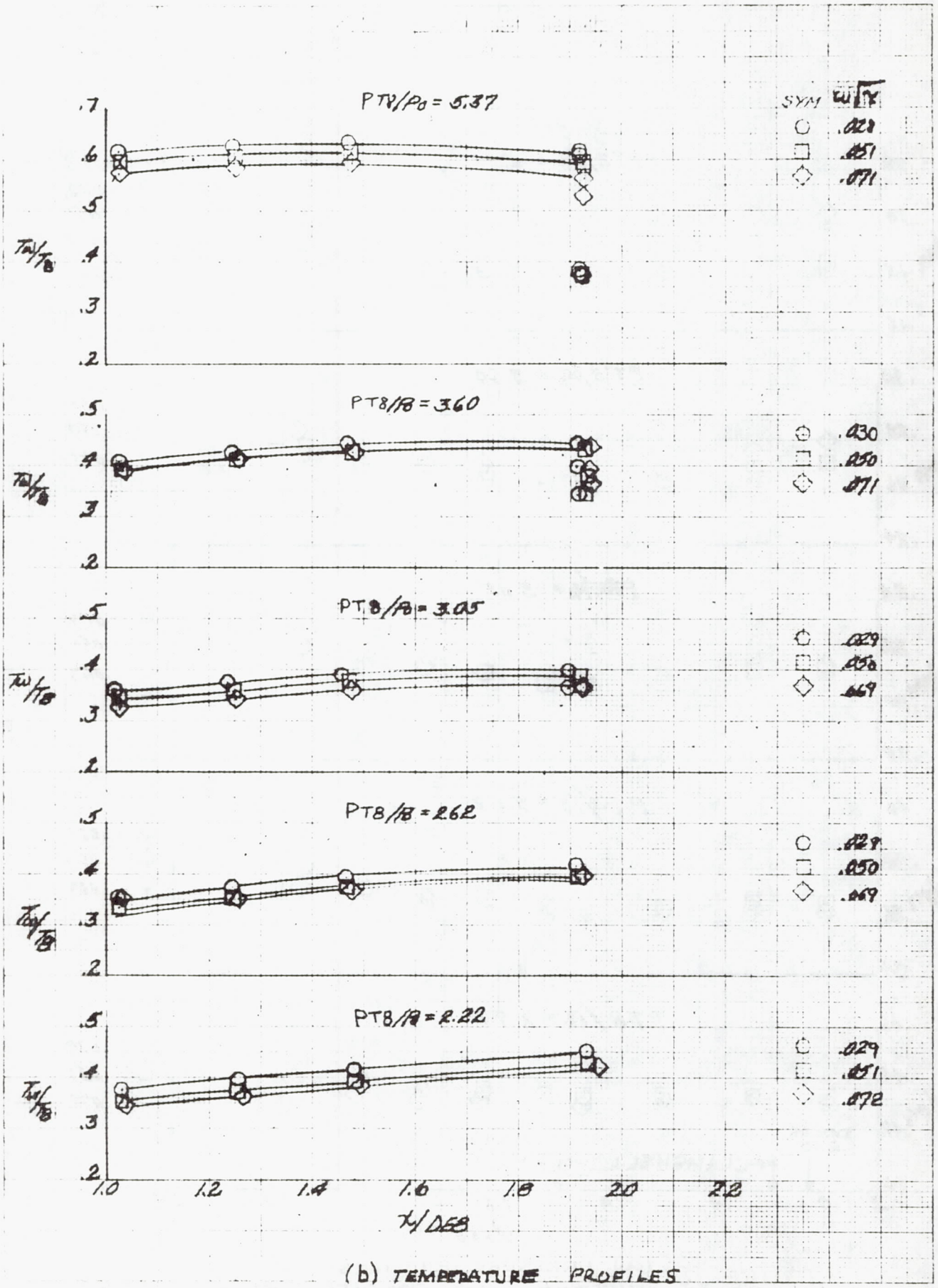

(b) TEMPERATURE PROFILES

FIGURE 33 CONCLUDED

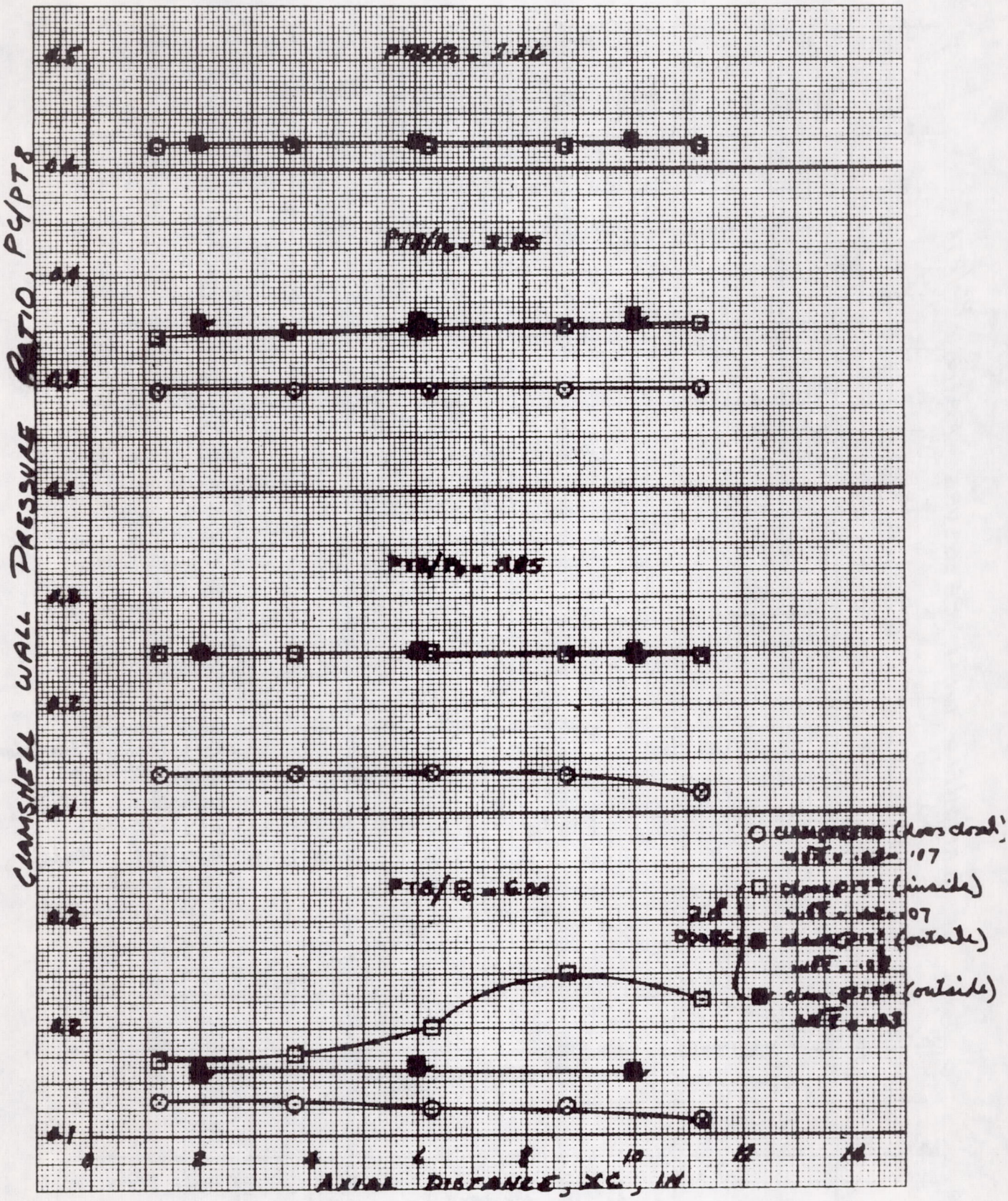

(a) $A_9/A_8 = 3.115$, $L_8/D_8 = 2.21$, $T_8 = 1630°R$

FIGURE 34 PRESSURE PROFILES @ CENTER OF CLAM. WALL

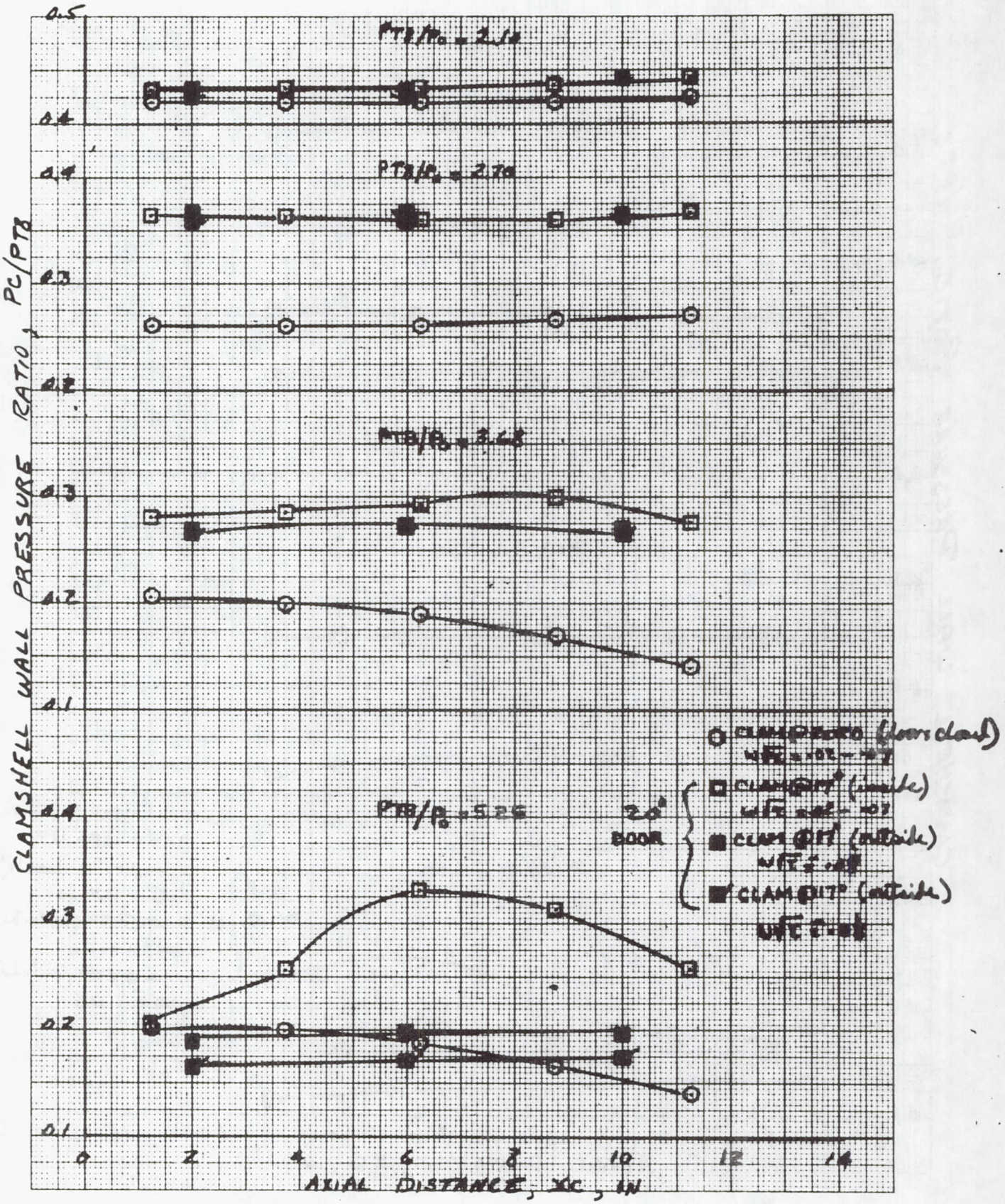

(b) $A_9/A_8 = 2.25$, $L_e/D_8 = 1.935$, $T_8 = 2510°R$

FIGURE 34 CONCLUDED

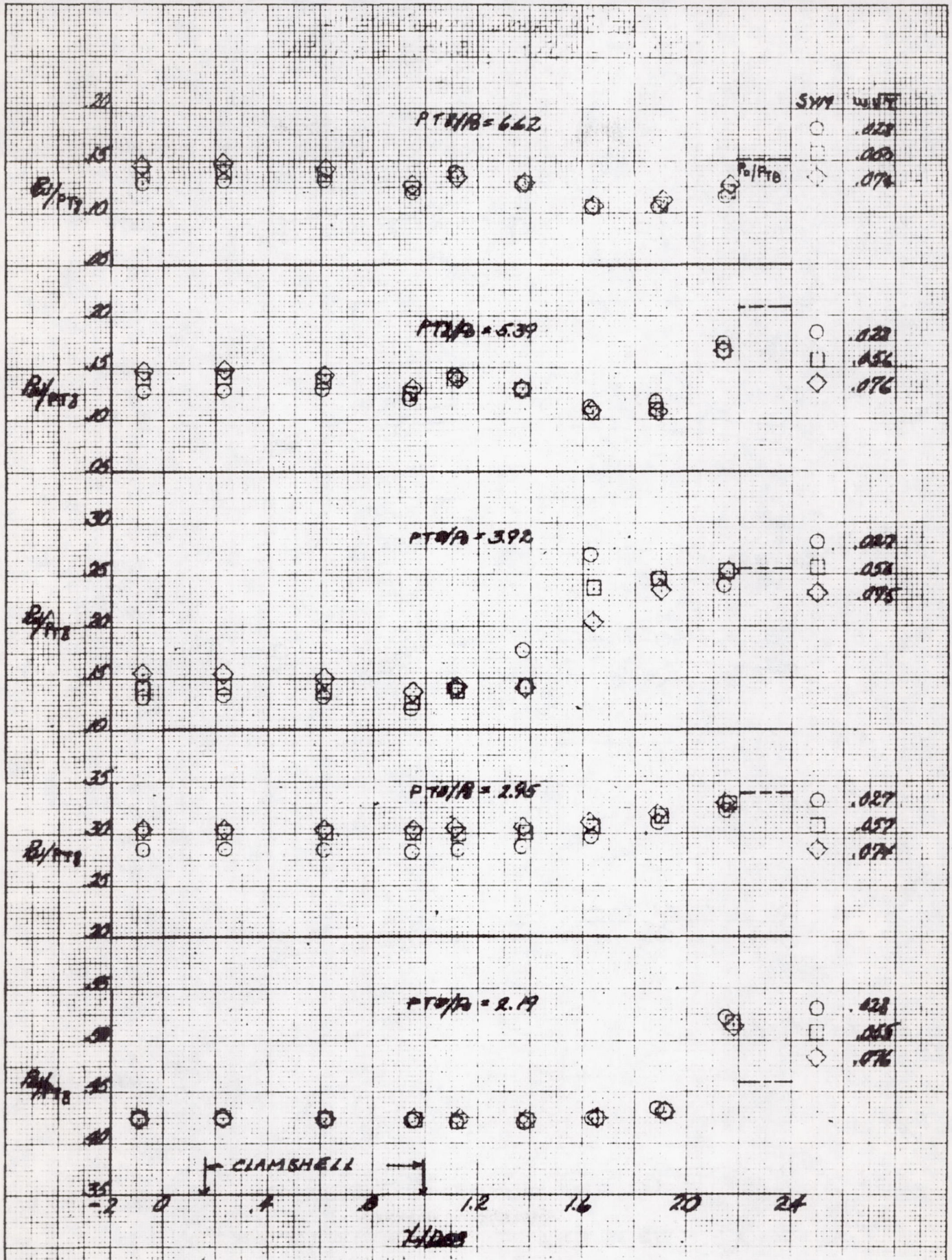

(a) PRESSURE PROFILES

FIGURE 35 EJECTOR WALL PROFILES (TRANSONIC EJECTOR)

$A_9/A_8 = 3.028$, $L_e/D_8 = 2.185$, $T_8 = 1630°R$

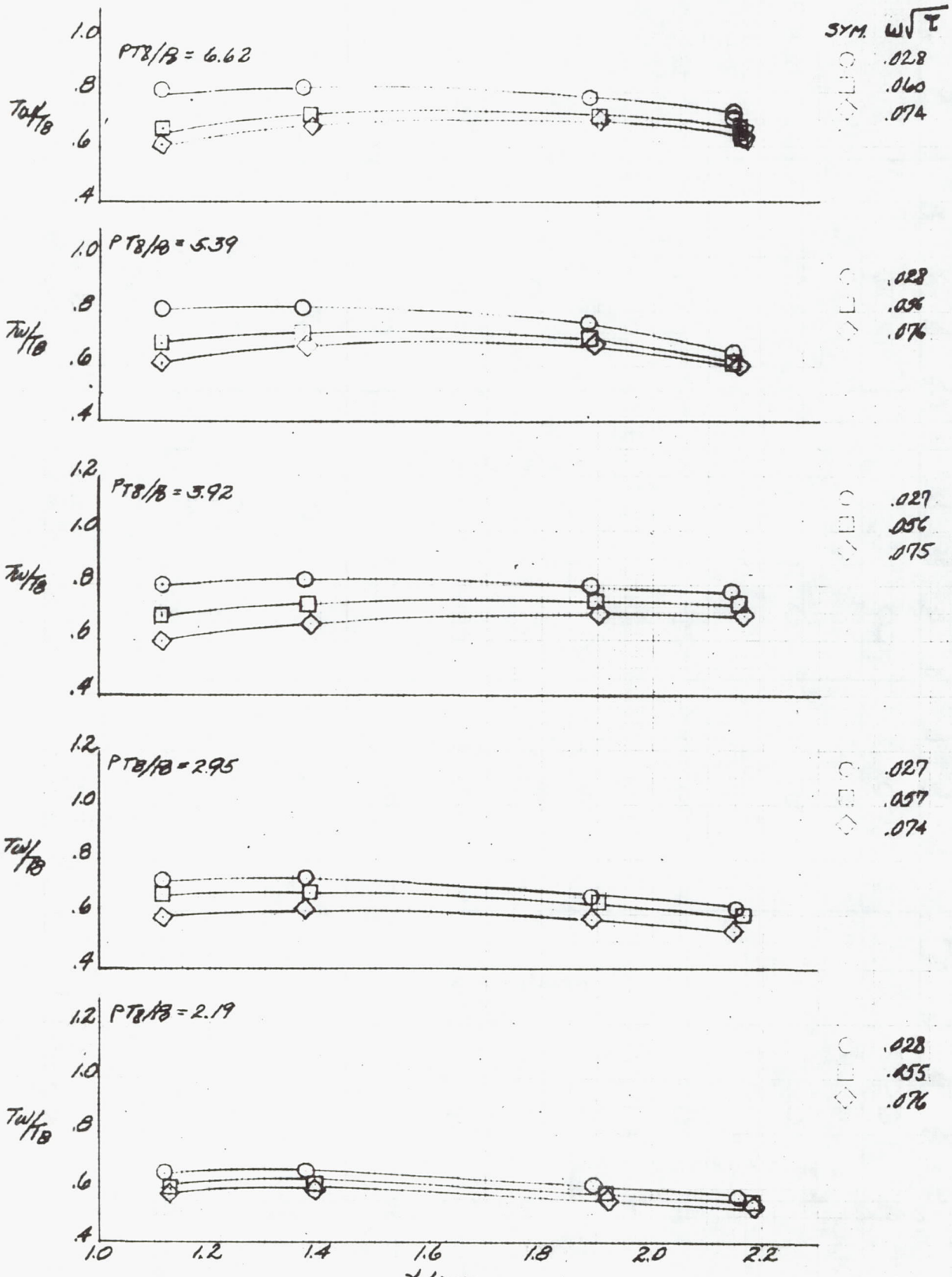

(b) TEMPERATURE PROFILES

FIGURE 35 CONCLUDED

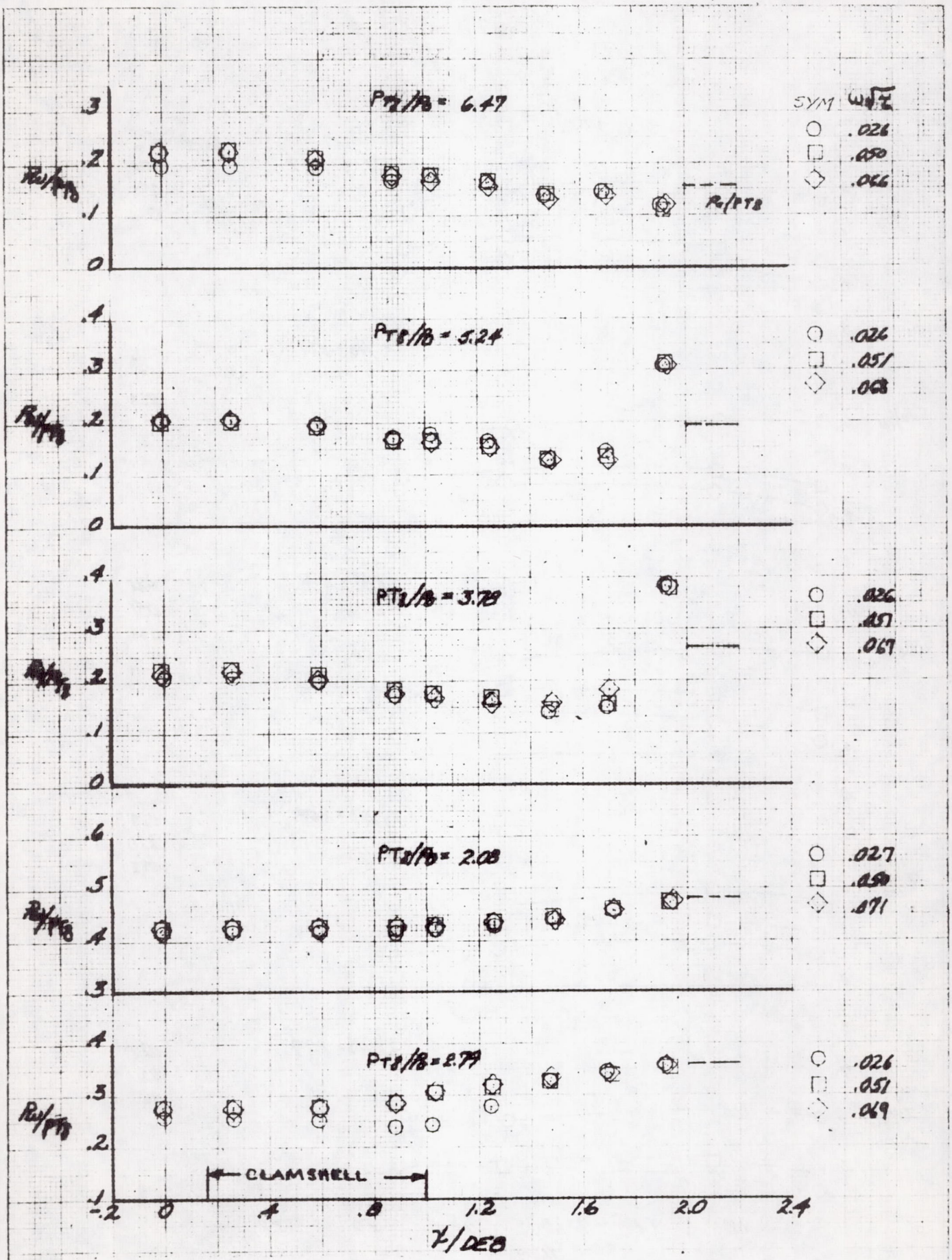

(a) PRESSURE PROFILES

FIGURE 36 EJECTOR WALL PROFILES (TRANSONIC EJECTOR)

$A_9/A_8 = 2.250$, $L_e/D_8 = 1.935$, $T_8 = 2560°R$

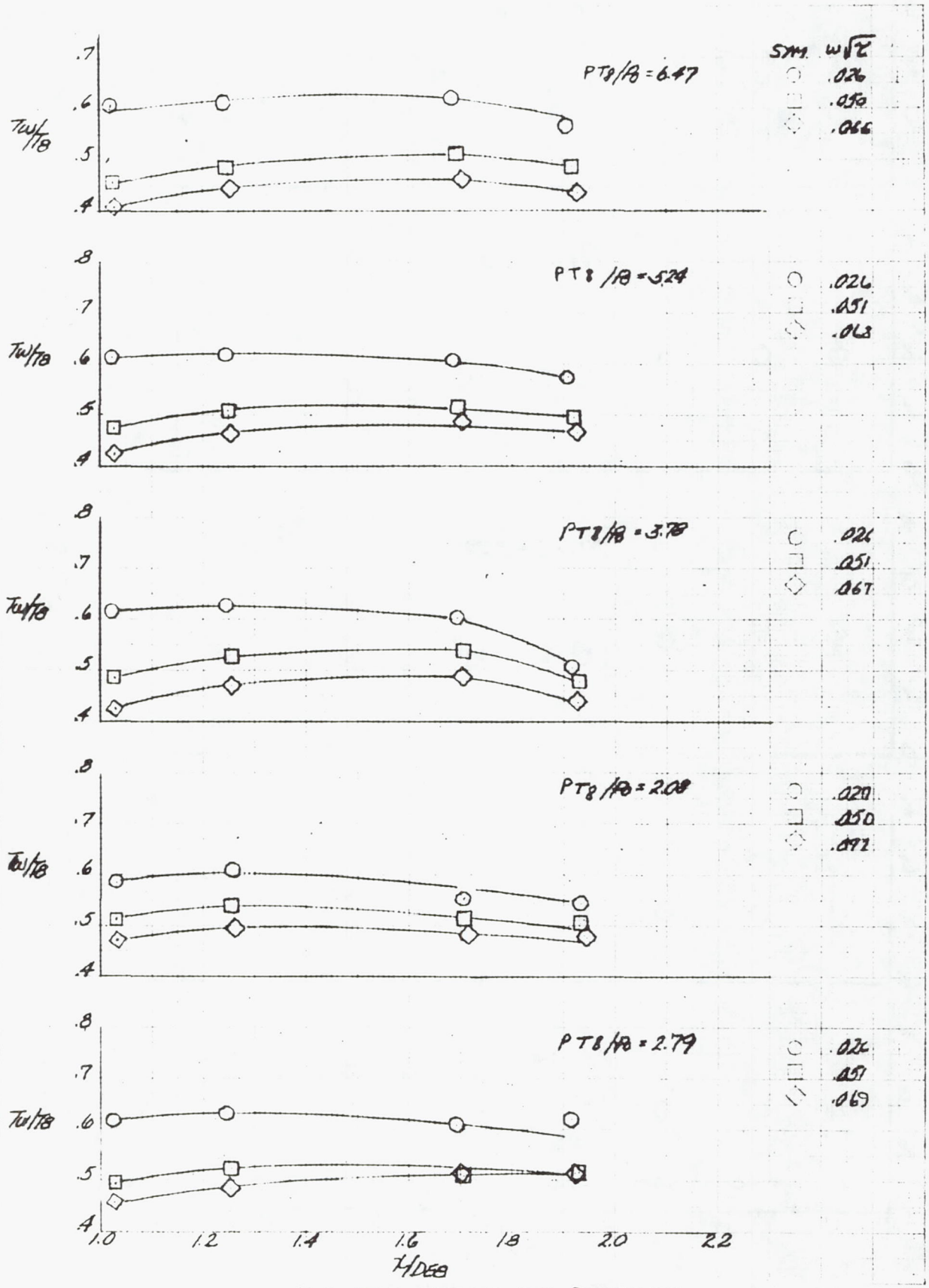

(b) TEMPERATURE PROFILES

FIGURE 36 CONCLUDED

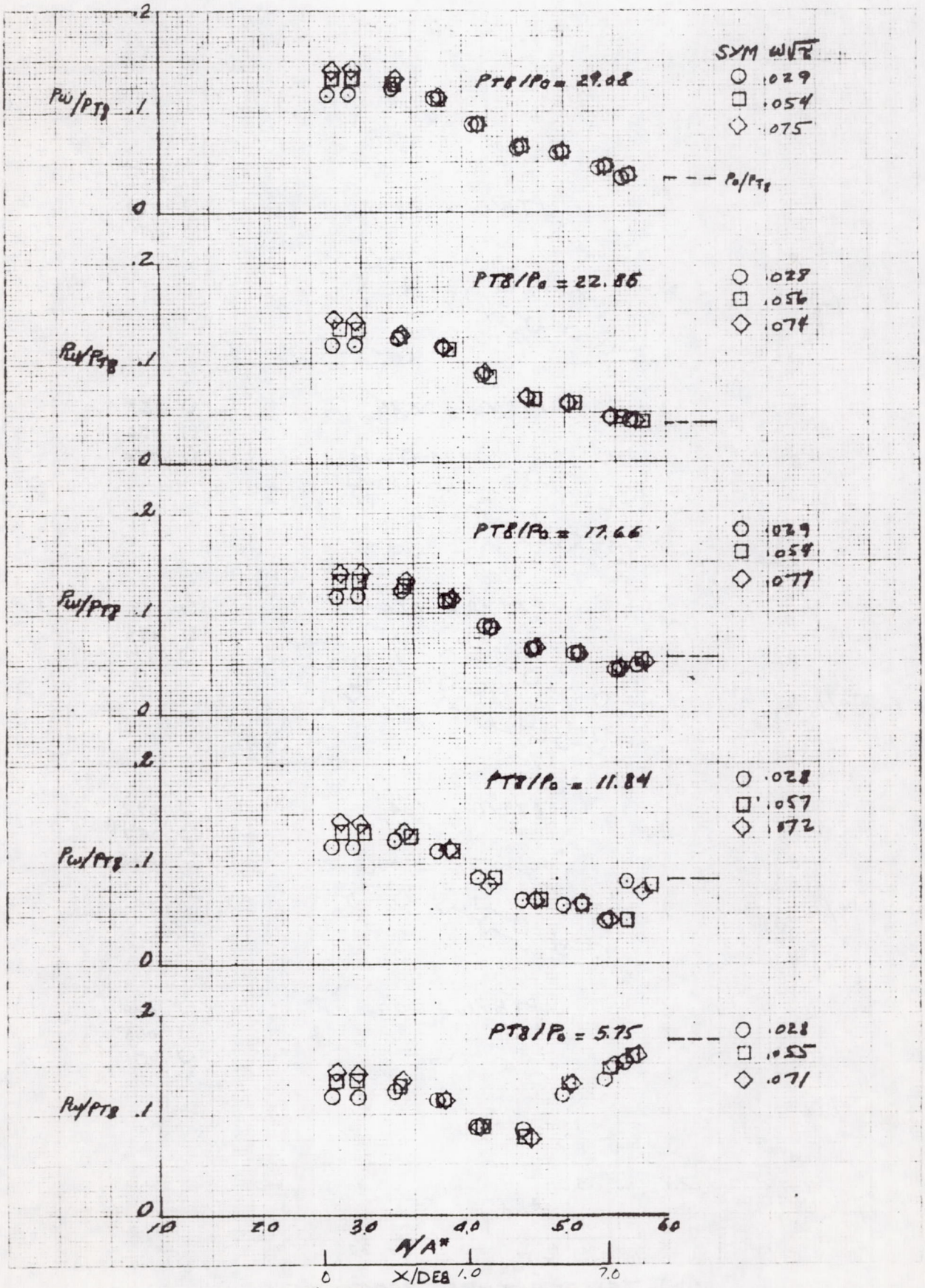

(a) PRESSURE PROFILES

FIGURE 37 EJECTOR WALL PROFILES (S.S. CRUISE EJECTOR)
$A_9/A_8 = 4.507$, $L_e/D_8 = 2.210$, $T_8 = 1635°R$

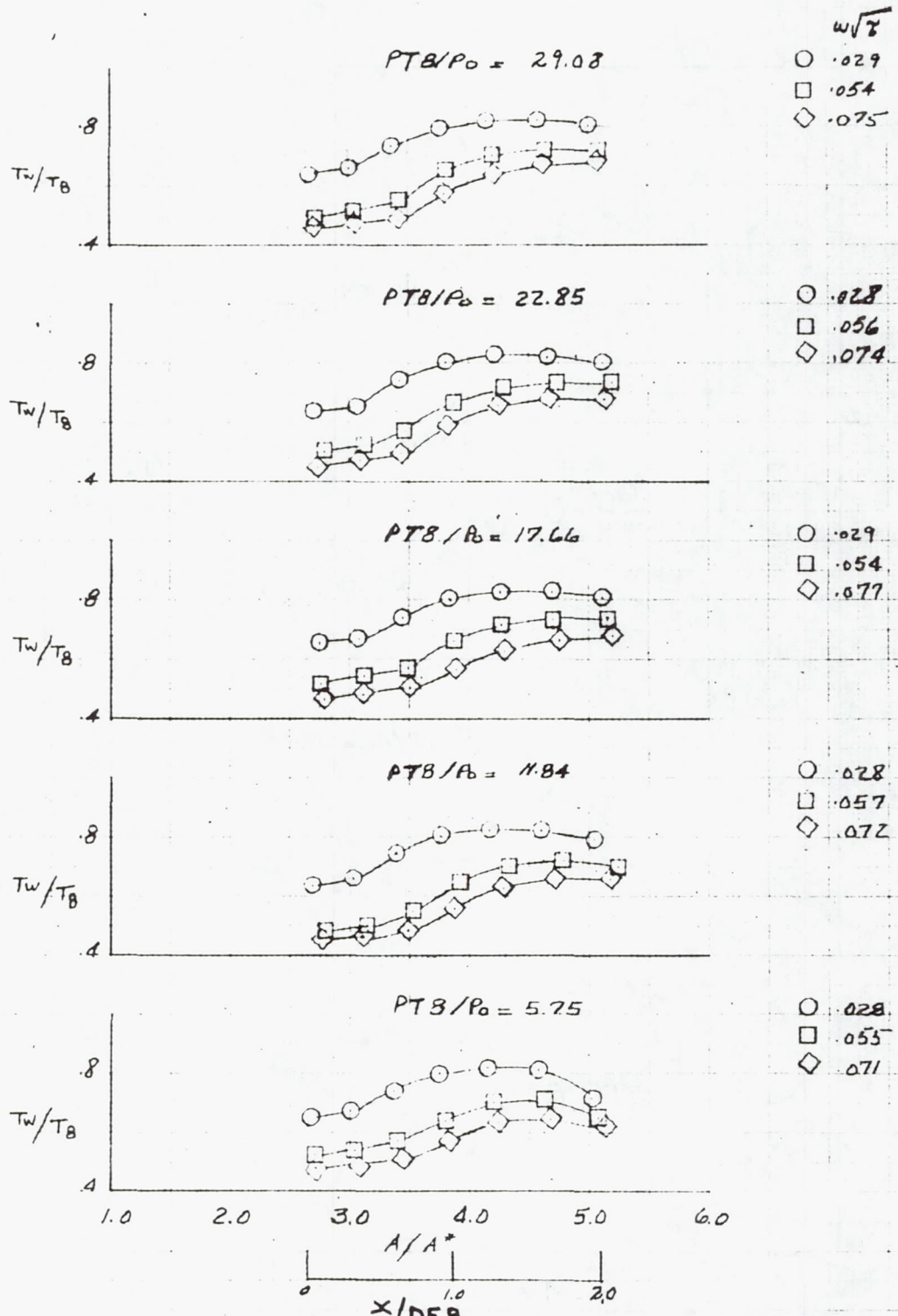

(b) TEMPERATURE PROFILES

FIGURE 37 CONCLUDED

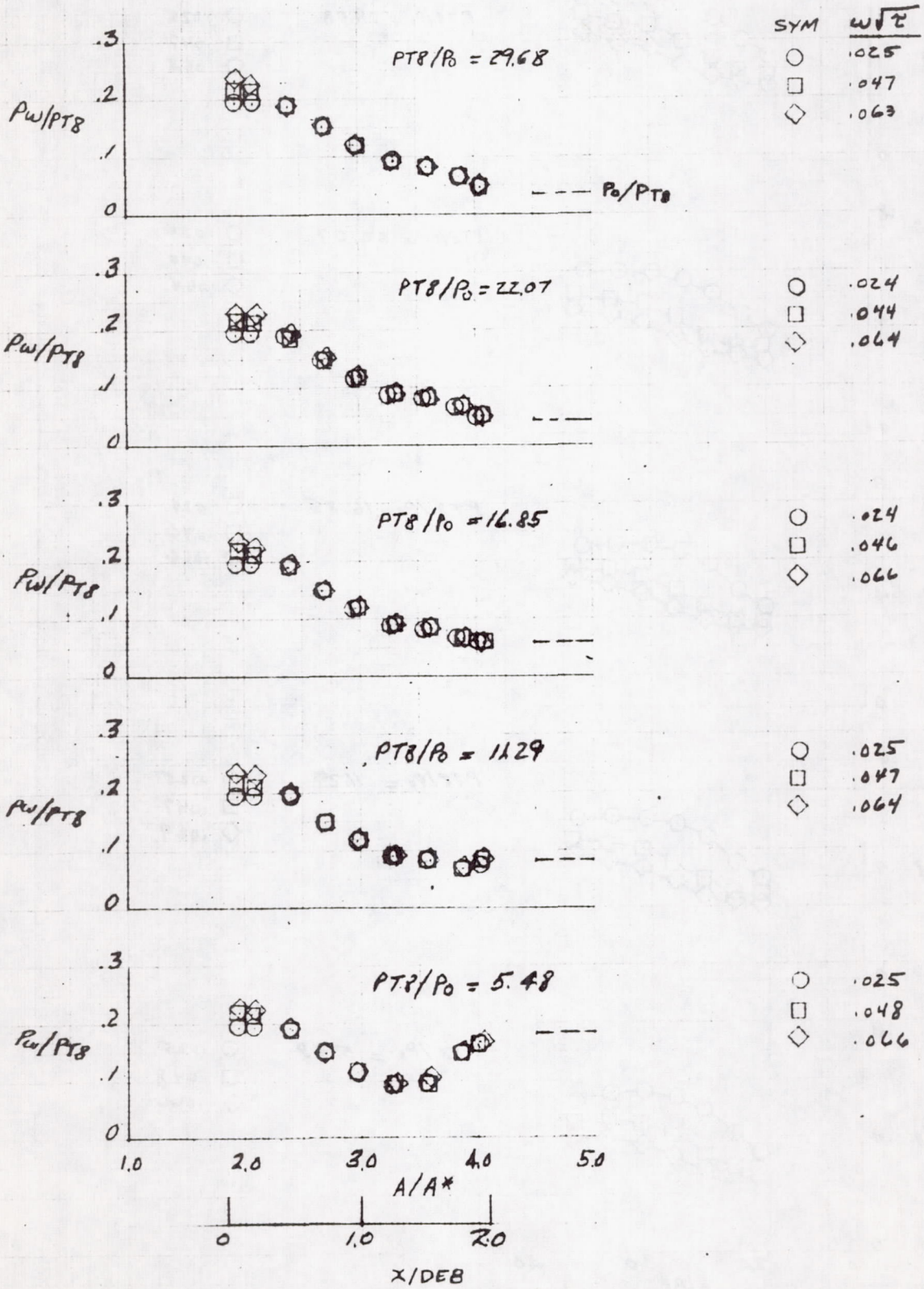

(a) PRESSURE PROFILES

FIGURE 38 EJECTOR WALL PROFILES (S.S. CRUISE EJECTOR)
$A_9/A_8 = 3.445$, $L_e/D_8 = 1.980$, $T_8 = 2475°R$

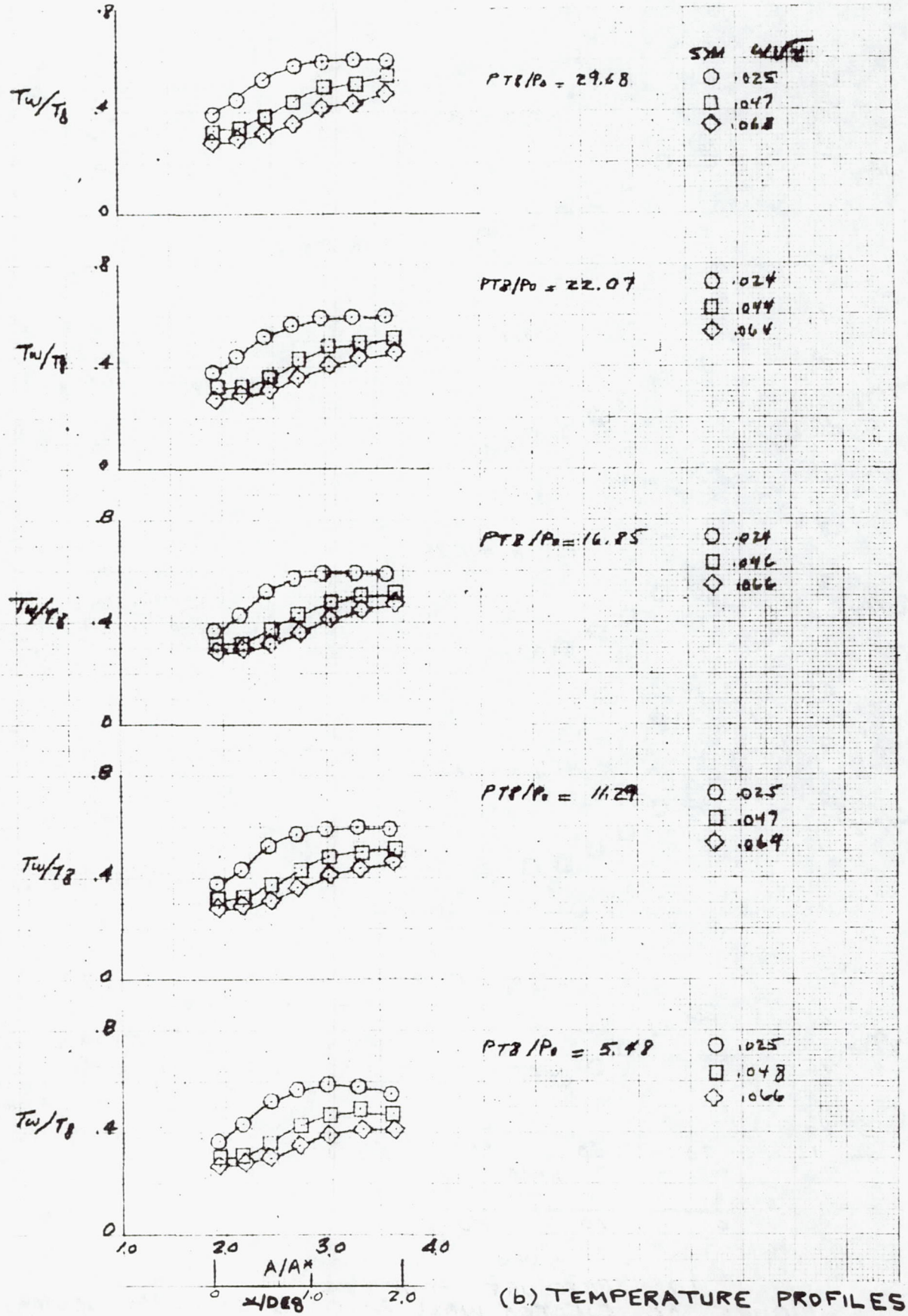

(b) TEMPERATURE PROFILES

FIGURE 38 CONCLUDED